Optimization of Common Reflection Surface (CRS) attributes based on conjugate direction approach using Powell search method

Dissertation

Zur Erlangung des Doktorgrades der Naturwissenschaften
im Fachbereich Geowissenschaften
der Universität Hamburg

vorgelegt von
Eko Minarto
aus
Jombang, Indonesia

Hamburg
2013

Als Dissertation angenommen vom Fachbereich Geowissenschaften der
Universität Hamburg
Auf Grund der Gutachten von Prof. Dr. Dirk Gajewski
und Dr. Claudia Vanelle
Hamburg, den 22 January 2014

Prof. Dr. Christian Betzler
Leiter des Fachbereichs Geowissenschaften

Abstract

Optimization is an important step in the analysis of physical problems to search for the optimal state. The goal is to find the best values of the variables that optimize the objective. It can be further increasing the accuracy of the Common Reflection Surface (CRS) wavefield attributes. The fastest optimization algorithms usually only seek a local minima, a point at which the objective function is smaller than at all other feasible points in its vicinity. They do not always find the best solution of all such minima, that is, the global minimum. Global solutions are highly desirable in some applications, but they are usually difficult to identify and even more difficult to locate.

I propose a new strategy for the optimization method of the simultaneous estimation of the CRS stack attributes, which allows to improve the image of pre-stack seismic reflection data. The method is based on the conjugate direction method with its well-known convergence properties and the Powell search method. The algorithm is robust and easy to implement. The main advantage of this approach is the use of the conjugate direction method leads to a highly efficient iterative search method to speed up the convergence rate while no derivatives of the objective function need to be calculated. The specific features of the Powell search method for the control of the search direction prevents the premature convergence into local minima.

Previous research has shown that Nelder Mead optimization method applied to estimate of the CRS stack attributes requires more iterations and is very time-consuming. An application to the complex Sigsbee 2A synthetic data and a field data example shows that the new method provides solutions with higher stability and faster convergence. The new method also has a substantial computational advantage against the Nelder Mead method currently used in the CRS attribute search. A factor of 2 in computing time was observed for the simultaneous search of the parameters in the 2-D CRS stack using the Powell conjugate direction approach for the field data example.

The application of the global optimization of the simultaneous estimation of the CRS stack method on the Sigsbee 2A synthetic data set and field data set shows that the new method provides very good solutions and can avoids being trapped into wrong solutions which can not be achieved by the Nelder Mead optimization method.

Contents

List of Figures

List of Tables

Chapter 1

Introduction

The aim of this thesis is the implementation of the optimization method for simultaneous estimation of the Common Reflection Surface (CRS) stack attributes, which allows to improve the image of pre-stack seismic reflection data. Optimization is an important step in the analysis of physical problems to search for the optimal state. The goal is to find the best values of the variables that optimize the objective. The objective depends on certain characteristics of the system, called variables or unknowns. The fastest optimization algorithms usually seek only a local minima, a point at which the objective function is smaller than at all other feasible points in its vicinity. They do not always find the best solution of all such minima, that is, the global minimum. Global solutions are highly desirable in some applications, but they are usually difficult to identify and even more difficult to locate. Optimization theory or optimization problem is the study of the extremal values of a function: its minimum and maximum. Topics in this theory range from conditions for the existence of a unique extremal value to methods, analytic and numeric for finding the extremal values and for what values of the independent variables the function attains its extremes.

Optimization procedure can be further increasing the accuracy of the CRS wavefield attributes. I try to devise a strategy for the optimization of the simultaneous estimation of the CRS stack attributes, which allows to improve the image of pre-stack seismic reflection data. The method comprises conjugate direction approach based on Powell search method. Previous research has shown the pragmatic approach of the CRS stack, which subdivides the 3-D global search in the full pre-stack data volume into three 1-D searches in data sub-volumes, and the simultaneous optimization using Nelder Mead (NM) method applied to estimate Common Reflection Surface (CRS) stack attributes. In this thesis, I introduced the new globally optimization method for simultaneous estimation of the Common Reflection Surface (CRS) stack attributes which prevents the premature convergence into local minima, without the needed of computing the gradient. The method is based on the conjugate direction method with its well-known convergence properties and Powell search method for the control of the search direction. The algorithm is robust and easy to implement. The use of the conjugate direction method leads to a highly efficient iterative search method to speed

up the convergence rate while using Hessian is avoided, also no matrix inversion and no storage of a sparse matrix required. The iterative Powell search method for the control of the search direction prevents the premature convergence into local minima, without the need of computing the gradient.

One of the most commonly used geophysical methods for oil and gas exploration is the reflection seismic method to generate a structural image of the subsurface. The reflection events in the recorded pre-stack data time domain has to be transformed into the reflectors of the medium properties in the depth domain. A crucial problem of the imaging task is the fact that many conventional imaging methods require a sufficiently accurate macro velocity model to yield correct results. The simulation of a zero-offset (ZO) stack section from multi coverage seismic reflection data is a widely used seismic reflection time domain imaging method that reduces the amount of data and enhances the signal-to-noise (S/N) ratio.

The Common Reflection Surface (CRS) stack is a model independent seismic imaging method without any ray tracing and macro velocity model estimation. Only the knowledge of the near-surface velocity is required. Application of the Common Reflection Surface (CRS) stack technique improves the signal-to-noise (S/N) ratio and the quality of reflection seismic images. Since, a multiparameter formula allows to sum up more traces during the stack compared to the Common Mid Point (CMP) stack and involves information about the shape of seismic reflectors, i.e., dip and curvature, into processing. In contrast to the conventional CMP stacking that does not use the full potential of the data set, the CRS stacked directly makes use of the inherent redundancy in the pre-stack data and parameterizes the reflection events in the time domain to improve the signal-to-noise (S/N) ratio and the quality of reflection's seismic images. Reflection events in the CRS stack sections appear clearer and more continuous compared to conventional CMP stack sections. The CRS stack is not only to provide a well-simulated zero-offset stack section but also to determine certain attributes of hypothetical wave fronts at the surface useful for a subsequent inversion. The 2-D CRS description of the reflection response is specified by three kinematic wave field attributes, namely the emergence angle α of the normal ray, the radius of curvature R_{NIP} and R_N of the NIP wave and the normal wave, respectively. Since for each new values of $\{\alpha, R_{NIP}, R_N\}$ the estimation of the semblance has a high computational cost in term of floating-point operations and data movement, the search process, if not correctly designed, might be very time-consuming. This lead to the introduction of the pragmatic approach which subdivides the 3-D global search in the full pre-stack data volume into three 1-D searches in data sub-volumes.

In the first part of this thesis, the processing of optimization method used the initial values from the result of the pragmatic approach, which subdivides the 3-D global search in the full pre-stack data volume into three 1-D searches in data sub-volumes. We have to split the three-parameters optimization problem into separate one-parameter searches. Furthermore, there is no guarantee that the resulting attributes may be wrong or linked to a local minimum. The second part of this thesis

global optimization methods may overcome some of these deficiencies and problems. The processing of the optimization procedure used the arbitrary guess based on a priori information from the geological structure, best guess or local slopes without any special treatment of the initial values.

1.1 Thesis structures

The thesis is structured as follows:

In Chapter 1, I briefly introduce and review the basic aim of this thesis. The optimization problem is described and applications on the simultaneous estimation of Common Reflection Surface (CRS) stacked attributes to improve the quality of pre-stack seismic reflection imaging is presented.

In Chapter 2, reviews the conventional and new seismic imaging techniques used in this work. In particularly, it introduces the CMP and CRS stack methods for time imaging, the pragmatic approach to define the initial values of the optimization and the global optimization problem.

In Chapter 3, discusses the optimization problem in detail. The fastest optimization algorithms usually seek only a local minima, a point at which the objective function is smaller than at all other feasible points in its vicinity. They do not always find the best solution of all such minima, that is, the global minimum. Global solutions are highly desirable in some applications, but they are usually difficult to identify and even more difficult to locate. A simplex method for finding a local minimum of a function of several variables is the Nelder Mead optimization method and compare with the conjugate direction approach using Powell search method. Demonstrate the numerical example of both method.

In Chapter 4, presents the results of the simultaneous optimized CRS stack attributtes using synthetic data. I apply the optimization procedure on Sigsbee 2A synthetic data which were generated designed in 2001 by the *Subsalt Multiples Attenuation and Reduction Technologies* (SMAART) JV consortium. The Sigsbee 2A data set was simulates for a marine 2-D model that represents a situation as observed in the Gulf of Mexico: a stratified background model associated with a relatively smooth macro-velocity model contains a salt body with a quite complicated geometry.

In Chapter 5, presents results of the simultaneous optimization for CRS stacked on field data set. The data set is marine data set from the North Sea close to the German coast line. Salt structures and complex fault systems characterize this region. The application of the new method has a substantial computational advantage against the Nelder Mead method currently used in the CRS attributes search. A factor of 2 in computing time was observed for the simultaneous search of the parameters in the 2-D CRS stacked using the conjugate direction approach for field data example. Whereas

we do not see specific differences in the stack or attributes sections for the Powell conjugate direction or Nelder Mead approach.

In Chapter 6, presents the results of the application of the global optimization CRS stack used an arbitrary initial values. I investigated the optimization results based on the choice of the initial values to demonstrate the advantages of this method finding the solution. In this implementation we still using the pragmatic approach results for the R_{NIP} and R_N as an initial values, and the arbitrary value for the angle. To show the advantages this method I apply the optimization procedure on Sigsbee 2A synthetic data set and field data set. The application of the simultaneous optimization of the CRS stack method on the Sigsbee 2A synthetic data set and field data set shows that the new method provides very good solutions and can avoids being trapped into wrong solutions which can not be achieved by the Nelder Mead optimization method. The results show that the new method can find the right solution in comparison with the Nelder Mead method without any special treatment of the initial values.

In Chapter 7, I conclude the experiences and summarize the results of the thesis and give an outlook on various future extensions and generalizations of the CRS stack approach.

Chapter 2

Theoretical review

Seismic method is one of the most commonly used techniques for geophysical investigations for the petroleum exploration, ground water searches, or civil engineering. The method allows to image of the Earth's interior using indirect measurements carried out at the Earth's surface. The detail image of subsurface structures is the goal of geophysical investigation to provide data are used to analyze potential petroleum reservoirs and mineral deposits, locate groundwater, and assess sites for environmental remediation.

2.1 Reflection seismic method

Seismic reflection is one branch of geophysics which utilizes the concept of wave propagation. The reflection seismic method is the most important method in the hydrocarbon exploration industry, due to high accuracy, high resolution and deep penetration. The reflection seismic method based on the generation and measurement of elastic waves at the earth's surface. The purpose of this method is to get an image of the subsurface from the traveltimes and amplitudes of the elastic waves measured at the earth's surface. This method allows the investigation of the subsurface structures for possible oil and natural gas deposit. Explosive or vibrator sources are used to generate the elastic waves, which propagate through the subsurface and are reflected as well as refracted at seismic interface (show in Figure 2.1(a)). These interfaces are boundaries between geological formations, where the velocity or density distribution in the earth changes. A series of receivers spread on the surface capture the returning energy at the earth's surface, recording the traveltime and amplitude of the elastic wave.

The simplest type of acquisition would be to use a single coincident source and receiver pair and profile the earth along a line as shown in the adjacent figure. Such an

experiment would be called a zero-offset (ZO) experiment because there is no offset distance between source and receiver (both marked as a yellow dot on the Figure 2.1(b)). The resulting seismic data will be single-fold because there will be only a single trace per sub-surface position. The zero-offset (ZO) concept is an important one and the method might be used in practise if noise could be ignored. In order to overcome the noise problem and additionally to estimate earth velocity, the method of acquisition most commonly used is the Common Mid Point (CMP) method.

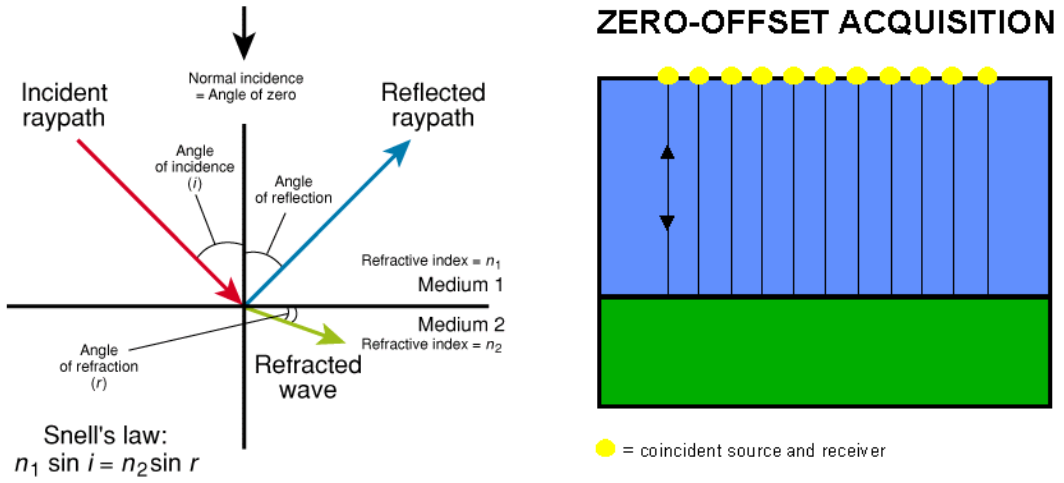

(a) (b)

Figure 2.1: Propagation of seismic wave (a) and zero-offset geometry acquisition (b).

2.2 Conventional CMP stack

In a typical 2-D seismic data acquisition experiment sources and receivers are distributed along a straight line (Sheriff and Geldart, 1995; Yilmas, 2001). Seismic energy travels into the subsurface from the source location $(x_s, 0)$. Seismic trace resulting from the reflected and diffracted portions of this released energy are recorded at the receiver location $(x_g, 0)$. In the field, seismic data are acquired as Common Source (CS) gathers and then sorted into Common Mid Point (CMP) gathers. CMP location (x_m) is defined as the midpoint between a source and a receiver. The location x_m on the seismic line can be calculated from the source location x_s and the receiver location x_g. The distance between source and receiver is called offset. Source and receiver pairs with the same CMP location are gathered into a CMP gather. Thus the lateral position of each trace in the prestack data is transformed according to:

$$x_m = \frac{x_s + x_g}{2}, \qquad h = \frac{x_g - x_s}{2}, \tag{2.1}$$

x_m is the horizontal location of the CMP and h is half the distance between source and receiver, respectively.

In the 2-D survey, source and the receiver together are moved along the line of acquisition (Figure 2.2(a)). Thereby, each subsurface point is repeatedly illuminated under varying angles. This so-called multi coverage seismic recording provides redundant information of the illumminated subsurface point. This repeated gathering of information from the same element with different offset is called redundancy. Since in field data is usually acquired in a redundant way, many traces contain information about the same region in the subsurface. A CMP gather includes all rays that illuminate the same point on a reflector with different offsets (Figure 2.2(b)). Thereby the same element of the subsurface is involved in several records with different source and receiver pair coordinates x_s and x_g. Thus, a CMP gather contains redundant information about the surface. This redundancy results in rapidly increasing storage demands and can efficiently be lowered by the technique of stacking. This is the basic idea for the CMP stack method (Mayne, 1962). Not only does this technique allow to considerably lower the demanded storage capacity, since the trace from different offsets contain information for a common point on a horizontal reflector, the redundant information can be summed up constructively to increases the signal-to-noise (S/N) ratio. The signal-to-noise ratio is improved by constructive summation of the reflection events and destructive summation of incoherent noise.

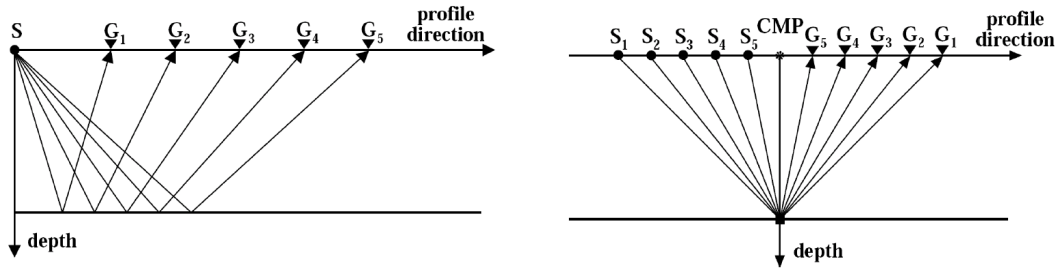

(a) (b)

Figure 2.2: Reflection seismic geometry: shot configuration (a) and CMP configuration (b). In homogeneous and horizontally-layered model, all rays in a CMP gather reflect from the same depth point under varying angles. The CMP gather contains exactly the same information about one point in depth, the Common Depth Point (CDP).

2.2.1 Normal move out and velocity analysis.

In general a CMP gather consist of traces with different half-offsets to the CMP, the coherent energy recorded in the data is now summed constructively, as one desires. The delay of reflection arrival times with offset is called Normal Move Out (NMO). The traveltime curve defines the increase in traveltime t with offset x (Figure 2.3). The time $\triangle t_{NMO}$ is the difference between the traveltime $t(h)$ for a specific offset and the zero-offset traveltime t_0. It is the additional propagation time $\triangle t_{NMO}(x) = t(x) - t_0$ that a seismic wave requires if source and receivers are not coincident and an offset

remains, compared to the traveltime for coincident source-receiver location. Summation or stacking of the gathered traces to zero-offset requires the NMO correction of each trace to the same level t_0 at zero-offset.

To overcome this problem, the variation of traveltime with offset has to be estimated. Conventional CMP stacking involves summing the primary reflection along the calculated moveout curves which best approximate the actual reflection traveltimes curves. For the simplest case of small offset a planar horizontal reflector, constant velocity layer over a homogeneous half-space, the traveltime curves can be approximated according Pythagorean theorem described by a hyperbola formula:

$$t^2(h) = t_0^2 + \left(\frac{4h^2}{v^2}\right), \tag{2.2}$$

with h is the half-offset between source and receiver, v is the medium velocity and t_0 is the zero-offset traveltime (traveltime that measured for coincident source and receiver, $h = 0$). This equation describes a hyperbola whose curvature is characterized by the moveout velocity parameter.

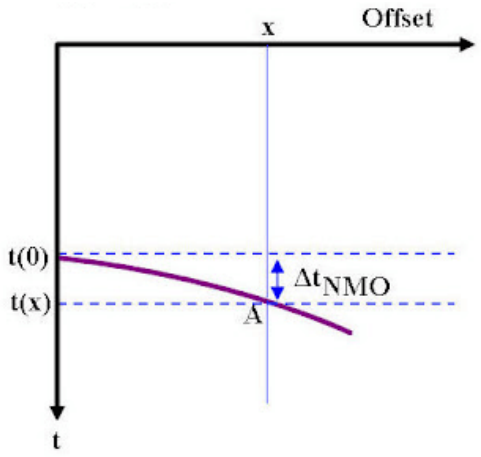

Figure 2.3: NMO correction: increase in traveltime t with offset x.

The removed of the effects of offset on traveltime is called normal moveout correction, which implies mapping of traveltime $t(h)$ to zero-offset traveltime t_0 by:

$$\triangle\, t_{NMO}(h) = t(h) - t_0 = t_0 \left\{ \left(1 + \left(\frac{2h}{vt_0}\right)^2\right)^{1/2} - 1 \right\}, \tag{2.3}$$

The square of the traveltime (equation 2.2) is allow for vertical inhomogeneity in the overburden can be expanded into its Taylor series (Hubral and Krey, 1980):

$$t^2(h) \approx t_0^2 + \left(\frac{4h^2}{v_{RMS}^2}\right), \tag{2.4}$$

where the root mean square velocity is given by v^2_{RMS}

$$v^2_{RMS} = \frac{1}{t(0)} \sum_{i=1}^{n} v_i^2 \triangle t_i(0), \tag{2.5}$$

with $\triangle t_i(0)$ being the vertical two-way traveltime through the i^{th} layer, v_i is the velocity in the i^{th} layer and $t(0) = \sum_{i=1}^{n} \triangle t_i$.

2.3 Common Reflection Surface (CRS) stack

The simulation of a zero-offset stack section from multicoverage seismic reflection data is a widely used seismic reflection imaging method that significantly reduces the amount of data and increases the signal-to-noise ratio (S/N). But a sufficiently accurate stacking velocity model is required to yield correct result. Common reflection surface (CRS) stack is a new zero-offset simulation method in seismic processing (Müller, 1999), new model independent in seismic imaging method. There are no need macro velocity model, consequently without velocity analysis, just near surface velocity. Common reflection surface stack is the use of analytical formulae that describe the kinematic reflection moveout response for inhomogeneous media with curved interface and the kinematic multicoverage response for inhomogeneous media. The aim of the common reflection surface stack is not only to provide a well-simulated zero-offset stack section but also to determine certain parameters useful for a subsequent inversion. Use coherency analysis (Taner and Koehler, 1969) to determined stack operator: reflection segmen location, curvature, and orientation.

The CRS stacking surface (Figure 2.4) can be calculated using the approximation of the true subsurface reflector by a reflector element that locally has the same curvature as the true reflector. The hyperbolic second order Taylor expansion formula derived from paraxial ray theory (Schleicher et al., 1993; Tygel et al., 1997) given by

$$t^2(x_m, h) = \left(t_0 + 2\frac{\sin\alpha}{v_0}(x_m - x_0) \right)^2 + 2\frac{t_0 cos^2\alpha}{v_0} \left(\frac{(x_m - x_0)^2}{R_N} + \frac{h^2}{R_{NIP}} \right), \tag{2.6}$$

with t_0 is the zero-offset traveltime, α is the angle of emergence of the ZO ray, v_0 is the near surface velocity, x_m and h midpoint and half-offset coordinate, respectively, R_N and R_{NIP} are radius of curvature of the normal (N) wave and normal incident point (NIP) wave, respectively. Half offset h and midpoint x_m can be calculated from the source location x_s and the receiver location x_g is given by equation 2.1.

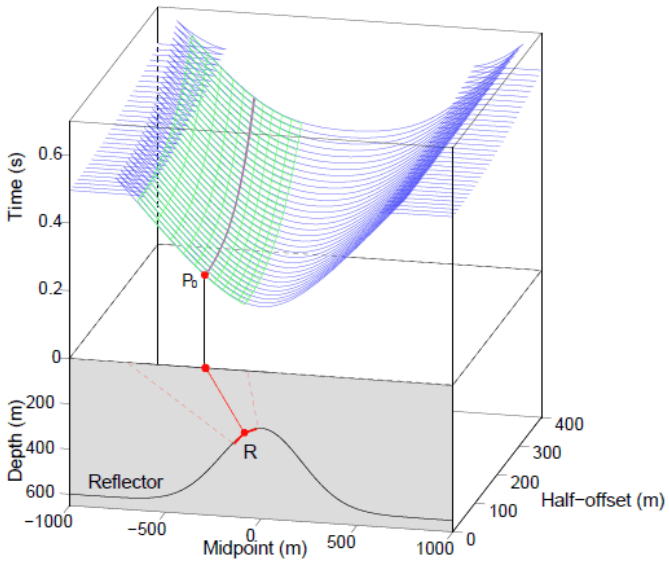

Figure 2.4: CRS stacking surface: illustration of the common reflection surface in a midpoint-offset-time (m, h, t) domain. Reflector curvature and dip can better be taken into account and a higher signal to noise ratio achieved. Due the summation not only takes place in offset but also to the extend in midpoint direction (Müller, 1999).

The three kinematic wavefield attributes α, R_N, and R_{NIP} were introduced by (Hubral, 1983). The N-wave is a wave generated by an exploding reflector model, where dense point sources cover the common reflector surface (CRS) around the NIP and explode simultaneously. The NIP-wave can be considered as a wave that propagates from a point source at the NIP for a specific reflector. R_N is the distance from the reflector element and local reflector curvature to the surface (Figure 2.5(a)), and R_{NIP} is the distance from the reflector element to the observation surface (Figure 2.5(b)).

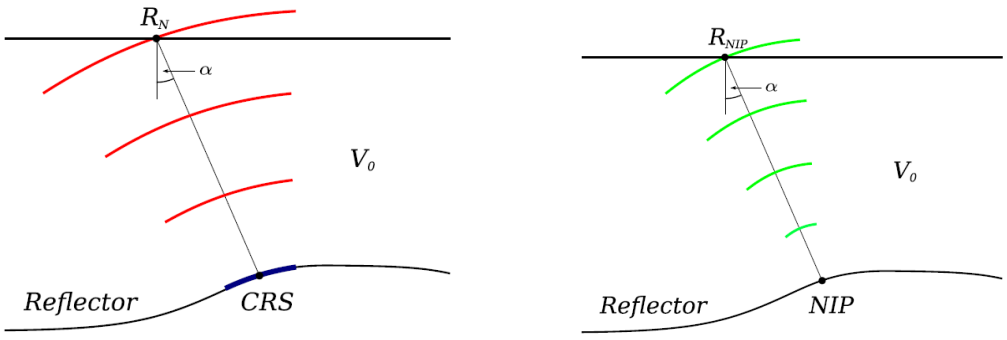

Figure 2.5: Illustration of physical interpretation of the kinematic CRS wavefield attributes. The radius of curvature of the N-wave (a) is the distance from the CRS curvature to the observation surface, and the radius of curvature NIP-wave (b) is measure from the NIP. The angle of emergence, α, defines the angular orientation of the CRS.

The respective sample of the zero-offset trace to be simulated is defined by (t_0, x_0). The remaining parameters are the angle of emergence α of the zero-offset ray, the curvature of the NIP-wave R_{NIP}, and the curvature of the N-wave R_N (Höcht, 1998). For each sample (t_0, x_0) in the stack section, we have to determine the stacking parameter triple (α, R_{NIP}, R_N) that yields the stacking operator that fits best to an event in the multicoverage data set. This is done by means of coherency analysis of the stacking operator with the measured data. It is given by (Taner and Koehler, 1969):

$$S = \frac{1}{N} \frac{\sum_t \left(\sum_{i=1}^{N} f_{i,t(i)} \right)^2}{\sum_t \sum_{i=1}^{N} f_{i,t(i)}^2}, \tag{2.7}$$

where $f_{i,t(i)}$ is the amplitude on the i^{-th} trace at traveltime $t(i)$ and N is the number of traces.

2.4 CRS processing

To perform the CRS stacking of seismic reflection the CRS parameters must be estimated. CRS processing starts with the search of initial values for the CRS parameters. Three kinematic wavefield attributes, emergence angle α, radius of curvature of the NIP wave R_{NIP}, and radius of curvature of the normal wave R_N, serve as parameters for the CRS operator.

2.4.1 Pragmatic approach

A simultaneous three parameters search for CRS parameters (α, R_N, R_{NIP}) would be computationally very expensive. The most efficient solution of the posed optimization problem with three parameters can be achieved if it can be decomposed into three separate optimization problem with one parameter searches (Müller, 1998). Here the 3-D search is subdivided into three subsequences 1-D searches is called the pragmatic approach. Three parameters α, R_N, and R_{NIP} search processes by automatic CMP stack, angle scan, and R_N scan. Starting with the generation of an automatic CMP stack section, the three CRS parameters are estimated step by step.

Automatic CMP stack

The hyperbolic equation traveltime formula (equation 2.6) depends on three unknown parameters α, R_N, R_{NIP} can be simplified in the CMP configuration ($x_m = x_0$). To split the three-parameter optimization problem into separate one-parameter searches,

the input data is confined to specific gathers. These yields initial attributes which can be used as first guess in a final optimization procedure. The hyperbolic approximation $x_m = x_0$ can be expressed by:

$$t_{CMP}^2(h) = t_0^2 + 2\frac{t_0 cos^2\alpha}{v_0}\frac{h^2}{R_{NIP}} = t_0^2 + 2\frac{t_0 h^2 q}{v_0}. \tag{2.8}$$

With the conventional stacking velocity V_{NMO} equation we obtain:

$$V_{NMO}^2 = \frac{2v_0 R_{NIP}}{t_0 cos^2\alpha} = \frac{2v_0}{t_0 q}, \tag{2.9}$$

where

$$q = \frac{cos^2\alpha}{R_{NIP}}, \tag{2.10}$$

$$t_{CMP}^2(h) = t_0^2 + \frac{4h^2}{V_{NMO}^2}. \tag{2.11}$$

Angle scan-plane wave search zero-offset

To determine initial values of emergence angle α, we consider the ZO section simulated in the preceeding step. For traces in the ZO gather the traveltime description depends only on the two parameters α and R_N. In the ZO configuration ($h = 0$) the CRS equation reduces to:

$$t_{ZO}^2(x_m) = \left(t_0 + 2\frac{sin\alpha}{v_0}(x_m - x_0)\right)^2 + 2\frac{t_0 cos^2\alpha}{v_0}\left(\frac{(x_m - x_0)^2}{R_N}\right). \tag{2.12}$$

In a first order approximation by neglecting second order (for $R_N = \infty$) this equation can be further simplified to yield a one-parametric equation:

$$t_{ZO}(x_m) = t_0 + 2\frac{sin\alpha}{v_0}(x_m - x_0). \tag{2.13}$$

Using this equation, an initial angle of emergence α is determined for every ZO time sample. Using a discrete number of angle of emergence α appliying coherency analysis. For each test parameter the traveltime is calculated and correlated with ZO data. The angle of emergence that yields the highest correlation is stored as the initial angle of emergence α for the initial CRS stack.

R_N scan-hyperbolic search zero-offset

After the values V_{NMO} and α are estimated, the R_{NIP} is defined through equation 2.9 as:

$$R_{NIP} = \frac{t_0 cos^2 \alpha V_{NMO}^2}{2v_0}. \tag{2.14}$$

In the zero-offset configuration ($h = 0$) equation 2.12 applies to estimated R_N. With the knowledge of angle of emergence α we can determine initial discrete R_N value for the initial CRS stack.

The simplified flowchart for the pragmatic approach procedure is shown in Figure 2.6.

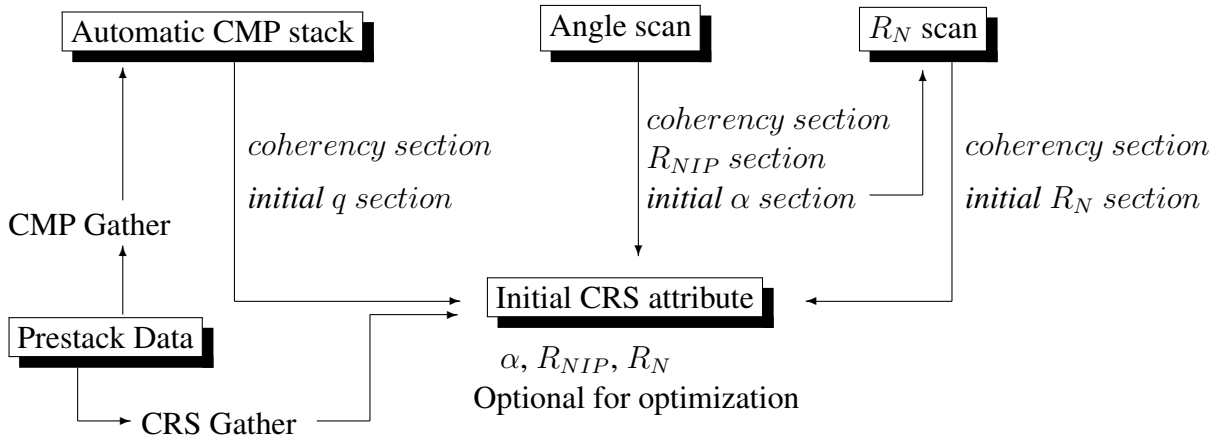

Figure 2.6: Flow chart for the pragmatic approach procedure for the CRS stack.

2.4.2 Simultaneous optimization

After the generation of the automatic CMP stack section, the CRS stack performs a parameter search using the zero-offset approximation and hyperbolic search of the CRS traveltime formula. The pragmatic approach procedure provides the CRS parameters α, R_N, R_{NIP} for every zero-offset (ZO) time sample in the target zone. These attributes are used as initial values in the final optimization process.

Current research implementation of the CRS stack used Nelder Mead optimization method. For a scalar objective function $f(x)$, where x is a vector with $N \geq 2$ components, optimization algorithm propagates a polyhedron with $N + 1$ vertices through the N-dimensional parameter space. Starting with a given initial polyhedron, the method only requires the values of the objective function f at the vertices x_i

and internally calculated new potential vertex locations. Derivatives of the objective function are not required.

In this thesis, a simple and robust local optimization is used, namely the conjugate direction approach using Powell method, compared to the Nelder Mead optimization procedure currently used as the optimization technique in the determination of CRS attributes. This method solved quadratic of N variables in N steps use iterative methods. An iterative method makes an initial guess at a solution to the system, and then tries to repeatedly improve the guess. Therefore three parameter CRS stack $\alpha, R_N,$ and R_{NIP} will be determined in three iterations. The method is based on the conjugate direction method with its well-known convergence properties and Powell search method for the control of the search direction. The algorithm is robust and easy to implement. The use of the conjugate direction method leads to a highly efficient iterative search method to speed up the convergence rate while using Hessian is avoided. The iterative Powell search method for the control of the search direction prevents the premature convergence into local minima, without the needed of computing the gradient. The simplified flowchart for the simultaneous optimization procedure is shown in Figure 2.7.

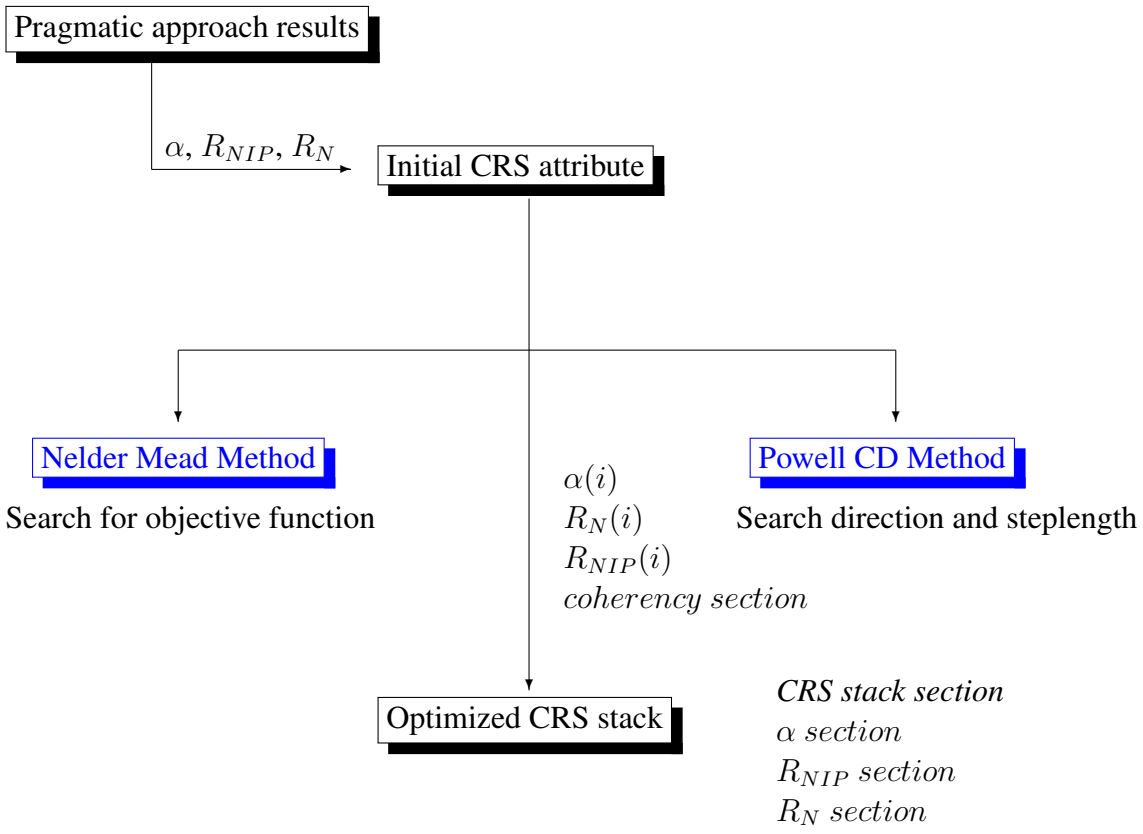

Figure 2.7: Flow chart for simultaneous optimization CRS stack procedure.

2.4.3 Global optimization

The main purpose of the optimization procedure is to find the best solution to minimize or maximize the function from all feasible solutions of the function. In many nonlinear optimization problems, the objective function has a large number of local minima and maxima, a point at which the objective function is smaller or larger than at all other feasible points in its vicinity (see Figure 2.8). Finding an arbitrary local optimum is relatively straightforward by using classical local optimization methods. Finding the global minimum or maximum of a function is far more difficult, where the largest or smallest value that the function takes at a point either within a given neighborhood (local or relative extremum) or on the function domain in its entirety (global or absolute extremum).

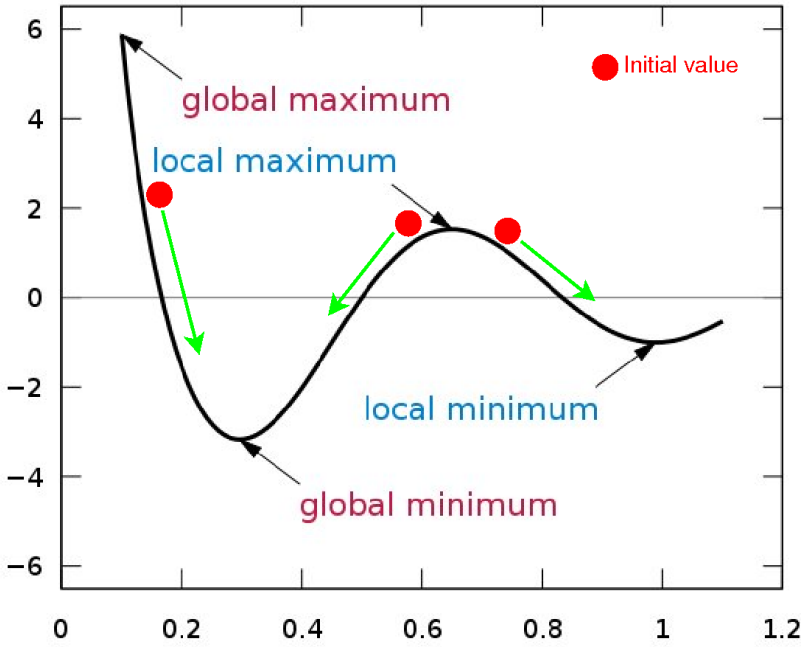

Figure 2.8: Local-global solution.

The objective of global optimization is to find the globally best solution of possibly nonlinear models, in the possible or known presence of multiple local optima. Formally, global optimization seeks global solutions of a constrained optimization model. Global optimization is the task of finding the absolutely best set of parameters to optimize an objective function. The task of global optimization is to find a solution in the solution set for which the objective function obtained its smallest value, the global minimum. Global optimization thus aims at determining not just "a local minimum" but "the smallest local minimum" with respect to the solution set. In general, the classical optimization techniques have difficulties in dealing with global optimization problems. One of the main reasons of their failure is that they can easily be entrapped in local minima.

Chapter 3

Optimization

Optimization is an important step in the analysis of physical problems to search for the optimal state. The goal is to find the best values of the variables that optimize the objective. To use it, we must first identify some objective, a quantitative measure of the performance of the system under study. This objective could be efficiency, time, accuracy, energy, or any certain quantity that can be represented by a single number. The objective depends on certain characteristics of the system, called variables or unknowns. Often the variables are restricted as can be constrained by a priori information. The process of identifying objective, variables, and constraints for a given problem is known as modeling. The construction of an appropriate model is the most important step in the optimization problem. If the model is too simplistic, it will not give useful insights into the practical problem, but if it is too complex, it may become too difficult to solve.

3.1 Optimization problem

Optimization theory or optimization problem is the study of the extremal values of a function: its minimum and maximum. Topic in this theory range from conditions for the existence of a unique extremal value to methods, analytic and numeric for finding the extremal values and for what values of the independent variables the function attains its extremes (Sun and xiang Yuan, 2006).

The simplest optimization problem is to find the minimum of a scalar-valued function of a scalar variable $f(x)$ the so-called objective function and where minimum is located. Assuming the function is differentiable, the well-known conditions for finding the minimum local and global are:

$$\frac{d}{dx}f(x) = 0, \tag{3.1}$$

$$\frac{d^2}{dx^2} f(x) > 0. \tag{3.2}$$

All values of the independent variable x satisfying these relations are locations of local minimum. Without the second condition, solution to the first could be either minimum, maximum or inflection points. Solution to the first equation are termed stationary points of the objective function. To find the global minimum where the function achieves its smallest value, each determined extremum must be tested, the objective function must be evaluated at each stationary point and the smallest selected.

The optimization problem can then be written as (Nocedal and Wright, 1999):

$$\underset{x \in \Re^n}{min} \qquad f(x), \tag{3.3}$$

x is the vector of variables, also called unknowns or parameters. f is the objective function, a function of x that we want to maximize or minimize.

The fastest optimization algorithms usually seek only a local minima (equation 3.4), a point at which the objective function is smaller than at all other feasible points in its vicinity (see Figure 2.8). They do not always find the best solution of all such minima, i. e., the global minimum (equation 3.5). Global solutions are highly desirable in some applications, but they are usually difficult to identify and even more difficult to locate (Weise, 2009). Optimization algorithms are iterative. They begin with an initial guess of the optimal values of the variables and generate a sequence of improved estimates until they reach a solution.

$$\hat{x_1} \in X, \;\; f : X \to \Re, \;\; f(\hat{x_1}) \leq f(x), \;\; \forall x \in X, \;\; \mid x - \hat{x_1} \mid < \varepsilon, \tag{3.4}$$

$$\check{x_1} \in X, \;\; f : X \to \Re, \;\; f(\check{x_1}) \leq f(x), \;\; \forall x \in X. \tag{3.5}$$

In this thesis, I present a new optimization method for simultaneous estimation of the CRS stack attributes, which allows to improve the image of pre-stack seismic reflection data. The method is based on a hybrid optimization, which comprises the conjugate direction method with its well-known convergence properties and an iterative considering the Powell search method for the control of the search direction. A specific feature of the Powell search method is its ability to avoid being trapped in local minima. The algorithm is robust and easy to implement. The use of the conjugate direction method leads to a highly efficient iterative search method to speed up the convergence rate while using Hessian is avoided. The iterative Powell search method for the control of the search direction prevents the premature convergence into local minima, without the need of computing the gradient.

3.2 Nelder Mead method

Before the Powell conjugate direction method is discussed I describe the Nelder Mead method which is currently use in the optimization. The Nelder Mead method or downhill simplex method or amoeba method is a commonly used nonlinear optimization technique. A simplex method for finding a local minimum of a function of several variables has been devised by (Nelder and Mead, 1965). It single-objective optimization approach for searching the N-dimensional space. The method uses the concept of a simplex, which is a special polytipe of N+1 vertices in N-dimensions using only function value information (Brent, 1973), where N is the number of variables that we are searching. For two variables, a simplex is a triangle, and the method is a pattern search that compares function values at the three vertices of a triangle. The worst vertex, where $f(x, y)$ is largest, is rejected and replaced with a new vertex. A new triangle is formed and the search is continued. The process generates a sequence of triangles which might have different shapes and the function value at the vertices get smaller and smaller. The goal is to replace the best vertex of the simplex with an even better one or ascertain that it is a candidate for the solution. The size of triangles is reduced and the coordinates of the minimum point are found.

The Nelder Mead algorithm starts with a simplex in a domain of the function to be minimized, then modifies the simplex five different ways until the simplex are very flat (function value is almost the same at all the vertices), at which point the minimum is the vertex with the smallest function value. Usually when the minimum is found the simplex is very small. The algorithm is stated using the term simplex (a generalized triangle in N dimension) and will find the minimum of function of N variables. It is effective and computationally compact. However, like hill climbing approaches, the downhill simplex may not converge to the global minimum and can get stuck at a local minimum. Random restarts, i. e., using different initial simplex can be helpful in this case (Lagarias et al., 1998).

3.2.1 Initial triangle BGW

Let $f(x, y)$ be the function that is to be minimized. To start, we are given three vertices of a triangle : $V_k = (x_k, y_k)$, $k = 1, 2, 3$. The function $f(x, y)$ is then evaluated at each of the three points : $z_k = f(x_k, y_k)$ for $k = 1, 2, 3$. The subscripts are then reordered so that $z_1 \leq z_2 \leq z_3$.
We use the notation :
$\vec{\mathbf{B}} = (x_1, y_1)$, $\vec{\mathbf{G}} = (x_2, y_2)$, $\vec{\mathbf{W}} = (x_3, y_3)$.

with $\vec{\mathbf{B}}$ is the best vertex, $\vec{\mathbf{G}}$ is good (next to best), and $\vec{\mathbf{W}}$ is worst vertex.

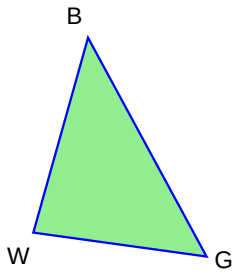

Figure 3.1: Initial triangle $\triangle$**BGW** for the Nelder Mead method.

3.2.2 Midpoint of the good side

The contruction process uses the midpoint of the line segment joining $\vec{\mathbf{B}}$ and $\vec{\mathbf{G}}$. It is found by averaging the coordinates and the midpoint gives us the search direction.

$$\vec{\mathbf{M}} = \frac{\vec{\mathbf{B}} + \vec{\mathbf{G}}}{2} = (\frac{x_1 + x_2}{2}, \frac{y_1 + y_2}{2}). \tag{3.6}$$

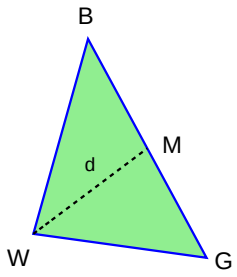

Figure 3.2: Midpoint the triangle.

3.2.3 Reflection using the point R

The function decreased as we move along the side of the triangle from $\vec{\mathbf{W}}$ to $\vec{\mathbf{B}}$, and it decreases as we move along side from $\vec{\mathbf{W}}$ to $\vec{\mathbf{G}}$. Hence it is feasible that $f(x, y)$ takes on smaller values at a point that lie away from $\vec{\mathbf{B}}$ on the opposite side of the line between $\vec{\mathbf{B}}$ and $\vec{\mathbf{G}}$. We choose a test point $\vec{\mathbf{R}}$ that is obtained by "reflecting" the triangle through the side $\overline{\mathbf{BG}}$. Then draw the line segment from $\vec{\mathbf{W}}$ to $\vec{\mathbf{M}}$ and call its length d. This last segment is extended a distance d through $\vec{\mathbf{M}}$ to locate the point $\vec{\mathbf{R}}$. The vector formula for $\vec{\mathbf{R}}$ is:

$$\vec{\mathbf{R}} = \vec{\mathbf{M}} + (\vec{\mathbf{M}} - \vec{\mathbf{W}}) = 2\vec{\mathbf{M}} - \vec{\mathbf{W}}. \tag{3.7}$$

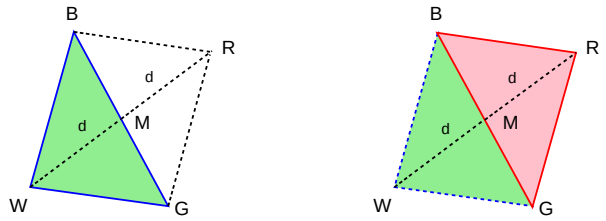

(a) (b)

Figure 3.3: The reflection point for the Nelder Mead method.

3.2.4 Expansion using the point E

If the function value at $\vec{\mathbf{R}}$ is smaller than the function value at $\vec{\mathbf{W}}$, then we have moved in the correct direction toward to the minimum. Perhaps the minimum is just a bit farther than the point $\vec{\mathbf{R}}$. So we extend the line segment through $\vec{\mathbf{M}}$ and $\vec{\mathbf{R}}$ to the point $\vec{\mathbf{E}}$. This forms an expanded triangle $\triangle\mathbf{BGE}$. The point $\vec{\mathbf{E}}$ is found by moving an additional distance d along the line joining $\vec{\mathbf{M}}$ and $\vec{\mathbf{R}}$. If the function value at $\vec{\mathbf{E}}$ is less than the function value at $\vec{\mathbf{R}}$, then we have found a better vertex than $\vec{\mathbf{R}}$. The vector formula for $\vec{\mathbf{E}}$ is:

$$\vec{\mathbf{E}} = \vec{\mathbf{R}} + (\vec{\mathbf{R}} - \vec{\mathbf{M}}) = 2\vec{\mathbf{R}} - \vec{\mathbf{M}}. \tag{3.8}$$

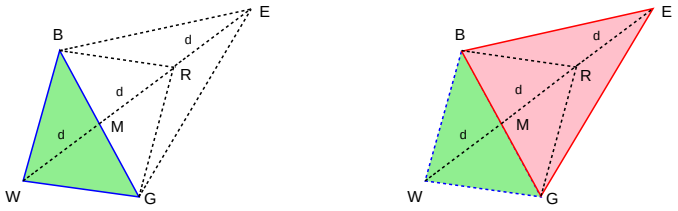

(a) (b)

Figure 3.4: The expansion point for the Nelder Mead method.

3.2.5 Contraction using the point C

If the function value at $\vec{\mathbf{R}}$ and $\vec{\mathbf{W}}$ are the same, another point must be tested. Perhaps the function is smaller at $\vec{\mathbf{M}}$, but we cannot replace $\vec{\mathbf{W}}$ with $\vec{\mathbf{M}}$ because we must have a triangle. Consider the two midpoints $\vec{\mathbf{C_1}}$ and $\vec{\mathbf{C_2}}$ of the line segments $\overline{\mathbf{WM}}$ and $\overline{\mathbf{MR}}$, respectively. The point with the smaller function value is called $\vec{\mathbf{C}}$, and the new triangle is $\triangle\mathbf{BGC}$.

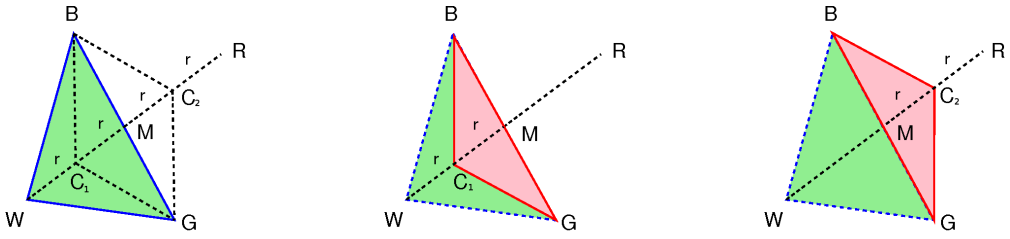

Figure 3.5: The contraction point C_1 and C_2 for the Nelder Mead method.

Note, the choice between C_1 and C_2 might seem inappropriate for the-two-dimensional case, but it is important in higher dimensions.

3.2.6 Shrink toward B

If the function value at $\vec{\mathbf{C}}$ is not less than the value at $\vec{\mathbf{W}}$, the point G and W must be shrunk toward $\vec{\mathbf{B}}$. Replace all vertices, except the best point, by the point halfway between each vertices and best point. The point $\vec{\mathbf{G}}$ is replaced with $\vec{\mathbf{M}}$, and $\vec{\mathbf{W}}$ is replaced with $\vec{\mathbf{S}}$, which is the midpoint of the line segment joining $\vec{\mathbf{B}}$ with $\vec{\mathbf{W}}$.

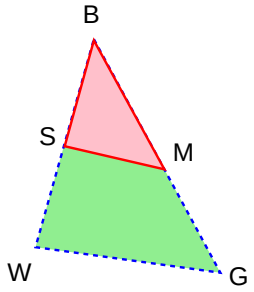

Figure 3.6: Shrinking the triangle toward B.

Nelder Mead algorithm

1. Order according to the value at the vertices:
   $f(x_1) \leq f(x_2) \leq \ldots\ldots \leq f(x_{n+1})$.
2. Calculate the midpoint x_M, the center of gravity off all points except x_{n+1}.
3. Reflection
   Compute reflected point $x_R = x_0 + \alpha(x_0 - x_{n+1})$.
   With α is the reflection coefficient. Standart values is $\alpha = 1$.
   If the reflected point is better than the second worst, but not better than the best:
   $f(x_1) \leq f(x_R) < f(x_n)$,
   the obtain a new simplex by replacing the worst point x_{n+1} with the reflected point x_R, and go to step 1.

4. Expansion
   If the reflected point is the best point so far, $f(x_R) < f(x_1)$,
   then compute the expanded point $x_E = x_0 + \gamma(x_0 - x_{n+1})$.
   With γ is the expansion coefficient and standart values is $\gamma = 2$.
   If the expanded point is better than the reflected point, $f(x_E) < f(x_R)$,
   then obtain a new simplex by replacing the worst point x_{n+1} with the expanded point x_E, and go to step 1. Else obtain a new simplex by replacing the worst point x_{n+1}, with the reflected point x_R, and go to step 1. Else (reflected point is worse than second worst) continue at step 5.

5. Contraction
   Here, it is certain that $f(x_R) \geq f(x_n)$.
   Compute contracted point $x_C = x_{n+1} + \rho(x_0 - x_{n+1})$
   With ρ is the contraction coefficient and standart values is $\rho = 1/2$.
   If the contracted point is better than the worst point, $f(x_C) \leq f(x_{n+1})$,
   then obtain a new simplex by replacing the worst point x_{n+1} with the contracted point x_C, and go to step 1. Else go to step 6.

6. Reduction
   For all but the best point, replace the point with
   $x_i = x_1 + \sigma(x_i - x_1)$ for all $i \in 2, ..., n + 1$.
   With σ is the shrink coefficient. Standart values is $\sigma = 1/2$. Then go to step 1.

The simplified logical decisions for the Nelder Mead algorithm procedure is shown in Figure 3.7.

IF $f(R) < f(G)$, THEN Perform Case (i) either reflect or extend
ELSE Perform Case (ii) either contract or shrink

BEGIN Case (i)	BEGIN Case (ii)
IF $f(B) < f(R)$ THEN	IF $f(R) < f(W)$ THEN
replace W with R	replace W with R
ELSE	Compute $C = (W + M)/2$
	or $C = (M + R)/2$ and $f(C)$
Compute E and $f(E)$	IF $f(C) < f(W)$, THEN
IF $f(E) < f(B)$, THEN	replace W with C
replace W with E	ELSE
ELSE	Compute S and $f(S)$
replace W with R	replace W with S
ENDIF	replace G with M
ENDIF	ENDIF
END Case(i)	END Case(ii)

Figure 3.7: Logical decisions for the Nelder Mead algorithm.

3.3 Conjugate direction method

Solving linear systems with direct methods are very difficult to adapt for distributed memory systems when the coefficient matrix is sparse. So most of the sparse linear system solvers for distributed memory system use iterative methods. An iterative method makes an initial guess at a solution to the system, and then tries to repeatedly improve the guess.

The conjugate direction method is a highly efficient iterative search technique because it allows to speed up the convergence rate of the steepest descent while using Hessian matrix evaluation is avoided (Stewart, 1973). This method solved quadratic of N variables in N steps. There are no Hessian matrix evaluation, also no inversion matrix and no storage of n x n matrix is required. The iterations converge quadratically, starting from any initial guess and then trying to repeatedly improve the values.

Each iteration computes a search direction d_i and then decides how far to move along that direction. The old value is replaced by the new one with a special choice of direction and step length. In every iteration a direction, d_i, and step length, α_i, are calculated to determine the next approximation of a new value in the line search method.

$$x_{k+1} = x_k + \alpha_k d_k. \tag{3.9}$$

The success of this search method depends on effective choices of both the direction d_i and step length α_i.

Iterative methods like the conjugate direction are suited for use with sparse matrices. Conjugate direction method is the most popular iterative method for solving large systems of linear equations. The conjugate direction is effective for systems of the form

$$Qx = b, \tag{3.10}$$

where Q is a known, square, symmetric positive definite matrix, x is an unknown vector, and b is a known vector. We are concerned with the problem of unconstrained optimization:

$$Q = [Q_{ij}] = \begin{pmatrix} Q_{11}Q_{12}...Q_{1n} \\ Q_{21}Q_{22}...Q_{2n} \\ . \quad . \quad . \\ Q_{n1}Q_{n2}...Q_{nn} \end{pmatrix}, \tag{3.11}$$

$$x = \begin{pmatrix} x_1 \\ x_2 \\ . \\ x_n \end{pmatrix}, \qquad b = \begin{pmatrix} b_1 \\ b_2 \\ . \\ b_n \end{pmatrix}. \tag{3.12}$$

A matrix Q is a symmetric positive definite matrix if for every nonzero vector x,

$$x^T Q x > 0, \tag{3.13}$$

and $Q^T = Q$, $Q_{ij} = Q_{ji}$ for i, j = 1,....,n.

A quadratic form is simply a scalar, quadratic function of a vector with the form

$$f(x) = \frac{1}{2} x^T Q x - b^T x. \tag{3.14}$$

If Q is symmetric positive definite, $f(x)$ is minimized by the solution to $Qx = b$. Conjugate direction definition: two vectors d_1 and d_2, are Q-orthogonal (or conjugate with respect to Q) if $d_1^T \, Q \, d_2 = 0$. The gradient of a quadratic form is defined to be

$$f^{'}(x) = \begin{pmatrix} \frac{\partial}{\partial x_1} f(x) \\ \frac{\partial}{\partial x_2} f(x) \\ \cdots \\ \frac{\partial}{\partial x_n} f(x) \end{pmatrix}. \tag{3.15}$$

One can minimize $f(x)$ by setting $f^{'}(x)$ equal to zero. And apply equation 3.14 to equation 3.15, and derive

$$f^{'}(x) := \frac{1}{2} Q^T x + \frac{1}{2} Q x - b. \tag{3.16}$$

If Q is symmetric, equation 3.16 reduces to

$$f^{'}(x) = Qx - b. \tag{3.17}$$

Then with the initialization $x_0 \in R^n, g_0 = \nabla f(x_0), d_0 = -g_0$, for any x_0 the sequence x_k generated by

$$x_{k+1} = x_k + \alpha_k d_k, \tag{3.18}$$

with

$$\alpha_k = -\frac{g_k^T d_k}{d_k^T Q d_k}, \tag{3.19}$$

$$d_{k+1} = -g_{k+1} + \beta_k d_k, \tag{3.20}$$

$$\beta_k = \frac{g_{k+1}^T Q d_k}{d_k^T Q d_k}. \tag{3.21}$$

3.3.1 Powell method

The essence of Powell's method is to add two steps to the process described in the preceding paragraph. The vector $P_n - P_0$ represents, in some sense, the average direction moved over the n intermediate steps $P_0, P_1, P_2, ..., P_n$ in an iteration. Thus the point x_1 is determined to be the point at which the minimum of the function f occurs along the vector $P_n - P_0$.

As before, f is a function of one variable along this vector and the minimization could be accomplished with an application of the iterative line search method. Finally, since the vector $P_n - P_0$ was such a good direction, it replaces one of the direction vectors for the next iteration. The iteration is then repeated using the new set of direction vectors to generate a sequence of points $\{x_k\}_{k=0}^{\infty}$. In one step of the iteration instead of a zig-zag path the iteration follows a "dog-leg" path. The process is outlined below.
Let x_0 be an initial guess at the location of the minimum of the function

$$z = f(x) = f(x_1, x_2, ..., x_n). \tag{3.22}$$

Powell conjugate direction algorithm

1. Initialiaties: set $x_0 = p_0$ and choose $d_1, d_2, ..., d_n$ linearly independent
2. FOR $1 \leq i \leq n$ DO
   Line search: find $\alpha_{LB} \leq \alpha_i \leq \alpha_{UB}$ minimizing $f(p_i + \alpha_i.d_i)$
   Define the new point: $p_{i+1} = p_i + \alpha_i.d_i$
3. Find an integer $1 \leq k \leq n$, so that $\delta = f(p_{k+1}) - f(p_k)$ is maximum
4. Compute: $f_3 = f(2p_n - p_0)$ and $f_1 = f(p_0)$, $f_2 = f(p_n)$
5. IF $f_3 < f_1$ AND $(f_1 - 2f_2 + f_3)(f_1 - f_2 - \delta)^2 < \frac{1}{2}\delta(f_1 - f_3)^2$ THEN
   Define the new direction : $d_k = p_n - p_0$
   Line search: find $\alpha_{LB} \leq \alpha_k \leq \alpha_{UB}$ minimizing $f(p_n + \alpha_k.d_k)$
   Define the new point: $x_{i+1} = x_i + \alpha_k.d_k$
   ELSE
   Keep all directions $d_1, d_2, ..., d_n$ for the next iteration and set $p_0 = p_n$
6. Repeat step 2 through 5 until convergence is achieved

If the conditions in step (5) are satisfied, then the set of direction vectors is left unchanged. The first inequality in step (5) indicates that there is no further decrease in the value of f in the average direction $P_n - P_0$. The second inequality indicates that the decrease in the function f in the direction of greatest decrease U_r was not a major part of the total decrease in f in step (2).

If the conditions in step (5) are not satisfied, then the direction of greatest decrease U_r is replaced with the average direction from step (2); $P_n - P_0$. The function is minimized in this direction. Stopping criteria are based on the magnitudes $\| x_i - x_{i-1} \|$ or $\| f(x_i) \|$.

3.3.2 Line search method

The line search, also called one-dimensional search, is a basic part of the optimization methods. This method refers to an optimization procedure for univariable functions. It is the base of multivariable optimization. As stated before, in multivariable optimization algorithms, for given x_k, the iterative scheme is:

$$x_{k+1} = x_k + \alpha_k d_k. \tag{3.23}$$

The key is to find the direction d_k and a suitable step length α_k:

$$h(\alpha) = f(x_k + \alpha d_k). \tag{3.24}$$

So, the problem that departs from x_k and finds a step length in the direction d_k such that:

$$h(\alpha) < h(0), \tag{3.25}$$

is just a line search about α.
If we find α_k such that the objective function in the direction d_k is minimized, i.e.,

$$f(x_k + \alpha_k d_k) =^{min}_{\alpha>0} \quad f(x_k + \alpha d_k), \tag{3.26}$$

$$h(\alpha_k) =^{min}_{\alpha>0} \quad h(\alpha), \tag{3.27}$$

such a line search is called exact line search, and α_k is called optimal step length. If we choose α_k such that the objective function has acceptable descent amount, i.e., such that the descent $f(x_k) - f(x_k + \alpha_k d_k) > 0$ is acceptable by users, such a line search is called inexact line search.

The basic idea of line search is determine the initial search interval which contains the minimizer. And then reduce the interval iteratively by evaluate the functions until the length of the interval is reduced to some desired degree. The minimizing a function over the interval is iteratively reducing the interval of uncertainty by comparing the function values of the observations. When the length of the interval of uncertainty is reduced less than some given tolerance, the points on the interval can be regarded as approximations of the minimizer.

The simplified flowchart for the Powell conjugate direction method algorithm procedure is shown in Figure 3.10.

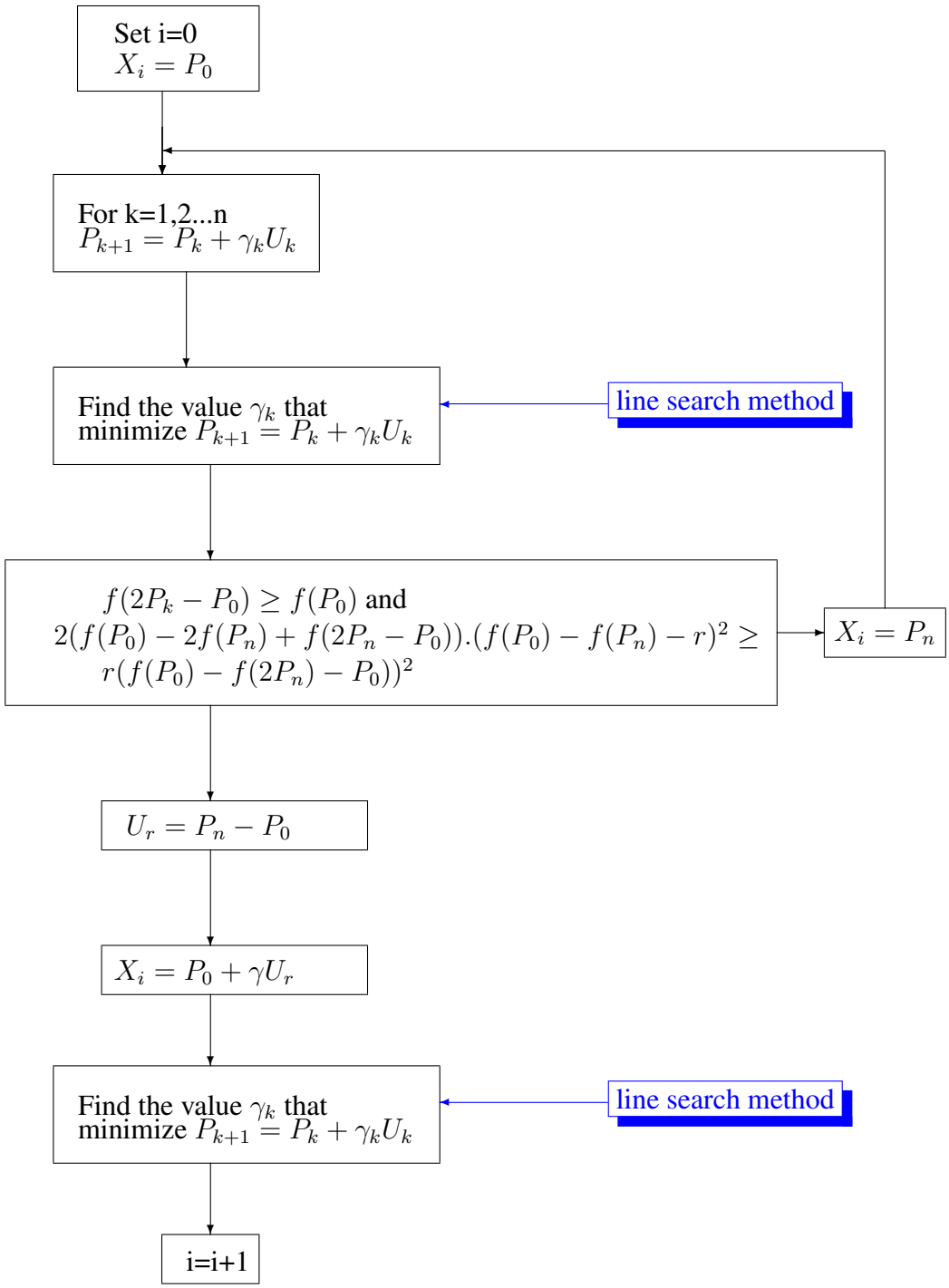

Figure 3.8: Powell conjugate direction method algorithm.

3.4 Numerical examples

We investigated the optimization procedure on an analytical example represents a simple mathematically function with 2 variables searches to see the behavior of two different optimization method with same initial values. To described the sensitivity of the initial values and the accuracy of the final solutions. For this purpose we consider the function $f(x_1, x_2) = x_1^2 + 2x_2^2 - 4x_1 - 2x_1x_2$ and $f(x_1, x_2) = x_1 - x_2 + 2x_1^2 + 2x_1x_2 + x_2^2$.

Figure 3.9 shows behavior of two different optimization method with same initial values for the first function: the Nelder Mead method with 10 iterations (a), 20 iterations (b), 27 iterations (c) and Powell conjugate direction method (d). And Figure 3.10 shows behavior of two different optimization method with same initial values for the second function: the Nelder Mead method with 10 iterations (a), 15 iterations (b), 23 iterations (c) and Powell conjugate direction method (d). Nelder Mead optimization method get final solutions better than Powell conjugate direction method when we use quite good initial values and more iterations.

To see the advantages this method to avoids being trapped into local minima, we test the optimization procedure on an analytical example represents a simple mathematically function with 2 variables and more than one local minima. And than compare it to the Nelder Mead optimization procedure currently used as the optimization technique in the determination of CRS attributes. We are particularly interested in its behavior in the presence of a local minima. For this purpose we consider the function $f(x_1, x_2) = \frac{1}{4}x_1 + 5x_1^2 + x_1^4 - 9x_1^2x_2 + 3x_2^2 + 2x_2^4$.

Figure 3.11 shows two different optimization methods with two different initial values. The Nelder Mead method (Figure 3.11(a)) and (Figure 3.11(c)) gets trapped into local minima for both initial values and also needs considerably more iterations. The Powell conjugate direction method (Figure 3.11(b)) and (Figure 3.11(d)) avoids the premature convergence and gets fairly close to the global minimum at (-2.1817, 1.6069).

Figure 3.12 shows how both optimization methods reached the solution. The first initial condition (Figure 3.12(a)) was chosen close to the first local minimum (2.1482, 1.5875) and the second initial condition (Figure 3.12(b)) was chosen close to the second local minimum (-0.0250, 0.0009). In the conjugate direction approach the number of iterations corresponds to the number of variables of the function to optimize, i.e., 2 for the analytical example above, 3 for the 2-D ZO CRS operator and accordingly for the 3-D and offset operators.

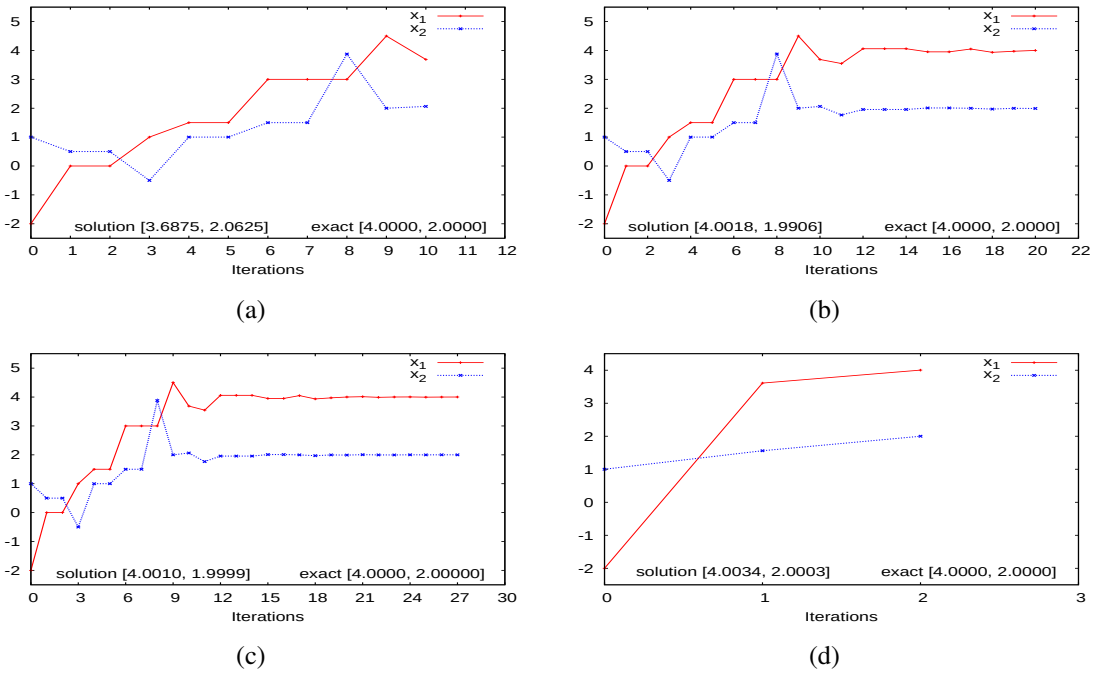

Figure 3.9: Behavior of two different optimization methods with same initial values for function-1: the Nelder Mead method with 10 iterations (a), 20 iterations (b), 27 iterations (c) and Powell conjugate direction method (d).

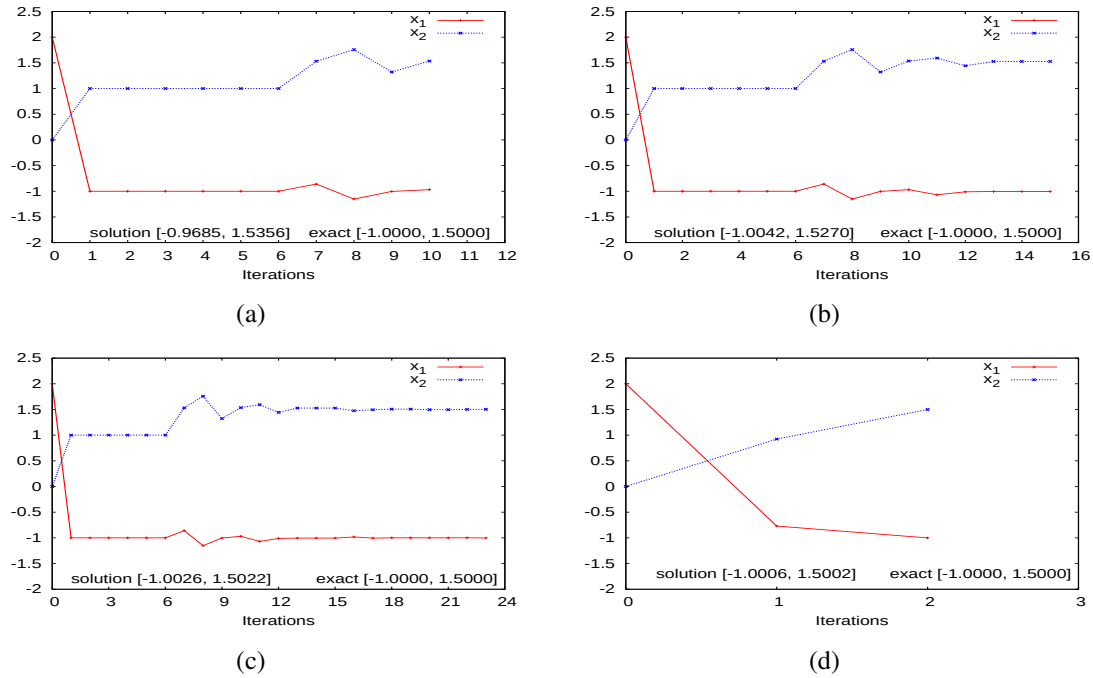

Figure 3.10: Behavior of two different optimization methods with same initial values for function-2: the Nelder Mead method with 10 iterations (a), 15 iterations (b), 23 iterations (c) and Powell conjugate direction method (d).

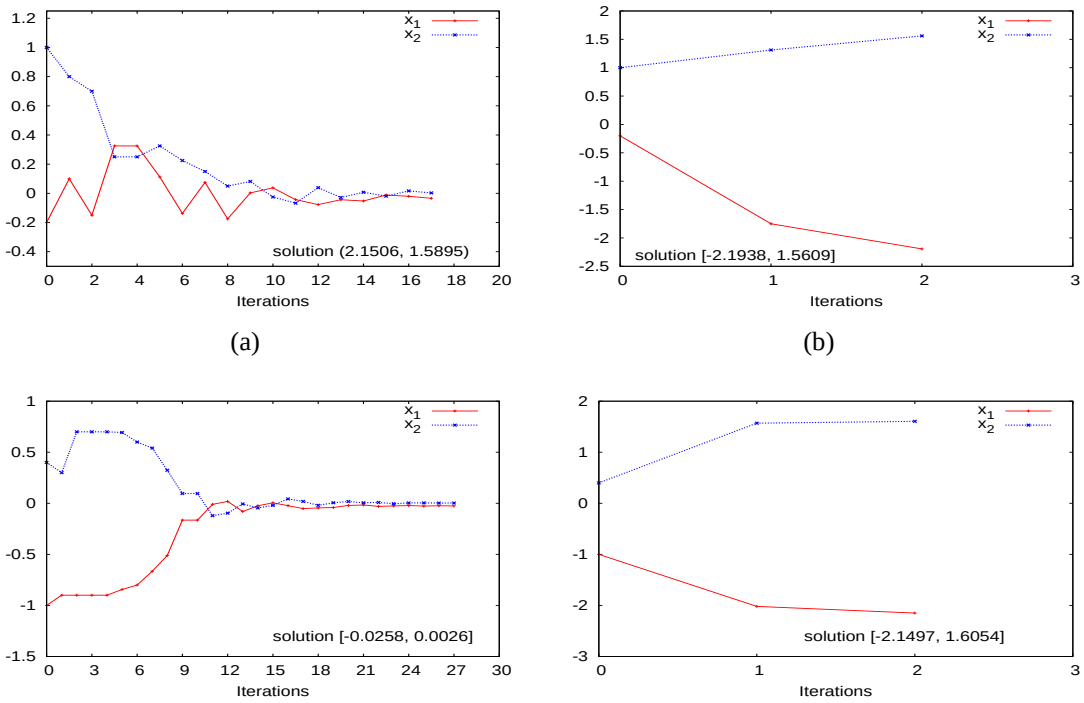

Figure 3.11: Two different optimization methods with two different initial values: the Nelder-Mead method (a) and (c) gets trapped in local minima. The Powell conjugate direction method (b) and (d) avoids the premature convergence into local minima and gets close to the global minimum at (-2.1817, 1.6069).

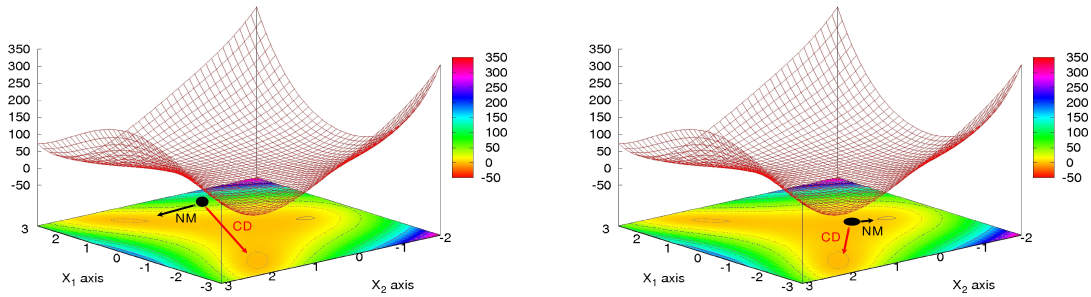

Figure 3.12: Path both method to reach the solution: the first initial condition was chosen close to the first local minimum (2.1482, 1.5875) (a) and the second initial condition were chosen close to the second local minimum (-0.0250, 0.0009) (b). The Nelder Mead method get trapped in local minima. The Powell conjugate direction method avoids the premature convergence into local minima and gets close to the global minima.

Chapter 4

Synthetic data example

This chapter shows the application of the pragmatic approach and the simultaneous optimization of the CRS stack method on the Sigsbee 2A synthetic data set. To demonstrate the advantages of the simultaneous optimization using the new method compared to the current implementation of the CRS stack are presented. The simultaneous optimization of CRS processing the data set started with the search of initial values for the CRS parameters. The automatic search for CRS parameters was applied to the preprocessed CMP gathers. I used the pragmatic approach based on the three one-parameter searches as described in (Müller, 1999), (Jäger et al., 2001) and (Mann, 2002). The initial values of the simultaneous optimization search were taken from the results of the pragmatic approach. The simulated ZO sections of the CRS stack result from the pragmatic approach are compared to the conventional CMP stack section and also the simultaneous optimization of the CRS stack used Nelder Mead method are compared to the new method.

4.1 Model and simulated pre-stack data

In order to test the simultaneous optimization of the CRS stack method and to show its advantages, I test the optimization procedure on the Sigsbee 2A synthetic data set. The Sigsbee 2A data set simulates a marine 2-D model that represents a situation observed, e.g., in the Gulf of Mexico: a stratified background model associated with a relatively smooth macro-velocity model contains a salt body with a quite complicated geometry. The Sigsbee 2A data set is a constant density acoustic synthetic data set designed in 2001 by the *Subsalt Multiples Attenuation and Reduction Technologies* (SMAART) JV consortium. All layers of the Sigsbee 2A model are assumed to be isotropic.

The sea surface was not considered as a free surface, therefore water column related multiples were not simulated. A number of normal and thrust faults and diffractor points are present in the data. Sources and receivers are located 7.62 m

below the sea surface, the measured quantity is pressure. The data set consist of 500 shot gathers with an average shot spacing of 45.72 m with 348 channels per shot and the receiver group spacing was 22.86 m. The line consisting of 2053 CMP gathers, where the CMP interval is 6.25 m and the maximum CMP fold is 87. The data are sampled every 8 ms with total recording time of 12 s, traveltimes range from 2 s to 11 s. All results obtained from these data refer to the datum given by the source and receiver locations. The CMP aperture is defined from 1829 m at 2.3 s to 7620 m at 11 s. The ZO aperture is defined from 518 m at 2 s to 1777 m at 11 s. Table 4.1 and Table 4.2 summarizes all relevant acquisition parameters of the pre-stack data set and the basic processing parameters used for the ZO simulation of CRS stack, respectively.

Context	Processing parameter	Setting
Shot and receiver geometry	Number of shot	500
	Shot interval	45.72 m
	Number of receivers	348
	Receiver interval	22.86 m
Recording parameters	Recording time	12 s
	Sampling interval	8 ms
Midpoint and offset geometry	Number of CMP bins	2053
	Maximum CMP fold	87
	CMP bin interval	11.43 m
	Offset range	0...7932.42 m
Frequency content	Dominant frequency	20 Hz
	Maximum frequency	40 Hz

Table 4.1: Sigsbee 2A data: acquisition parameters of the pre-stack data set.

4.2 Application of CRS stack

4.2.1 Pragmatic approach

The input data is confined to specific data volumes to split the three-parameter optimization problem into separate one-parameter searches. The first data volume to be investigated is the CMP gather ($\triangle x = 0$) following the pragmatic approach (Müller, 1998) using equation 2.8. To determine initial values of the emergence angle α, we consider the ZO section simulated in the preceding step with $h = 0$ using equation 2.13. With the knowledge of α, the ZO data can now be considered using equation 2.14. This yields initial attributes which can be used as first guess in the simultaneous optimization of the CRS procedure.

Context	Processing parameter	Setting
General parameters	Dominant frequency	20 Hz
	Coherence measure	Semblance
	Data used for coherence analysis	Original traces
	Temporal width of coherence band	56 ms
Velocity and constraints	Near surface velocity	1500 m/s
	Tested stacking velocity	1300...6000 m/s
Target zone	Simulated ZO traveltimes	2...11 s
	Simulated temporal sampling interval	8 ms
	Number of simulated ZO traces	2053
	Spacing of simulated ZO traces	11.43 m
Aperture and taper	Minimum ZO aperture	518 m @ 2 s
	Maximum ZO aperture	1777 m @ 11 s
	Minimum CMP aperture	1829 m @ 2.3 s
	Maximum CMP aperture	7620 m @ 11 s
	Relative taper size	30 %
Automatic CMP stack	Initial moveout increament for largest offset	16 ms
	Number of refinement iterations	3
Linear ZO stack	Tested emergence angles	-60...60°
	Initial emergence angles increment	1°
	Number of refinement iterations	3
Hyperbolic ZO stack	Initial moveout increment for largest ZO distance	8 ms
	Number of refinement iterations	3
Conflicting dip handling	Maximum number of dips	1
	Absolute coherence threshold for global maximum	0.5
	Relative coherence threshold for local maximum	0.25
Local optimization	Coherence threshold for smallest traveltime	0.05
	Coherence threshold for largest traveltime	0.02
	Maximum number of iterations	100
	Maximum relative deviation to stop	10^{-4}
	Initial variation of emergence angles	6°
	Initial variation of R_{NIP}	5 %
	Initial variation of transformed R_N	6°
	Transformation radius for R_N	106 m

Table 4.2: Sigsbee 2A data: processing parameters used for the ZO simulation by means of the CRS stack.

The ZO CMP stacked section is depicted in Figure 4.1, the associated coherence section in Figure 4.2. The ZO CMP stacked section presented in Figure 4.1 displays a lower quality in the areas of fault structures and steep dipping layers. The bow-tie structures and diffraction pattern stemming from the top of salt are clearly visible.

The coherence section presented in Figure 4.2 helps to identify the detected events and to estimate where the given aperture is appropriate to fit a hyperbolic operator: the events above and left to the salt are associated with high coherence values, as well as the complicated events stemming from the top of salt. With increasing complexity of the overburden, the coherence reduces, indicating the non-hyperbolic moveout of the events.

Finally, conflicting dip situations are not yet resolved in the ZO CMP stacked section. In these case, the event asssociated with the higer coherence is selected, whereas the other event is not considered.

The CRS stacked section obtained with the initial attributes from the result of the pragmatic approach is depicted in Figure 4.3. Compared to the conventional ZO CMP stack (Figure 4.1), the pragmatic approach CRS stacked section presented in Figure 4.3 shows better continuity of horizons at all time levels and produced a better image in reflections and diffractions. The reflections are more continuous and appear clearer.

The coherence section for the pragmatic approach CRS stack depicted in Figure 4.4 displays the reflection events clearly defined correspond with high coherence values and associated with the reflector. Most reflections better defined compared to the coherence section of the CMP stack shown in Figure 4.2.

The CPU times strongly depend on the used hardware, but in general, not differences in computational time was observed for the simultaneous search of the parameters in the 2-D CRS stack on the Sigsbee 2A data using the Powell conjugate direction approach and the Nelder Mead method currently used in the CRS attribute search (Table 4.3).

Processing step	NM method	Powell CD method
Automatic CMP stack	00:08:29	00:08:29
Zero-offset stacks	01:54:43	01:54:43
Initial stack	00:57:21	00:57:21
Optimized	18:42:10	17:52:50
Total	21:42:43	20:53:23

Table 4.3: Sigsbee 2A data: CPU times required for processing steps.

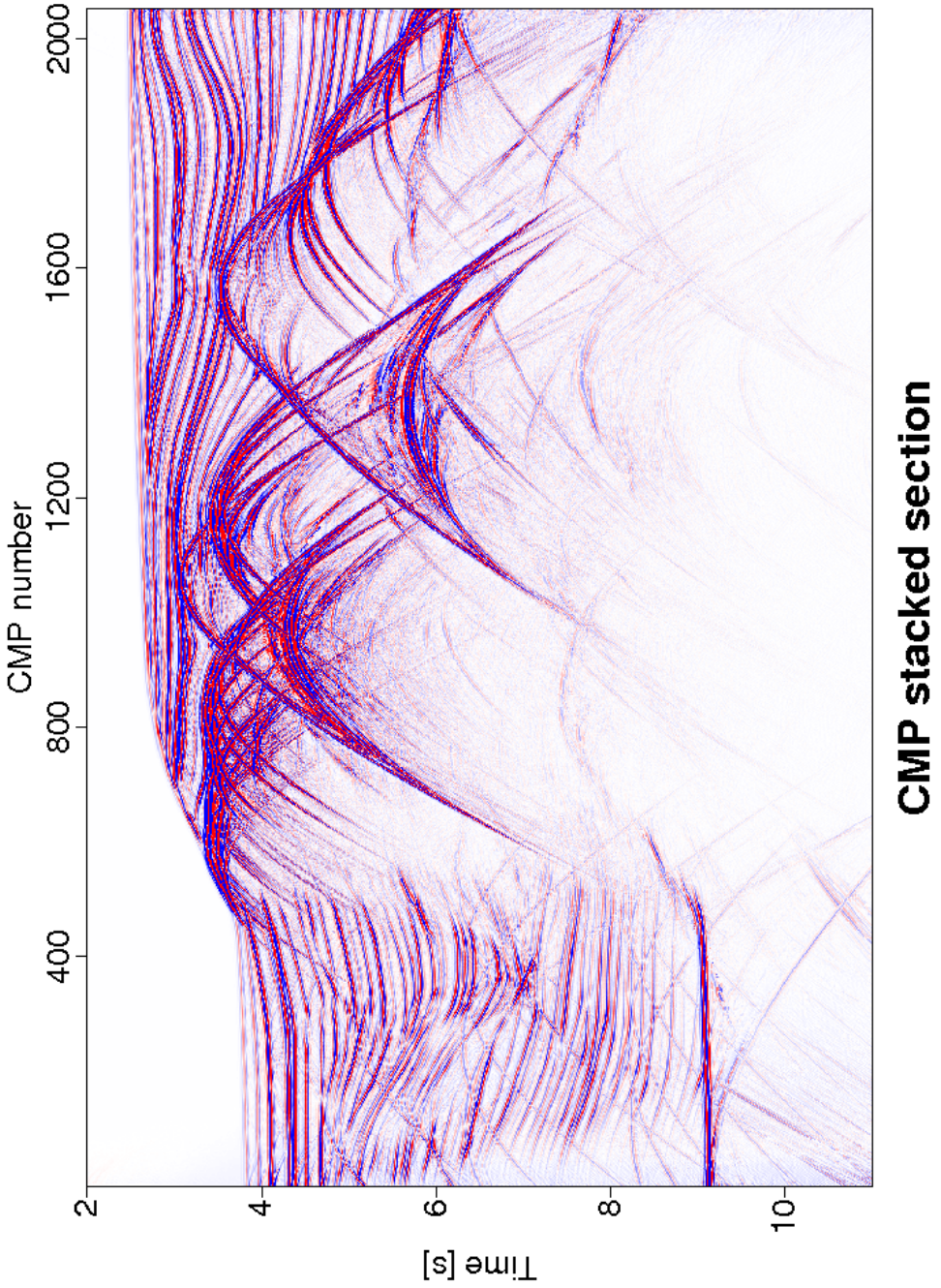

Figure 4.1: Sigsbee 2A data: result of CMP stack.

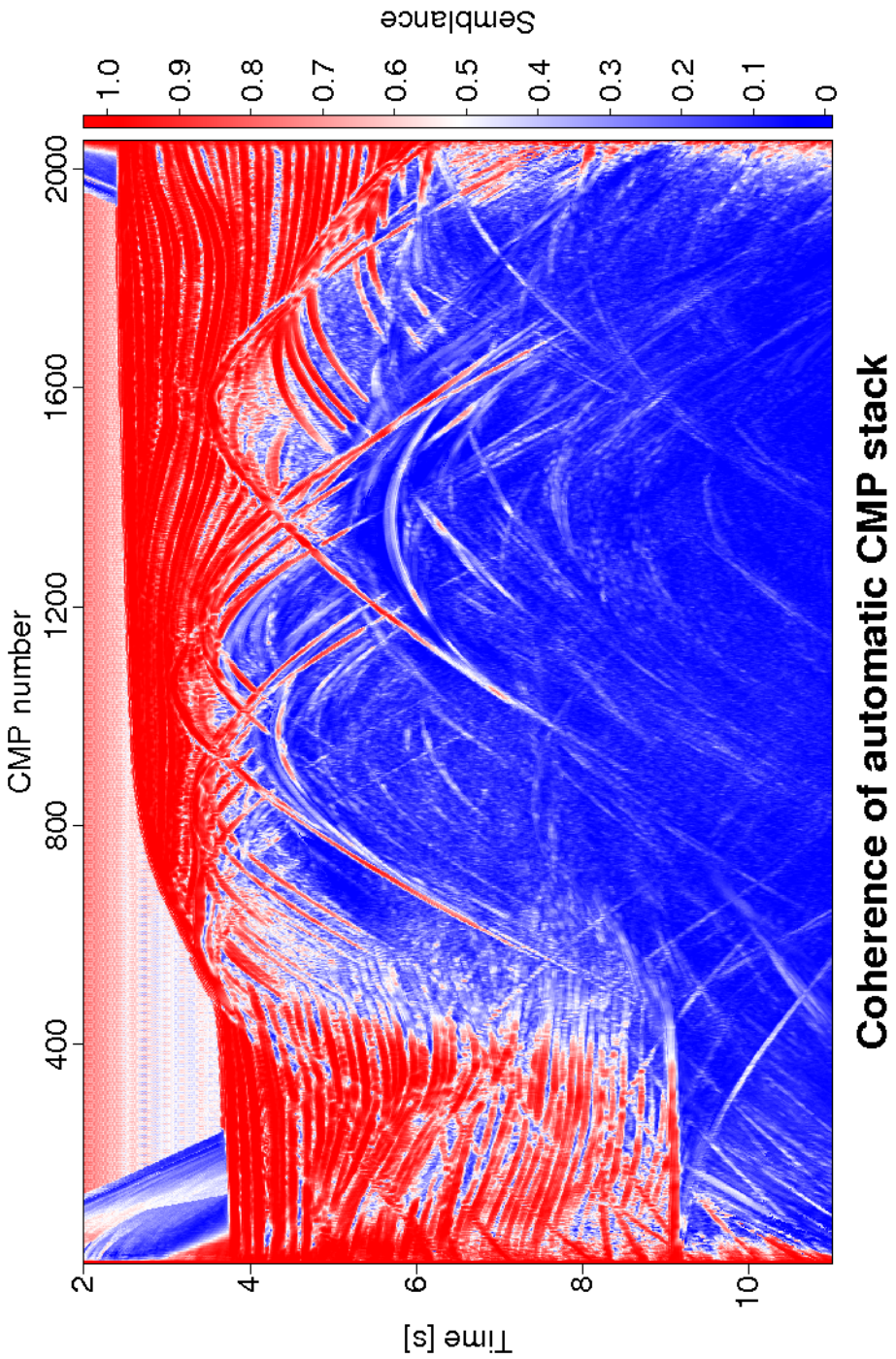

Figure 4.2: Sigsbee 2A data: coherence section associated with the CMP stacked section shown in Figure 4.1.

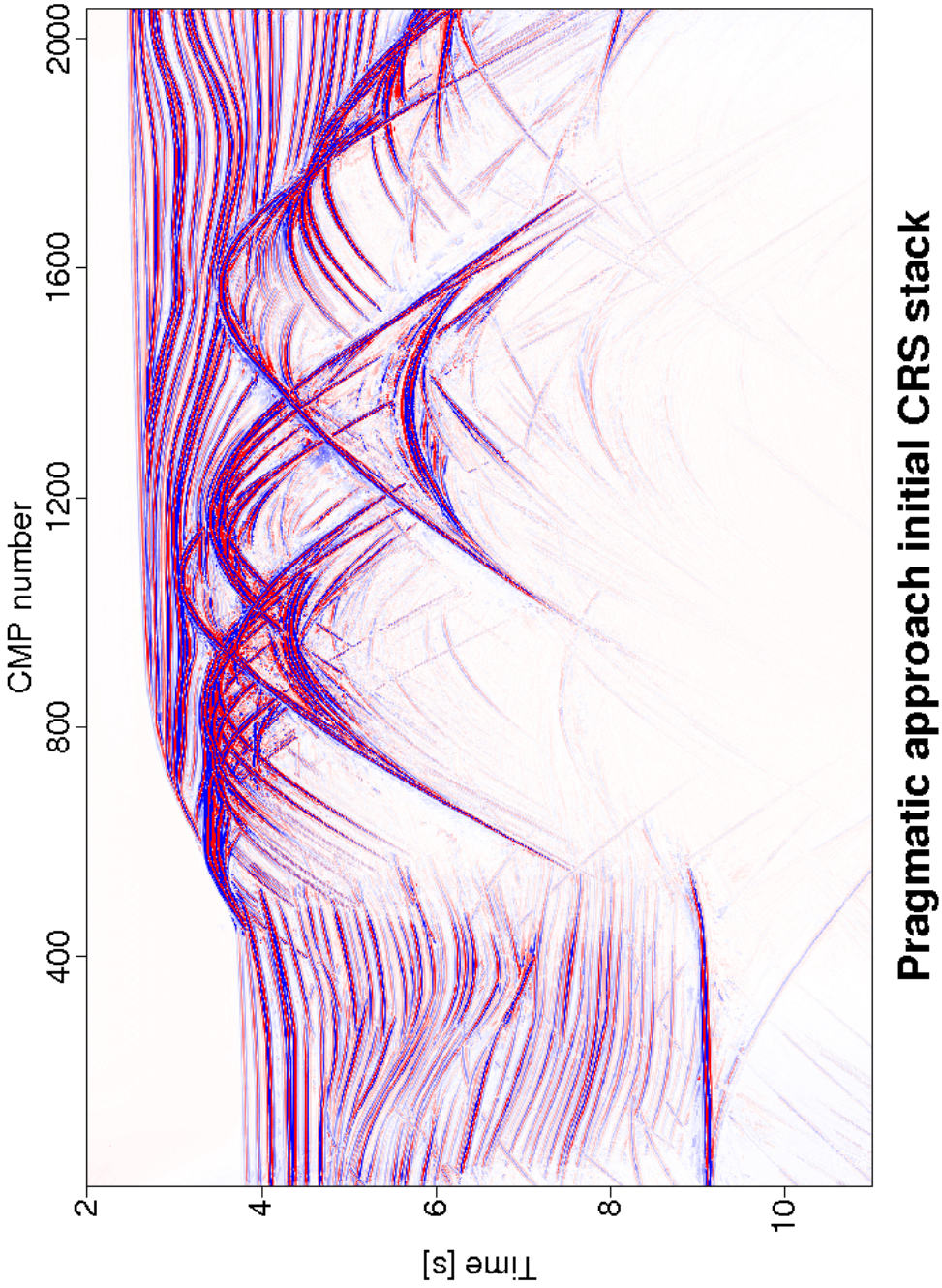

Figure 4.3: Sigsbee 2A data: result of the pragmatic approach CRS stack.

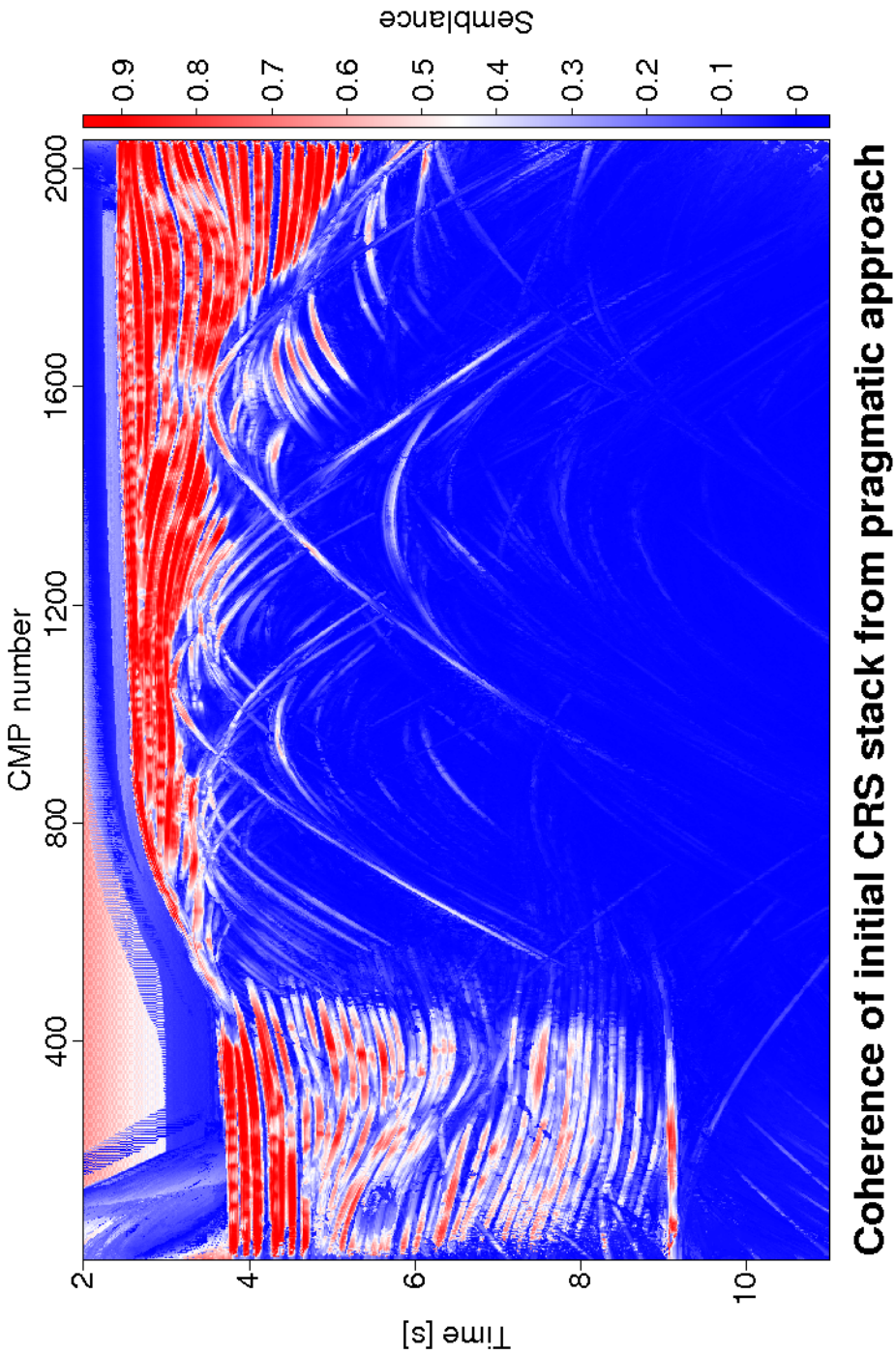

Figure 4.4: Sigsbee 2A data: coherence section associated with the pragmatic approach CRS stacked section shown in Figure 4.3

4.2.2 Simultaneous optimization of the CRS stack

Figure 4.5 to 4.16 display the resulting simultaneous optimized CRS stacked section. The CRS stacked section obtained with the initial attributes from the result of pragmatic approach in Figure 4.3 already has a sufficiently high quality. Optimization of the spatial CRS stacking operator with all three wavefield attributes can be further increasing the accuracy of the wavefield attributes. However, the optimization procedure is very time consuming.

For Sigsbee 2A synthetic data set, the initial wavefield attributes determined with pragmatic approach shown in Figure 4.3. We use the zero-offset CMP stacked section result as an input for the determination of the wavefield attributes. Associated with the near-surface velocity v_0, the wavefield attributes α, angle of emergence is directly related to the slopes. And the wavefiled R_N, radius of curvature of the normal wave is directly related to the curvatures of the events in the ZO section. Firstly, the slopes of the events are determined by means of a linear stacking operator within a relatively small aperture. Secondly, the curvatures of the events are determined with a hyperbolic operator separately for each detected slope. The coherence thresholds are applied again to reject events with too small lateral extension that are most likely artifacts. The wavefield R_{NIP}, radius of curvature of the NIP wave is calculated from the angle of emergence section of the dominant events and the stacking velocity section obtained from the automatic CMP stack.

We choose the pragmatic approach to define the initial wavefield attributes, since the initial wavefield attributes are very crucial in the optimization procedure. The optimization CRS stack result depends the choice of the initial wavefield attributes. If we choose wrong parameters for the initial wavefield attributes, e.g., near the local solutions, it will definitely lead to a wrong result.

Nelder Mead optimization method

The CRS stacked section obtained with the Nelder Mead optimized method is displayed in Figure 4.5. It shows better continuity of horizons at all time levels and produced a better image of conflicting dip areas. Compared to the CMP stacked section (Figure 4.1) and the pragmatic approach CRS stacked section (Figure 4.3), the CRS stacked section increase the lateral resolution in the areas with significant variation of the event curvature. The reflections are more continuous and appear clearer.

The coherence section for the dominant events associated with the Nelder Mead optimized CRS stack is shown in Figure 4.6. The events associated with the highest coherence at each particular ZO location allow to identify the detected events and

to estimate the reliability of the image as well of its associated wavefield attributes. The high coherence values are associated with the top salt and the events left to the salt.

The optimized emergence angle sections for the dominant events are shown in Figure 4.7. The improvement of the emergence angle section can readily be observed, due to the simple relation between the emergence angle and the slopes of the ZO events.

The optimized radius of curvature of the normal wave section for the dominant events are depicted in Figure 4.8. The same condition as above applies to this section.

And the optimized radius of curvature of the NIP wave for the dominant events are shown in Figure 4.9. For the stratified areas above and left to the salt, the values of R_{NIP} continously increases with increasing traveltime. Below the salt, the section is dominated by the tails of bow-tie structures and diffraction patterns stemming from the top and possibly also the botttom of the salt body.

The improvement of the coherence section can readily be observed at the coherence section associated with the Nelder Mead optimized section. The differences coherence between the pragmatic approach initial CRS stacked (Figure 4.4) and the Nelder Mead optimized CRS stack (Figure 4.6) is shown in Figure 4.10.

Powell conjugate direction optimization method

The CRS stacked section obtained with the Powell conjugate direction optimized method is displayed in Figure 4.11. It shows better continuity of horizons at all time levels and produced a better image of conflicting dip areas. We do not see specific differences in the stack or attribute sections for the Powell conjugate direction or the Nelder Mead approach. No differences in computational time was observed for the simultaneous search of the parameters in the 2-D CRS stack on the Sigsbee 2A data using the Powell conjugate direction approach and the Nelder Mead method currently used in the CRS attribute search. For multi-parameter stacking approaches with more than 3 attributes (offset formulas, converted waves, 3-D) its possible of computing time can be reduced.

The coherence section for the dominant events associated with the Powell conjugate direction optimized CRS stack is shown in Figure 4.12. The coherence section of the Powell conjugate direction method displays a little bit more scatter than the coherence section of the Nelder Mead method (Figure 4.6), but both sections are very similar and it does not appear that the difference in coherence has a major effect on the attributes. The events associated with the highest coherence at each particular ZO location, allows to identify the detected events and to estimate the reliability of the image as well of its associated wavefield attributes.

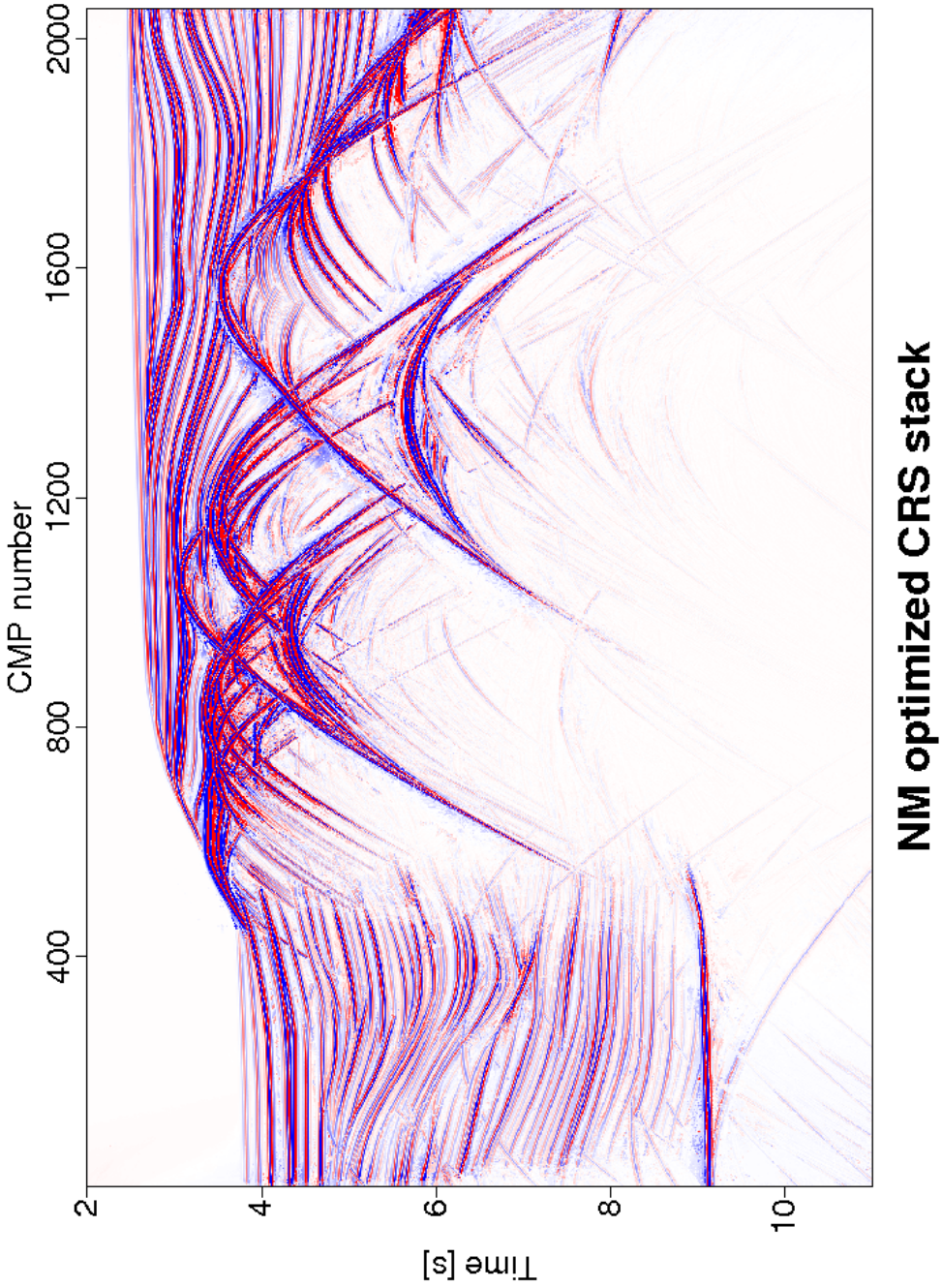

Figure 4.5: Sigsbee 2A data: CRS stack result of the Nelder Mead optimization.

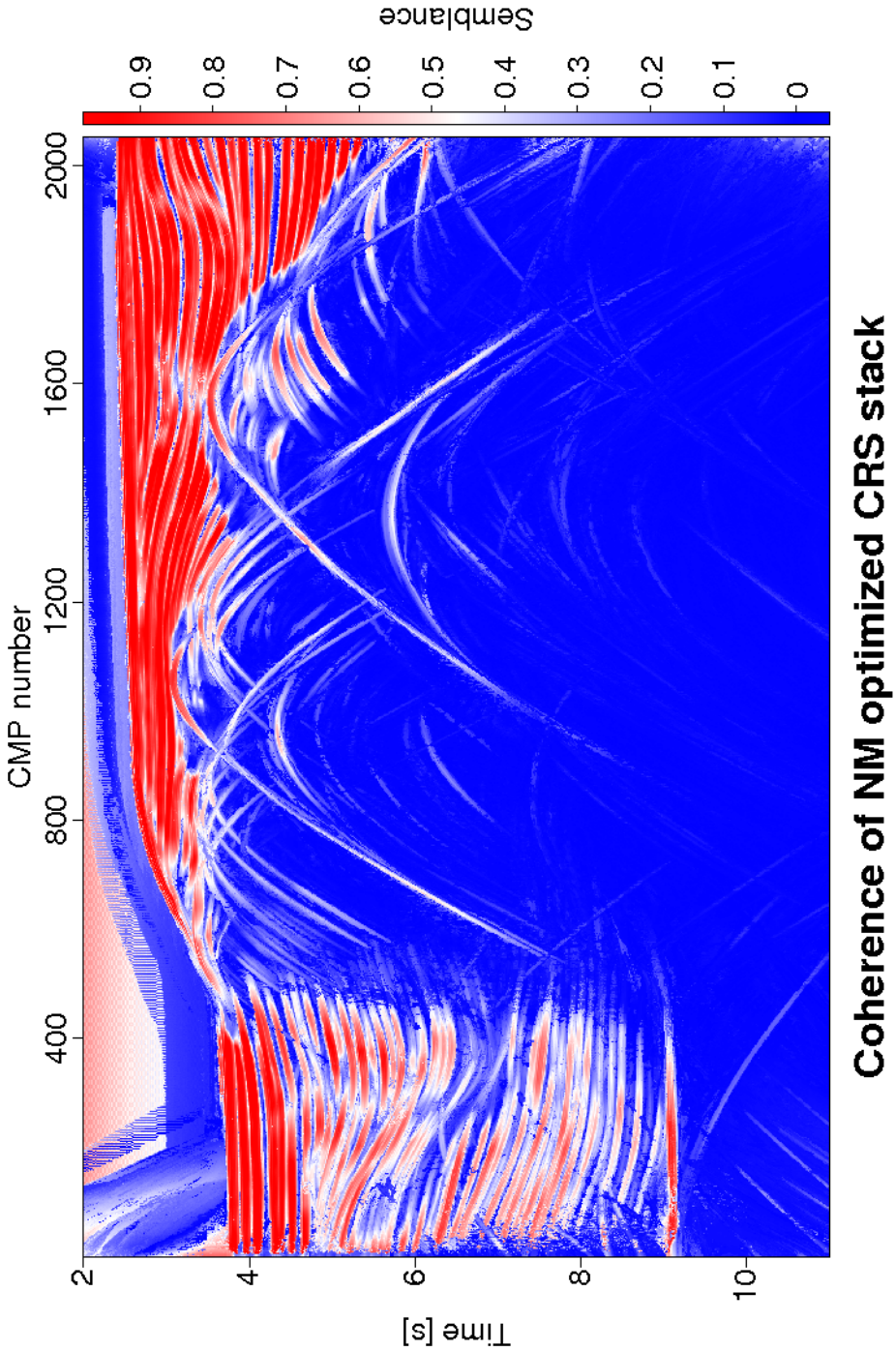

Figure 4.6: Sigsbee 2A data: coherence section associated with the Nelder Mead optimized CRS stacked section shown in Figure 4.5 smoother than coherence section of the pragmatic approach shown in Figure 4.4.

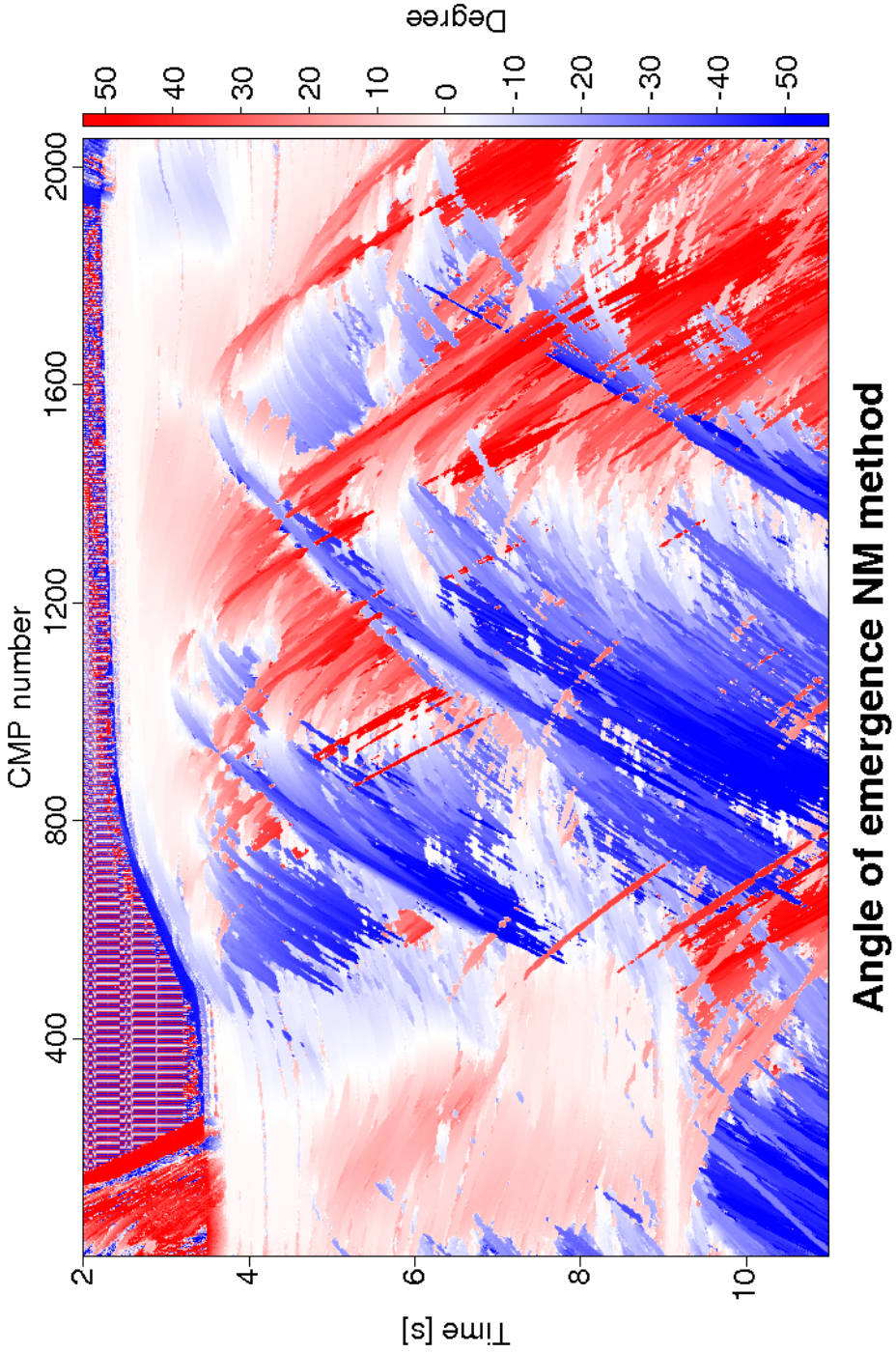

Figure 4.7: Sigsbee 2A data: angle of emergence associated with the Nelder Mead optimized CRS stacked section shown in Figure 4.5. These attributes are directly related to the slopes of the events.

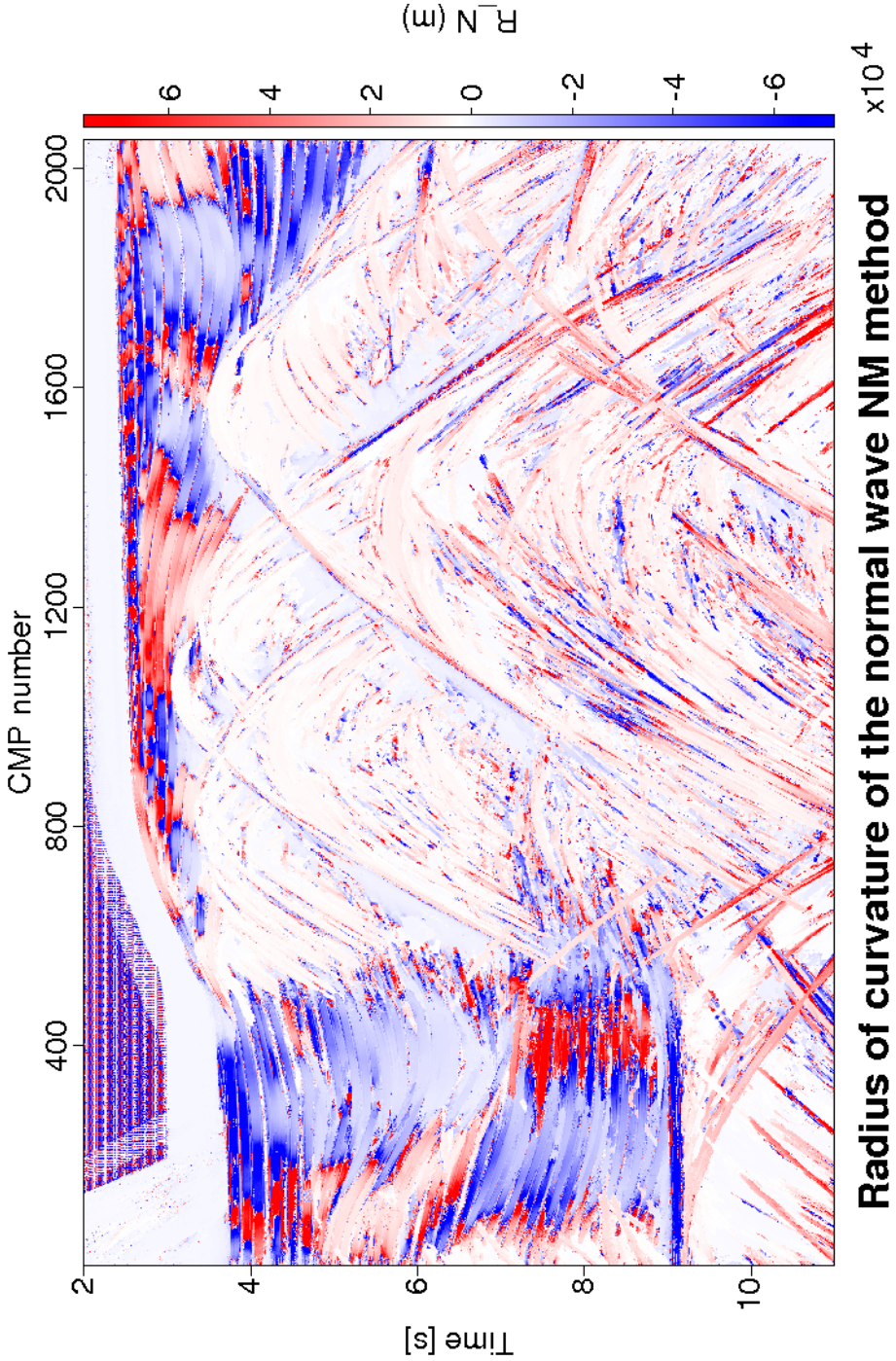

Figure 4.8: Sigsbee 2A data: radius of curvature of the normal wave associated with the Nelder Mead optimized CRS stacked section shown in Figure 4.5. These attributes are directly related to the curvatures of the events in the ZO section.

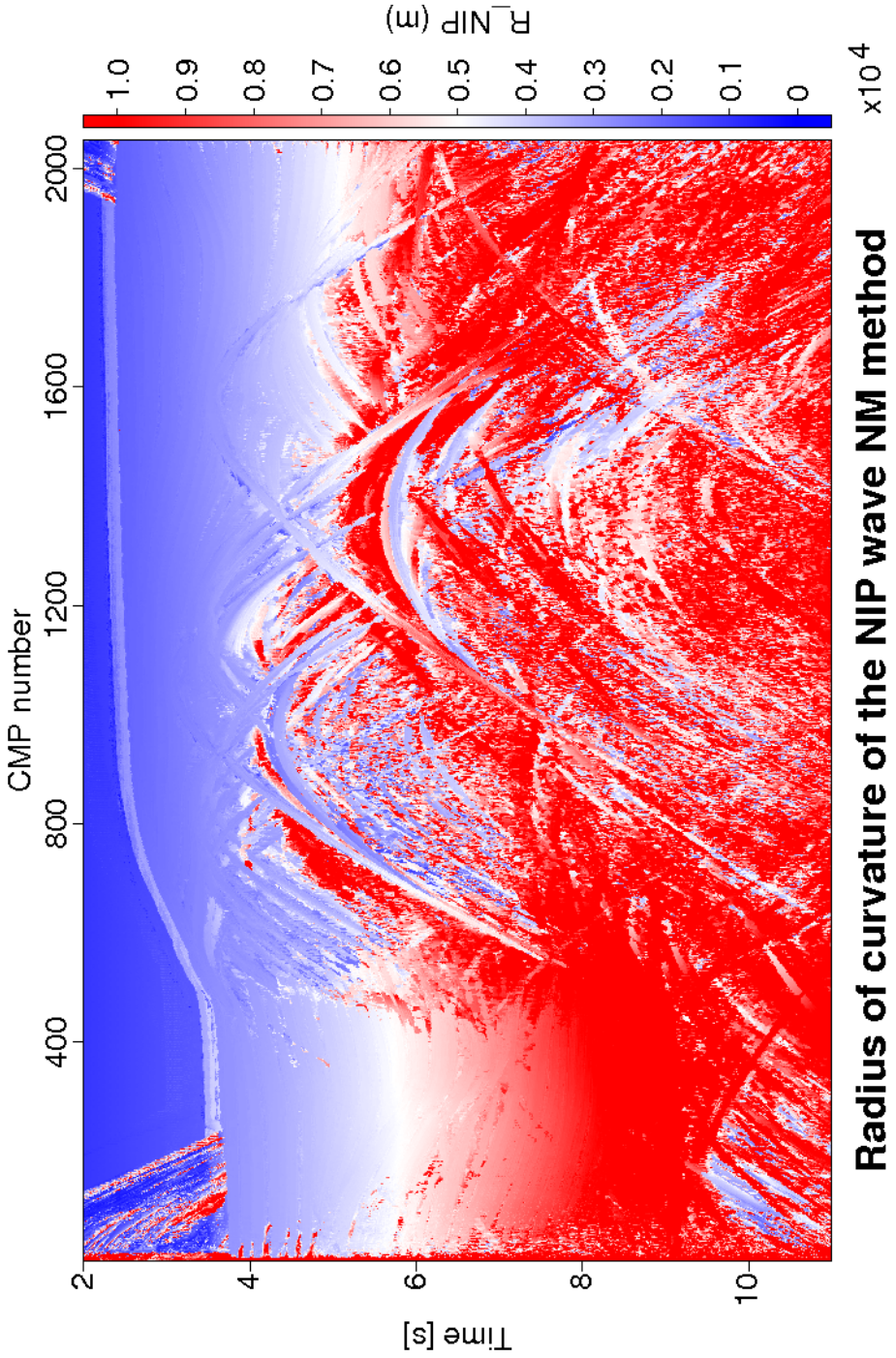

Figure 4.9: Sigsbee 2A data: radius of curvature of the NIP wave associated with the Nelder Mead optimized CRS stacked section shown in Figure 4.5. These section is calculated from the emergence angle section of the dominant events in Figure 4.6 and the stacking velocity section obtained from automatic CMP stack.

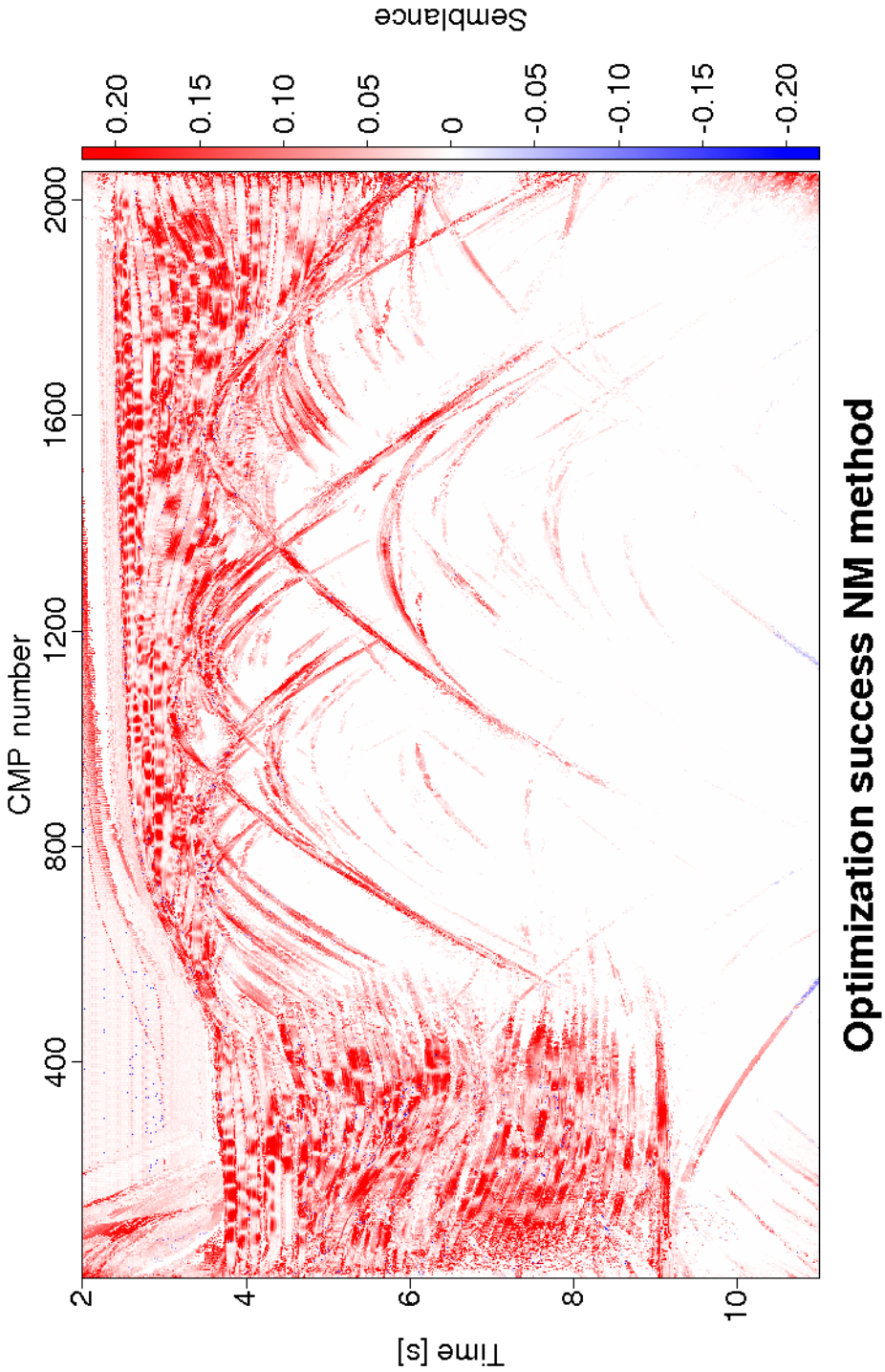

Figure 4.10: Sigsbee 2A data: difference in coherence between the pragmatic approach CRS stacked section (Figure 4.4) and the Nelder Mead optimized CRS stacked section (Figure 4.6).

The optimized emergence angle sections for the dominant events are shown in Figure 4.13. This image look similar to the optimized emergence angle section of the Nelder Mead method (Figure 4.7) and no specific differences can be observed. The consistency of the optimized emergence angle section can readily be observed, due to the simple relation between the emergence angle and the slopes of the ZO events.

The optimized radius of curvature of the normal wave section for the dominant events are depicted in Figure 4.14. This section looks similar to the Nelder Mead method (Figure 4.8) and no specific differences can be observed. The same applies to the section that is related to the curvature of the ZO events.

The optimized radius of curvature of the NIP wave for the dominant events are shown in Figure 4.15. For the stratified areas above and left to the salt, the values of R_{NIP} continously increases with increasing traveltime. Below the salt, the section is dominated by the tails of bow-tie structures and diffraction patterns stemming from the top and possibly also the botttom of the salt body.

The difference in coherence between the pragmatic approach initial CRS stacked (Figure 4.4) and the Powell conjugate direction optimized CRS stack (Figure 4.12) is shown in Figure 4.16. The minor improvement of the coherence section can readily be observed at the coherence section associated with the Powell conjugate direction optimized section compared to the Nelder Mead optimized section.

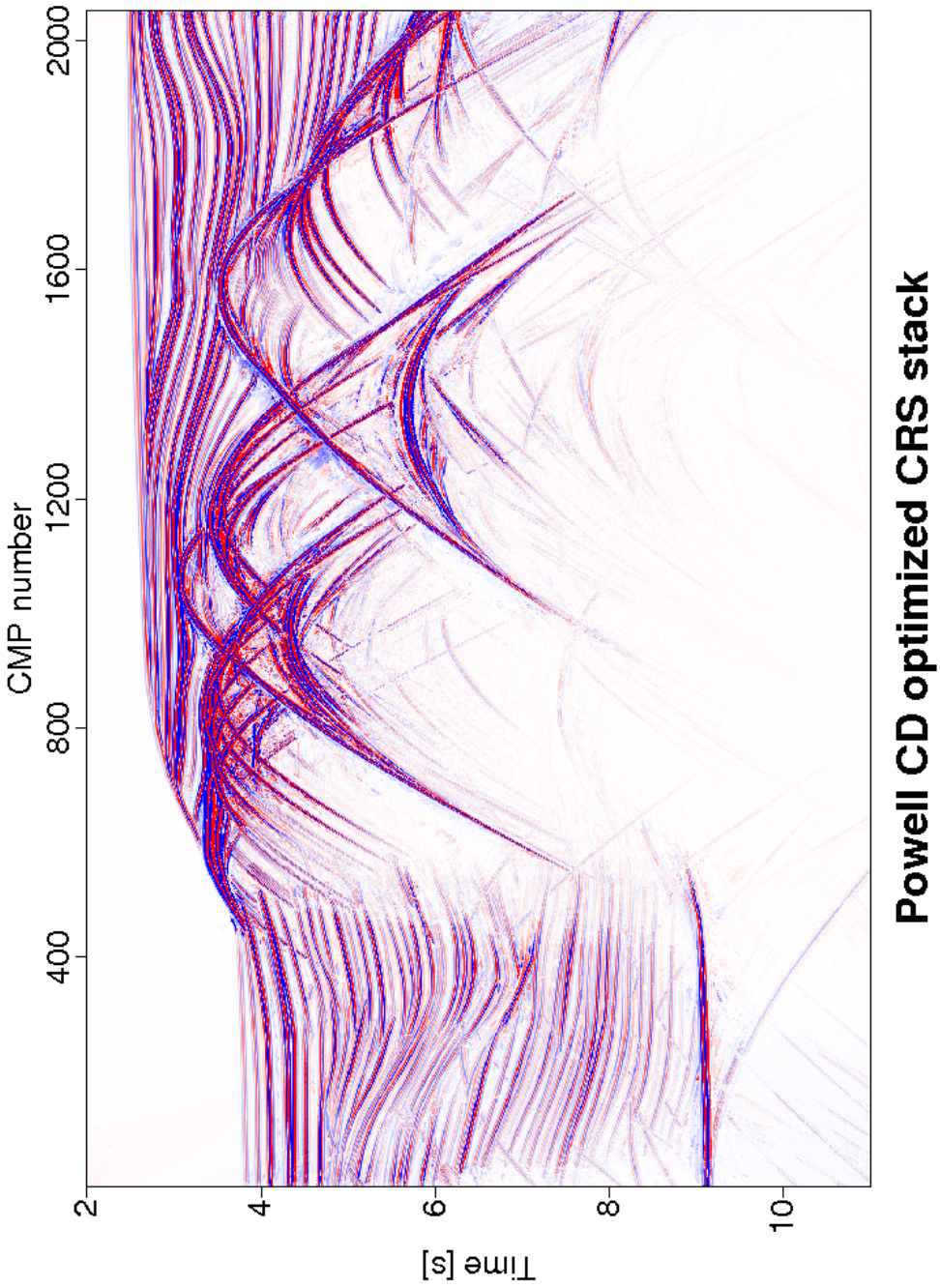

Figure 4.11: Sigsbee 2A data: CRS stack result of the Powell CD optimization.

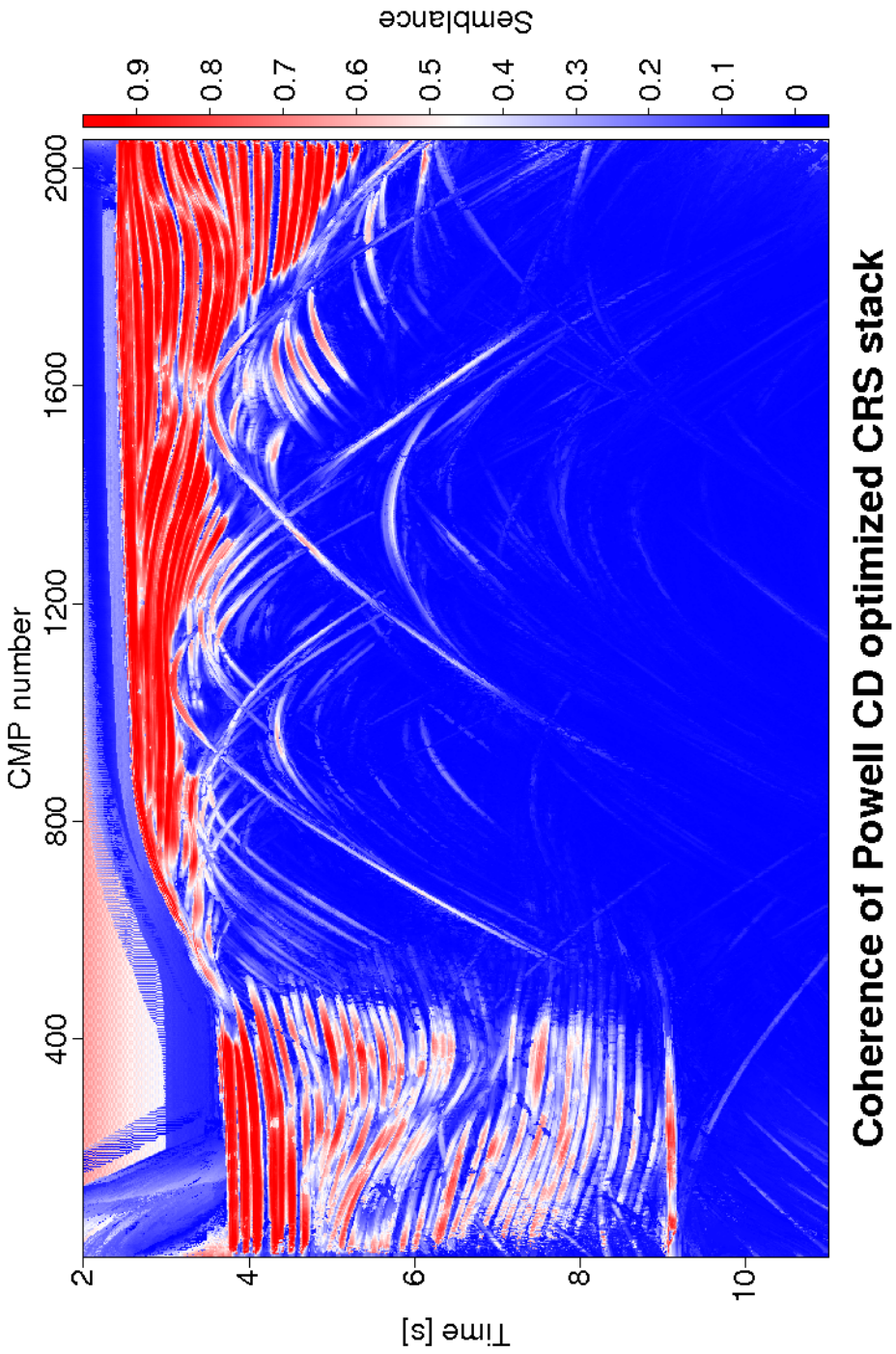

Figure 4.12: Sigsbee 2A data: coherence section associated with the Powell CD optimized CRS stacked section shown in Figure 4.9 smoother than coherence section of the pragmatic approach shown in Figure 4.4.

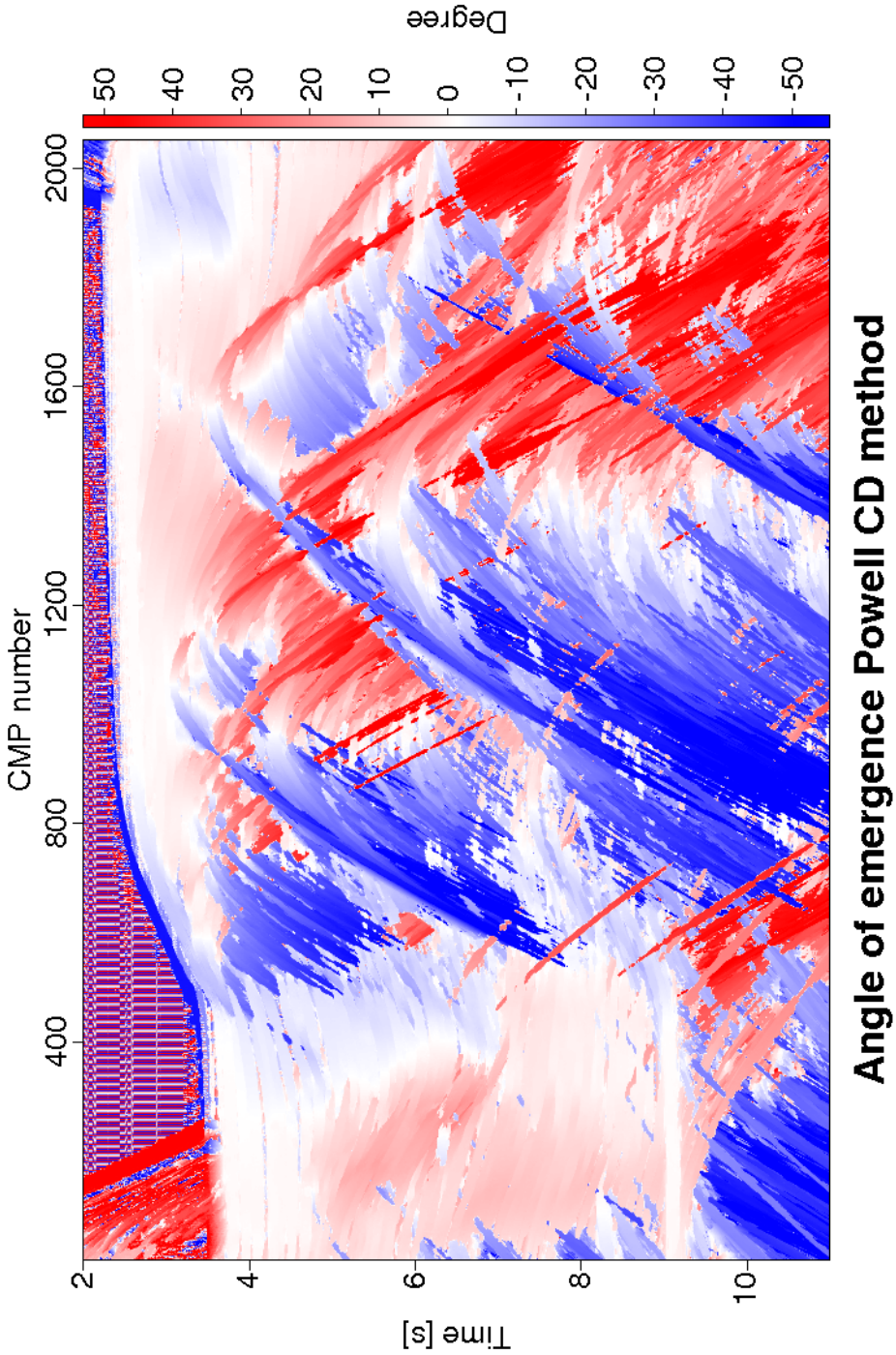

Figure 4.13: Sigsbee 2A data: angle of emergence associated with the Powell CD optimized CRS stacked section shown in Figure 4.9. These attributes are directly related to the slopes of the events.

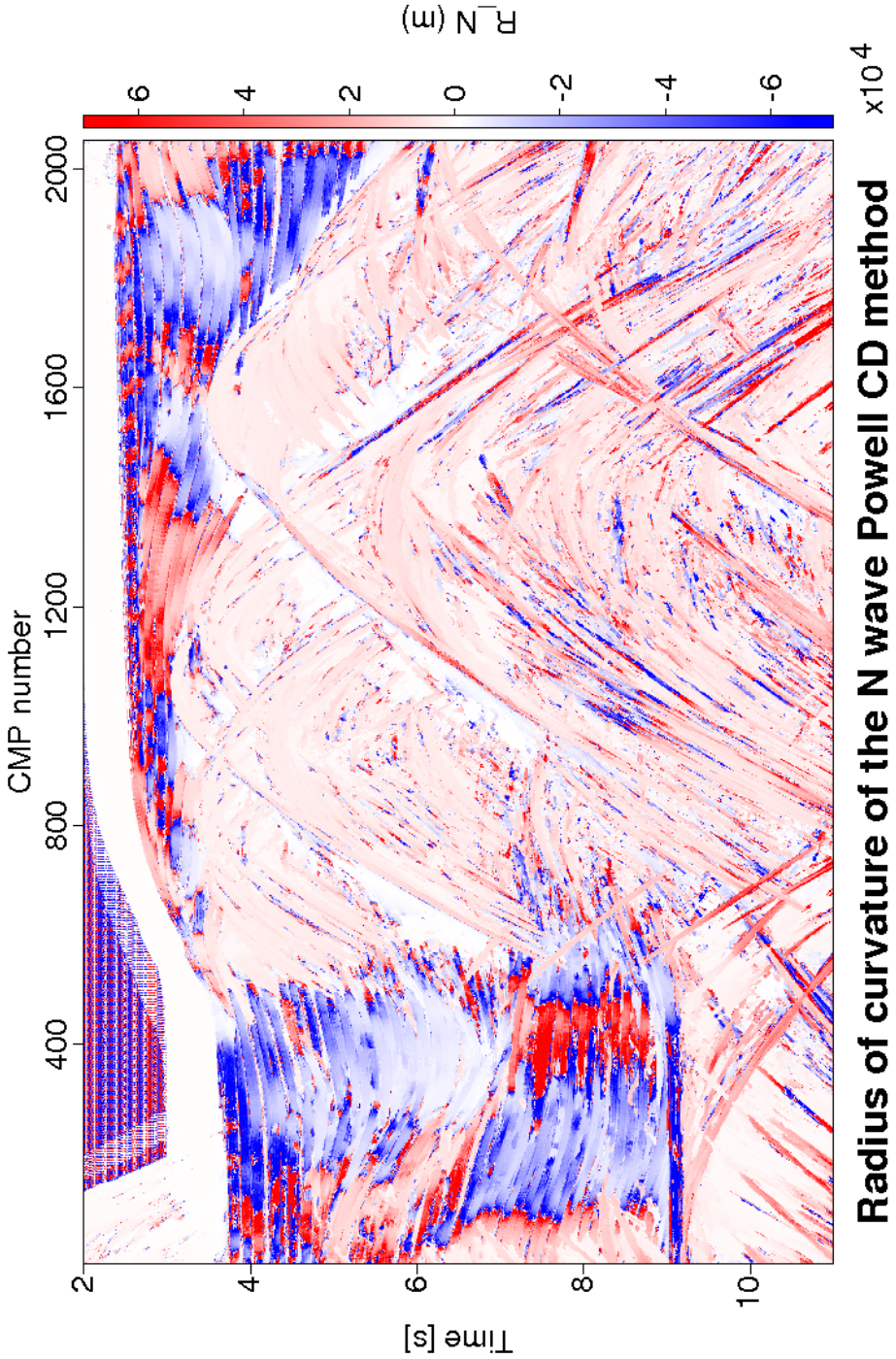

Figure 4.14: Sigsbee 2A data: radius of curvature of the normal wave associated with the Powell CD optimized CRS stacked section shown in Figure 4.9. These attributes are directly related to the curvatures of the events in the ZO section.

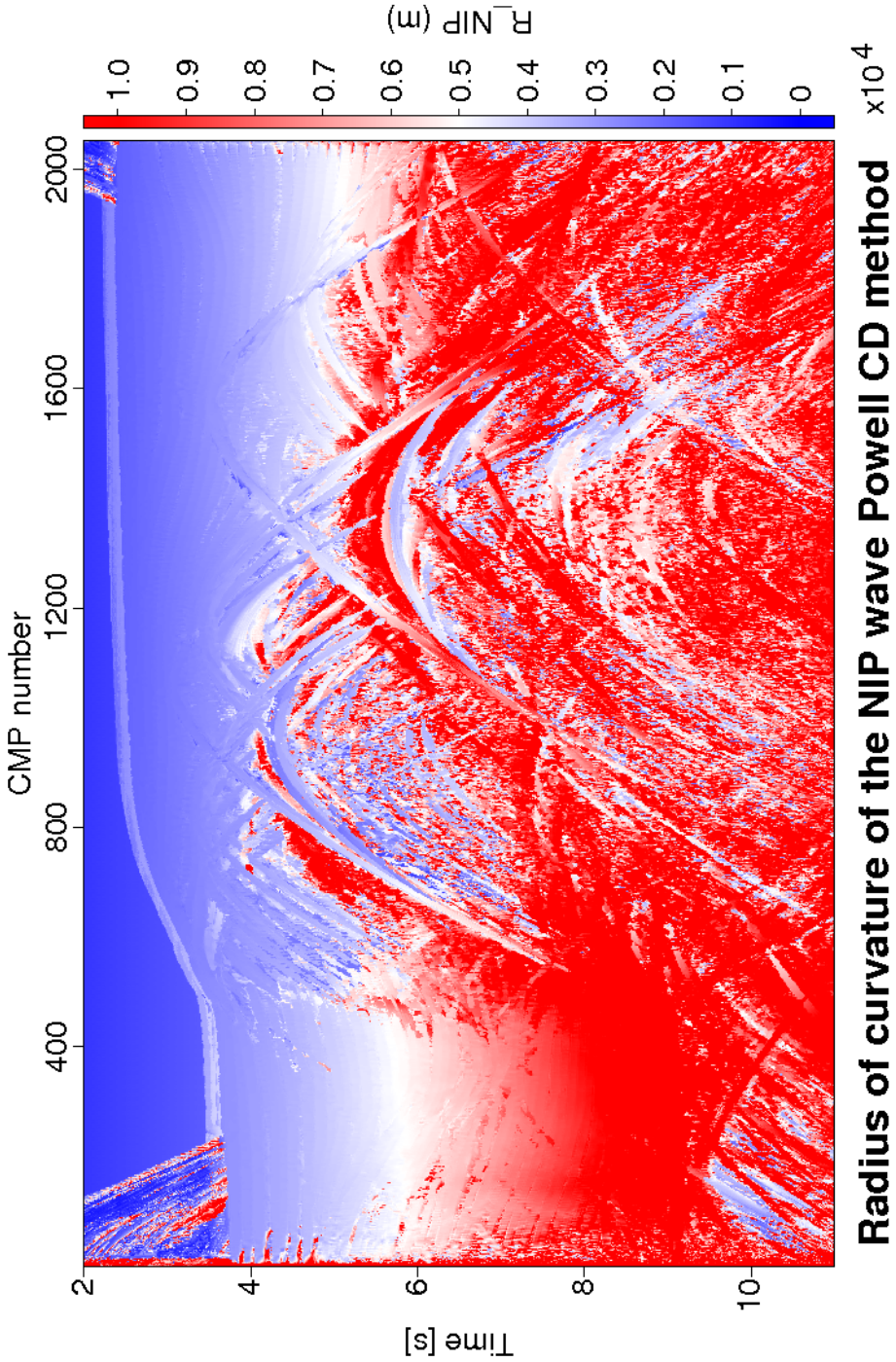

Figure 4.15: Sigsbee 2A data: radius of curvature of the NIP wave associated with the Powell CD optimized CRS stacked section shown in Figure 4.9. These section is calculated from the emergence angle section of the dominant events in Figure 4.11 and the stacking velocity section obtained from automatic CMP stack.

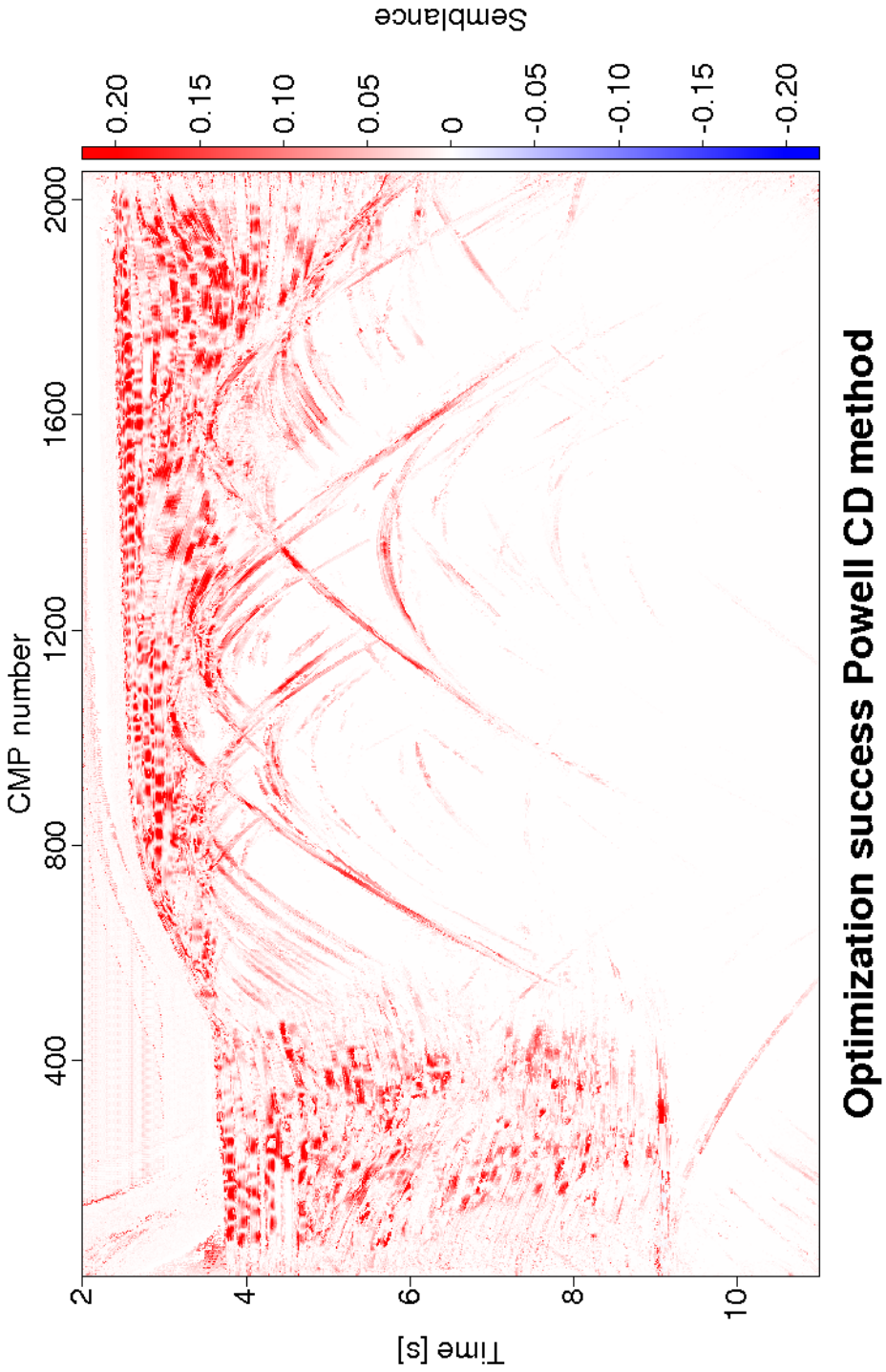

Figure 4.16: Sigsbee 2A data: difference in coherence between the pragmatic approach CRS stacked section (Figure 4.4) and the Powell conjugate direction optimized CRS stacked section (Figure 4.12).

Figure 4.17 shows enlarged images of the simultaneous optimized CRS stacked sections for the Nelder Mead optimization method and the Powell conjugate direction method. Both images look very similar between the Nelder Mead stacked section (Figure 4.17a) and the Powell conjugate direction stacked section (Figure 4.17b). And no differences can be observed from both images.

Figure 4.18 shows enlarged images of the coherence CRS stacked sections for the Nelder Mead optimization method and the Powell conjugate direction method. The Powell conjugate direction stacked section Figure 4.18b has a little bit scatter compared to the Nelder Mead stacked section Figure 4.18a. But both images look similar and it does not appear that the differences in coherence sections has a major effect on the atributes (shows in Figure 4.19, Figure 4.20, and Figure 4.21).

Figure 4.19 shows enlarged images of the emergence angle sections, α, for the Nelder Mead optimization method and the Powell conjugate direction method. Both sections are very similar and no differences can be observed.

Figure 4.20 and Figure 4.21 show enlarged images of the radius of curvature normal wave section, R_N, and the radius of curvature NIP wave section, R_{NIP}, for the Nelder Mead optimization method and the Powell conjugate direction method. Both sections are very similar and no differences can be observed.

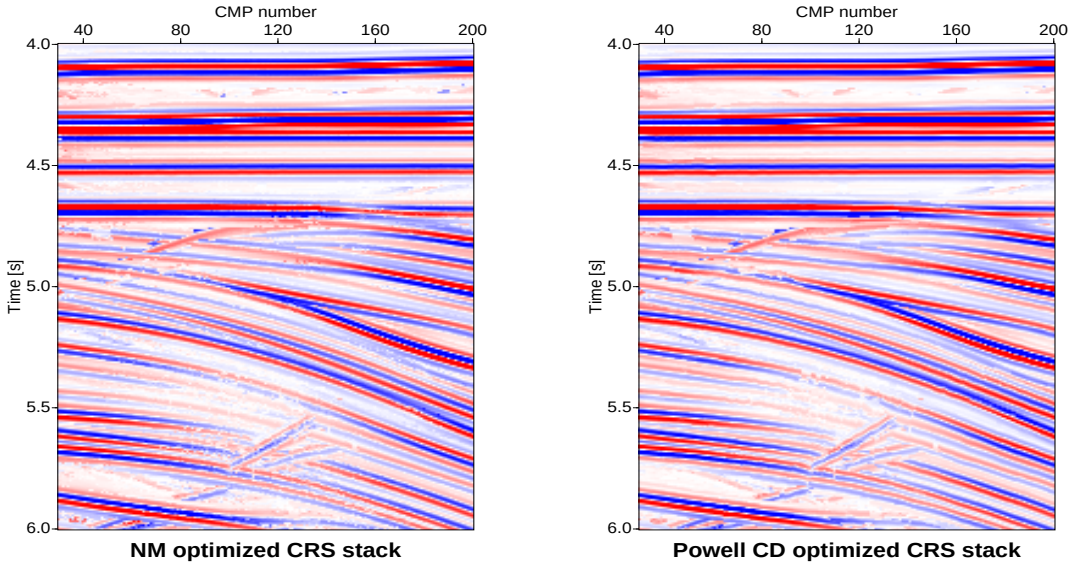

(a) (b)

Figure 4.17: ZO CRS stacked sections: comparison between the Nelder Mead optimization method and Powell conjugate direction optimization method with the same initial values from the pragmatic approach.

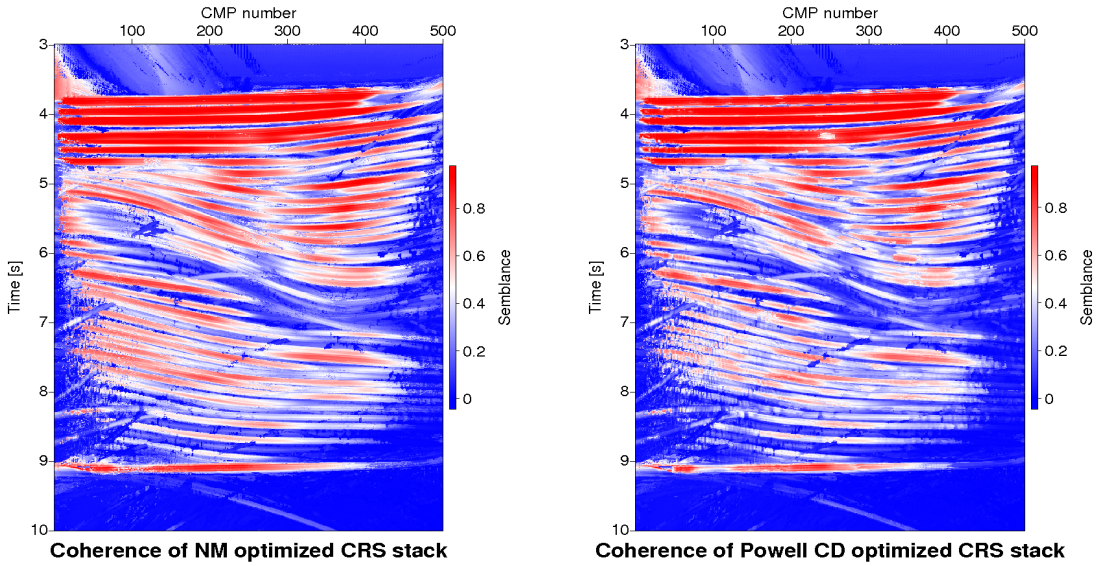

(a) (b)

Figure 4.18: Coherence section: comparison between the Nelder Mead optimization method (a) and Powell conjugate direction optimization method (b). The stacks of both method look similar and it does not appear that the differences in coherence has a major effect on the attributes.

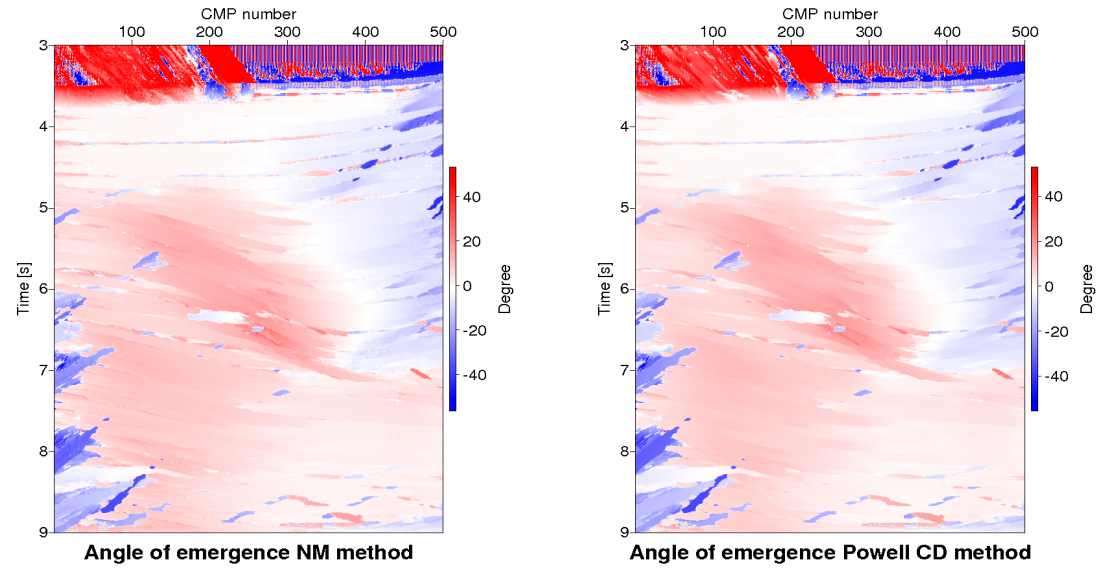

(a) (b)

Figure 4.19: Results of the automatic CRS parameter searches: α. Angle of emergence section for Nelder Mead optimization method (a) and angle of emergence section for Powell conjugate direction optimization method (b). Both section are very similar and no specific differences can be observed.

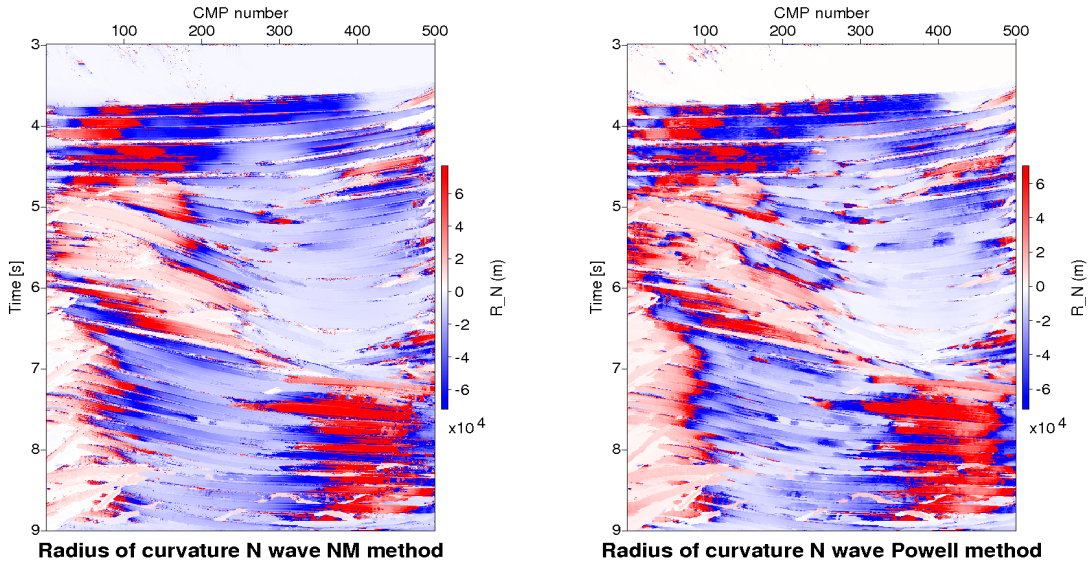

(a) (b)

Figure 4.20: Results of the automatic CRS parameter searches: R_N. Radius of curvature of the N wave section for Nelder Mead optimization method (a) and radius of curvature of the N wave section for Powell conjugate direction optimization method (b). Both section are very similar and no specific differences can be observed.

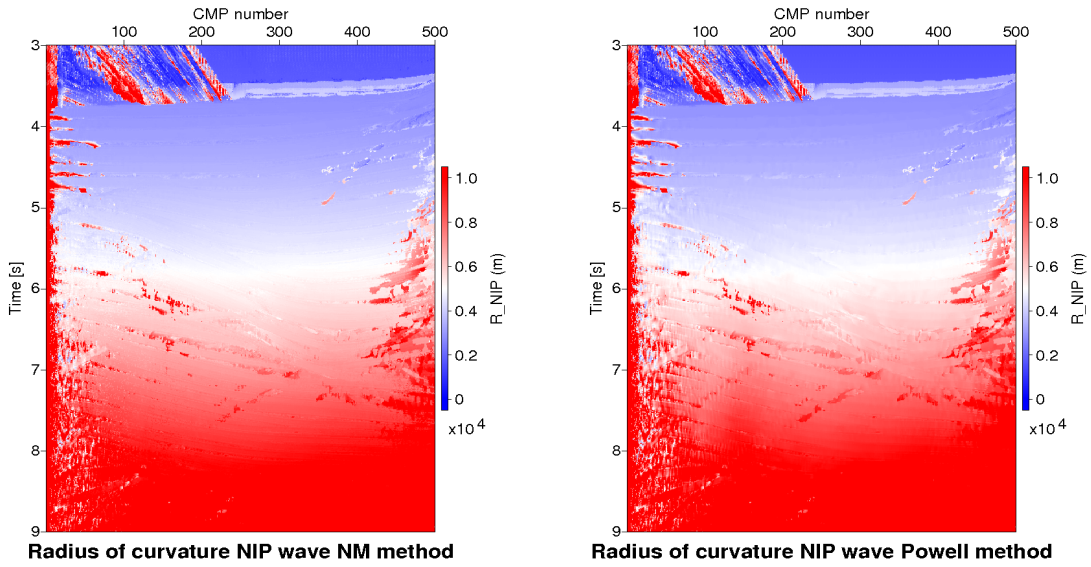

(a) (b)

Figure 4.21: Results of the automatic CRS parameter searches: R_{NIP}. Radius of curvature of the NIP wave section for Nelder Mead optimization method (a) and radius of curvature of the NIP wave section for Powell conjugate direction optimization method (b). Both section look similar and no specific differences can be observed.

4.3 Conclusions

We have introduced an alternative strategy for the optimization of the CRS attributes. The method is based on a hybrid optimization, which comprises the conjugate direction approach based on a Powell search method. The application of the simultaneous optimization of the CRS stack method on the Sigsbee 2A synthetic data set shows that the new method provides very good solutions. The results shows a better S/N ratio, improved continuity of reflections events and also a better image for the reflector compared to the CMP stacked section and the pragmatic approach CRS stacked section. This quality improvement is observed at the top of salt the bow-tie structures and diffraction patterns stemming are well simulated. Most horizons have continuous structures and can be easily identified. Application to a complex synthetic data example using this method provides the same result with the Nelder Mead method currently used in the CRS attribute search, overall no differences can be observed from both method. No differences in computational time was observed for the simultaneous search of the parameters in the 2-D CRS stack on the Sigsbee 2A data using the Powell conjugate direction approach and the Nelder Mead method currently used in the CRS attribute search.

Chapter 5

Field data example

This chapter shows the application of the pragmatic approach and the simultaneous optimization of the CRS stack method on the field data set from Northern Germany with a complex geology. The data set was kindly provided by RWE Dea AG (Hamburg). The automatic search for CRS parameters was applied to the preprocessed CMP gathers. CRS processing of the data set started with the pragmatic approach to search for the CRS parameters as initial values for the simultaneous optimization procedure. After the CMP stacked section was obtained, the automatic CRS parameter searches were carried out and the CRS stacked section was generated. The main targets of the optimization CRS processing of these data is the improvement of the image of seismic time-stacked sections. The pragmatic approach of the CRS stack section are compared to the conventional CMP stack section and also the simultaneous optimization of the CRS stack used Nelder Mead method are compared to the new method.

5.1 Acquisition geometry

The region of study area is located in the North Sea close to the German coast line (Figure 5.1). The area is characterised by salt structures and complex fault system. The area is a part of the intracratonic Southern Permian Basin formed at the end of the Variscan orogeny (Ziegler, 1990).

The data set consist of 1055 shot gathers recorded to 7 s time with 2 ms sampling rate. Airguns were used with an average shot spacing of 25 m with 240 channels per shot and the receiver group spacing was 12.5 m. Sources and receivers are located 6 m below the sea surface. With a total line length of ~26.5 km, consisting of 4243 CMP gathers ranging from CMP bin number 6757 to 11000. The CMP interval is 6.25 m and the maximum CMP fold is 60. The CMP aperture is defined from 400 m at 0.2 s to 3200 m at 2.3 s. I compiled all relevant acquisition parameters and the basic processing parameters used for the ZO simulation of CRS stack in Table 5.1 and Table 5.2, respectively.

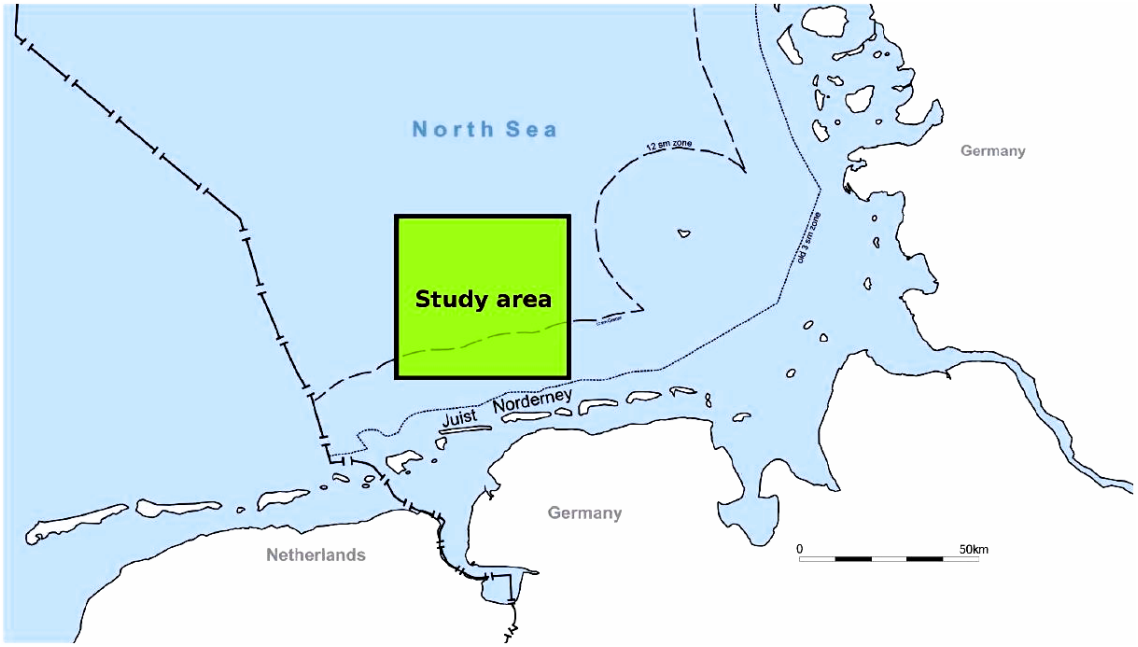

Figure 5.1: The region of study area is located approximately 30 km north of the German coast line in the southern part of the North Sea (Kindly provided by RWE Dea AG, Hamburg).

Context	Processing parameter	Setting
Shot and receiver geometry	Number of shot	1055
	Shot interval	25 m
	Number of receivers	240
	Receiver interval	12.5 m
Recording parameters	Recording time	7 s
	Sampling interval	2 ms
Midpoint and offset geometry	Number of CMP bins	4243
	Maximum CMP fold	60
	CMP bin interval	6.25 m
	Offset range	-250...-3238 m
Frequency content	Dominant frequency	50 Hz
	Maximum frequency	80 Hz

Table 5.1: Field data: acquisition parameters of the pre-stack data set.

Context	Processing parameter	Setting
General parameters	Dominant frequency	50 Hz
	Coherence measure	Semblance
	Data used for coherence analysis	Original traces
	Temporal width of coherence band	56 ms
Velocity and constraints	Near surface velocity	1500 m/s
	Tested stacking velocity	1500...5000 m/s
Target zone	Simulated ZO traveltimes	0...7 s
	Simulated temporal sampling interval	2 ms
	Number of simulated ZO traces	4243
	Spacing of simulated ZO traces	6.25 m
Aperture and taper	Minimum ZO aperture	500 m @ 0.2 s
	Maximum ZO aperture	500 m @ 2.3 s
	Minimum CMP aperture	400 m @ 0.2 s
	Maximum CMP aperture	3200 m @ 2.3 s
	Relative taper size	30 %
Automatic CMP stack	Initial moveout increament for largest offset	16 ms
	Number of refinement iterations	3
Linear ZO stack	Tested emergence angles	-60...60°
	Initial emergence angles increment	1°
	Number of refinement iterations	3
Hyperbolic ZO stack	Initial moveout increment for largest ZO distance	2 ms
	Number of refinement iterations	3
Conflicting dip handling	Maximum number of dips	1
	Absolute coherence threshold for global maximum	0.4
	Relative coherence threshold for local maximum	0.5
Local optimization	Coherence threshold for smallest traveltime	0.05
	Coherence threshold for largest traveltime	0.05
	Maximum number of iterations	100
	Maximum relative deviation to stop	10^{-4}
	Initial variation of emergence angles	6°
	Initial variation of R_{NIP}	5 %
	Initial variation of transformed R_N	6°
	Transformation radius for R_N	106 m

Table 5.2: Field data: processing parameters used for the ZO simulation by means of the CRS stack.

5.2 Application of CRS stack

5.2.1 Pragmatic approach

In order to generate a CMP stacked section, the automatic search estimates the best-fit stacking velocities for the preprocessed CMP gathers. CMP stacking of the preprocessed CMP gathers with the obtained velocity model provided the zero-offset (ZO) time section. The zero-offset (ZO) CMP stacked section is depicted in Figure 5.2. It displays steep dipping layers at 0-0.5 s traveltime. These section have a good quality at 0-2 s traveltime.

Structurally, the study area can be subdivided into three major part: Tertiary, Upper Cretaceous, and Zechstein. Horizontal reflections at 0.5 s and 1 s traveltime have continous structure corresponding to the Tertiary. These horizons can be easily identified and correlated due to strong impedance contrasts. The base of Tertiary at 1 s traveltime and the base of Upper Cretaceous at 1.5 s traveltime has cleary identified. These boundaries show a pull-up crossed by a set of faults at CMP 1500-1700.

In the areas of CMP 1450-1850 the base of Upper Cretaceous at 1.5 s traveltime was deformed during the salt movements. The same case for the areas of CMP 3100-3400. The presence of salt involved the complicated for the interpretation of salt boundaries and reflections below in the areas of the section at 1.5-2.5 s traveltime.

The image of the bottom part of the section below 2.5 s traveltime displays reflections with relatively low of the signal-to-noise (S/N) ratio and is poorly imaged. The base of Zechstein is well defined at about 2.5 s traveltime and is only interrupted below the salt bodies.

The coherence section (Figure 5.3) helps to identify the detected events and to estimate where the given aperture is appropriate to fit a hyperbolic operator. The reflection events are clearly defined for times 0-2.5 s traveltime and are linked with high coherence values of the reflections. Due of the lower signal-to-noise (S/N) ratio and geometrical spreading loss the coherence decreases with increasing recording time. And the image of seismic events below 2.5 s traveltime have a lower coherence values correspond with the salt plug areas.

Finally, conflicting dips situations are not yet resolved in the zero-offset (ZO) CMP stacked section. Due to dipping layers salt domes appear wider in this section than they are in reality. Moreover, a lot of conflicting dip situations are present at the salt-sediment boundaries.

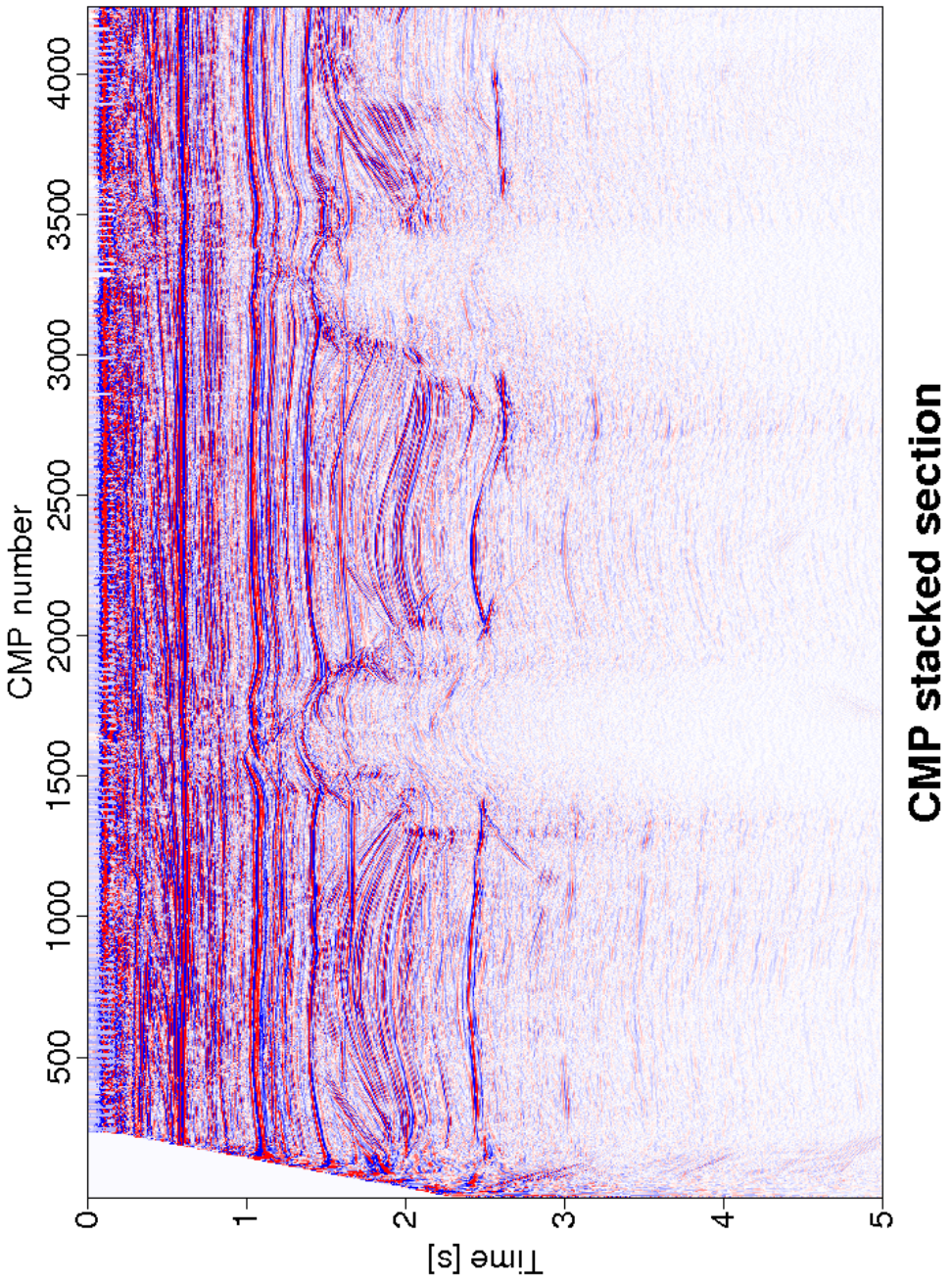

Figure 5.2: Field data: result of CMP stack.

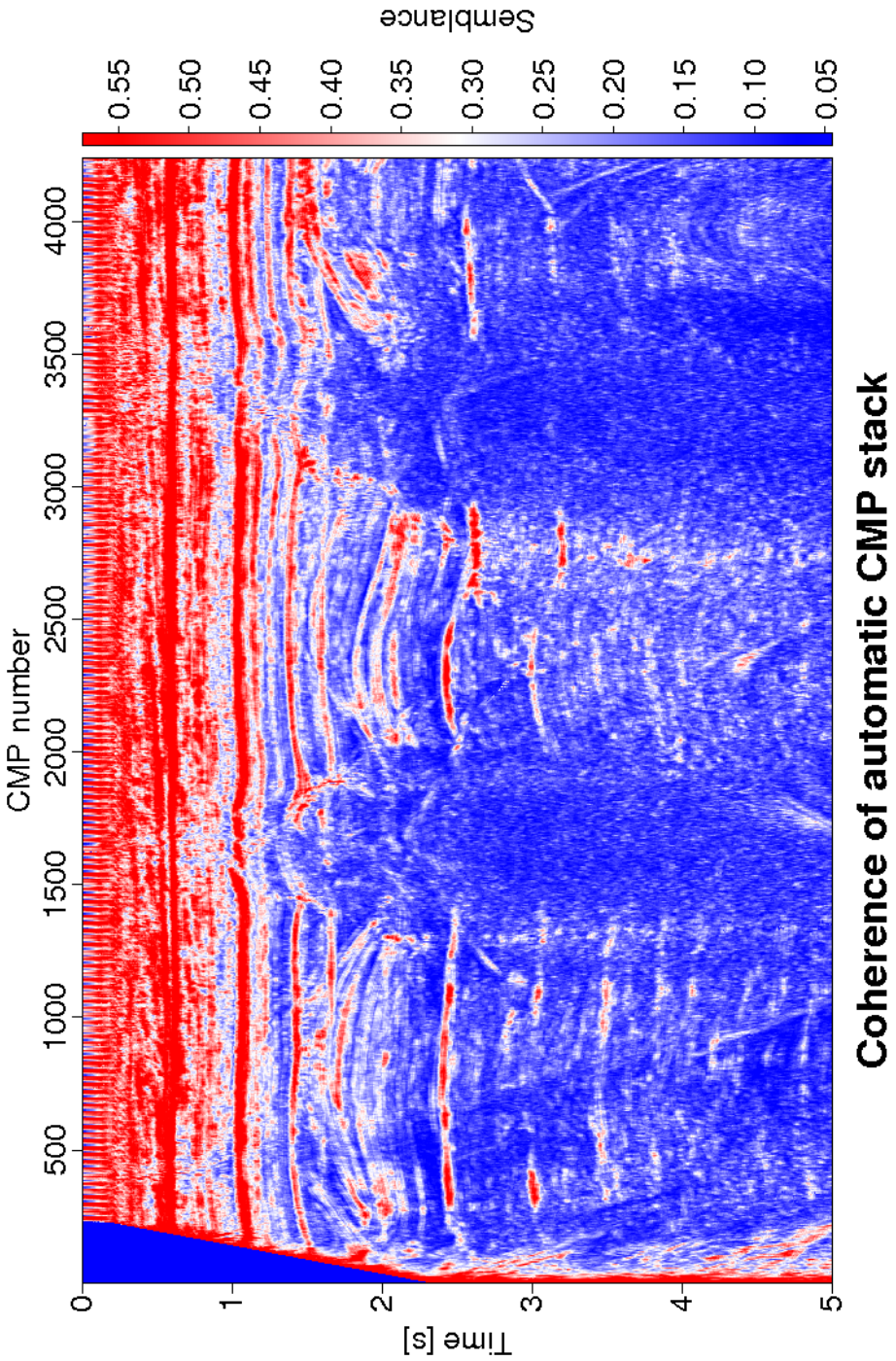

Figure 5.3: Field data: coherence section associated with the CMP stacked section shown in Figure 5.2

After the generation of he CMP stacked section, the automatic searches provided the CRS stacking parameters for the generation of the CRS stacked section. This yields initial attributes which can be used as first guess in a final optimization procedure. The pragmatic approach CRS stack result relies on a sufficiently high quality of the CMP stacked section generated in the first processing step.

Compared to the conventional zero-offset (ZO) CMP stack (Figure 5.2), the pragmatic approach CRS stacked section in Figure 5.4 shows better continuity of horizons at all time levels and produced a better image in reflections and diffractions. The reflections are more continuous and appear clearer. Then now we used these results to perform stack and coherence analysis along the entire spatial CRS stacking operators using the simultaneous optimization procedure.

The coherence section for the pragmatic approach CRS stack is shown in Figure 5.5. Most reflections better defined compared to the coherence section of the CMP stack shown in Figure 5.3 and the reflection events a clearly defined correspond with high coherence values and associated with the reflector.

The computational effort required for the sucessive processing steps is presented in Table 5.3. The CPU times strongly depend on the used hardware, but in general, the Powell conjugate direction method has a substantial computational advantage against the Nelder Mead method currently used in the CRS attribute search. A factor of 2 in computing time was observed for the simultaneous search of the parameters in the 2-D CRS stack using the Powell conjugate direction approach.

Processing step	NM method	Powell CD method
Automatic CMP stack	00:29:19	00:29:19
Zero-offset stacks	03:52:12	03:52:12
Initial stack	01:34:18	01:34:18
Optimized	32:54:52	15:02:59
Total	38:50:40	20:58:48

Table 5.3: Field data: CPU times required for processing steps.

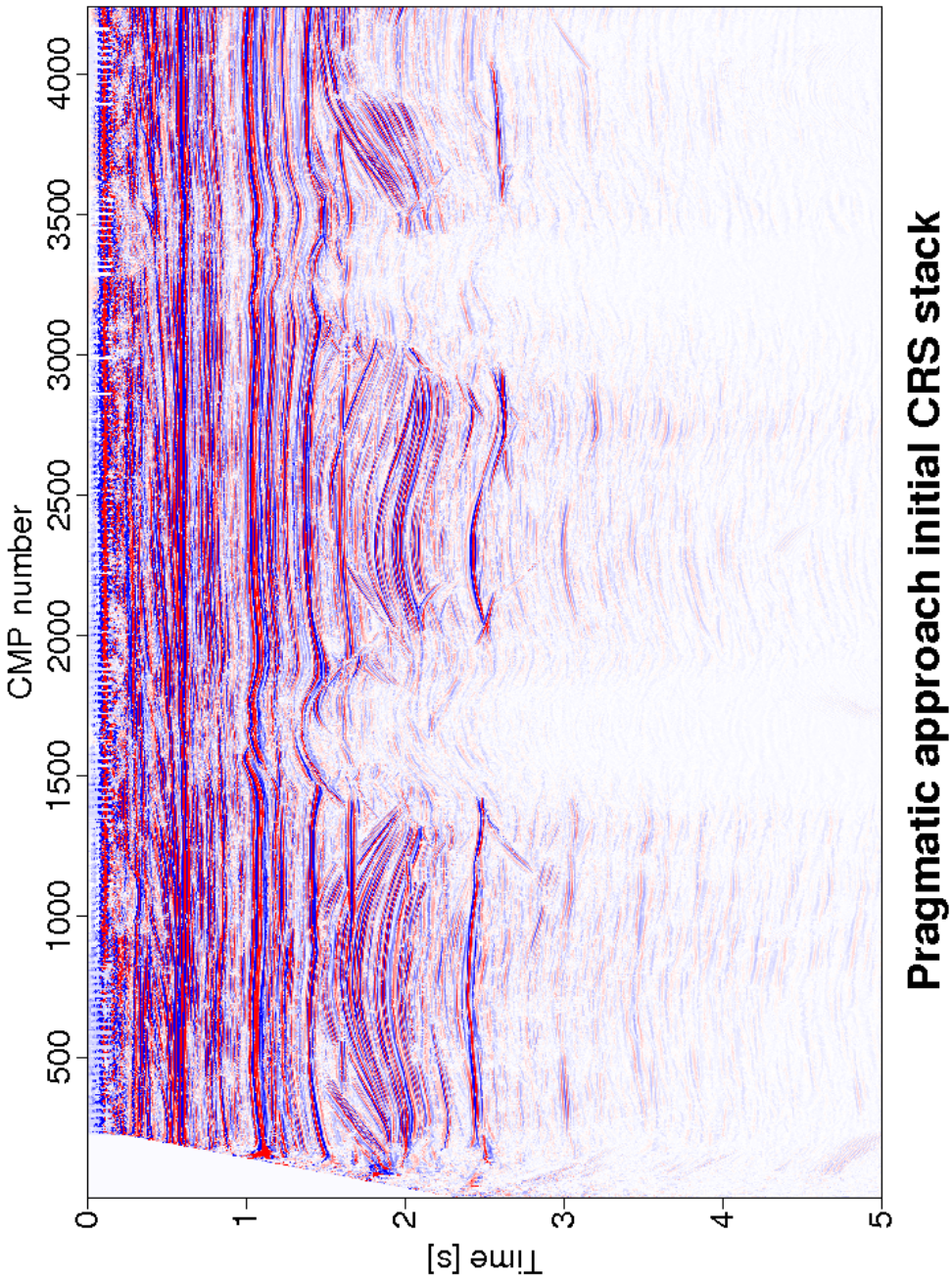

Figure 5.4: Field data: result of pragmatic approach CRS stack.

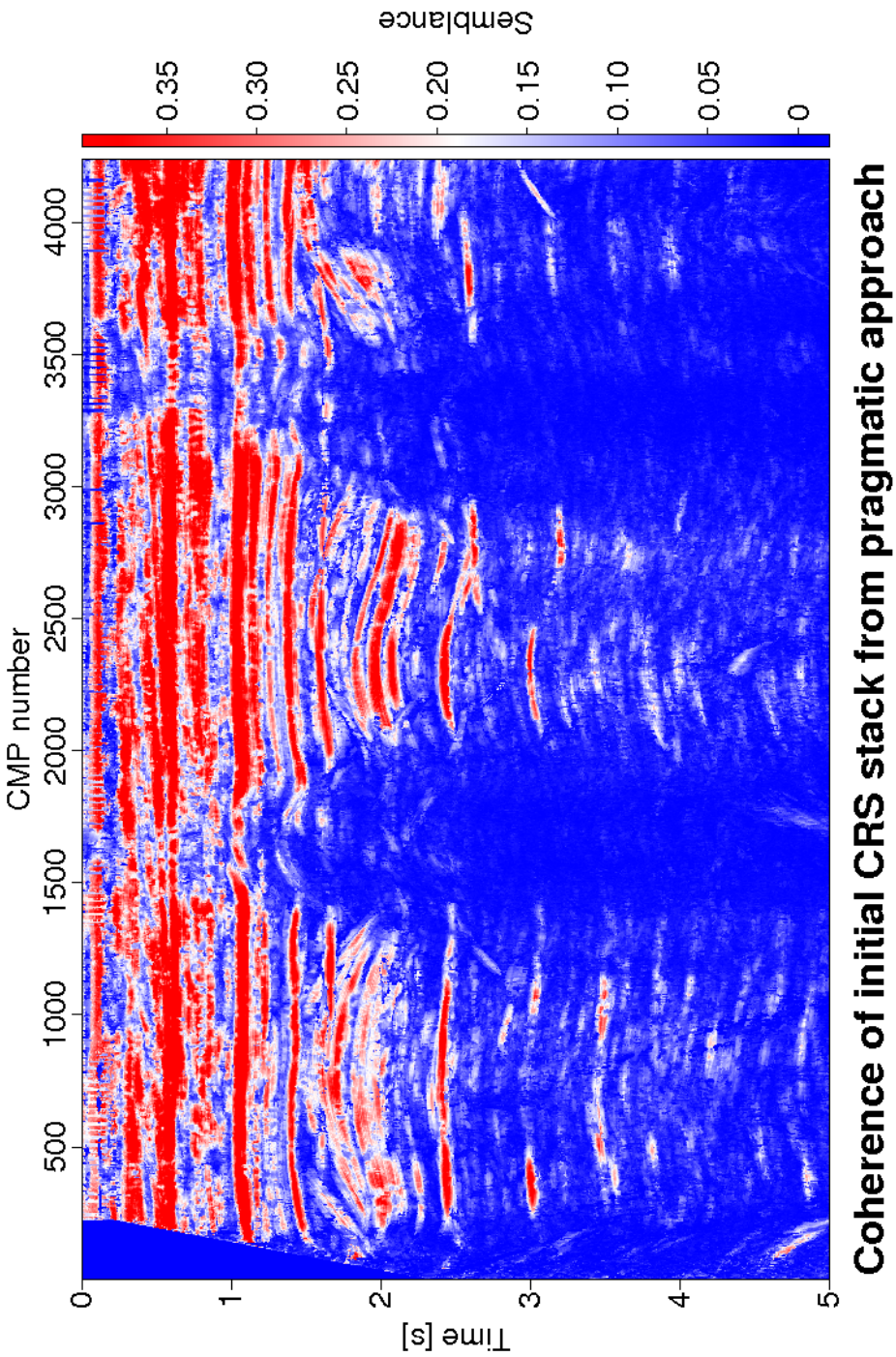

Figure 5.5: Field data: coherence section associated with the pragmatic approach CRS stacked section shown in Figure 5.4

5.2.2 Simultaneous optimization of the CRS stack

Optimization of the spatial CRS stacking operator with all three wavefield attributes can further increase the accuracy of the wavefield atributes. However, the optimization procedure is very time consuming.

For the field data I used the same approach as for the Sigsbee synthetic data, the CRS stack using initial wavefield attributes determined with pragmatic approach is shown in Figure 5.4. We use the zero-offset (ZO) CMP stacked section result as an input for the determination of the wavefield attributes. The optimization CRS stack results it depends the choice of the initial wavefied attributes. If we choose wrong parameters for the initial wavefield attributes, e.g., near the local solution, it will definitely lead to a wrong result.

Figure 5.6 to 5.17 display the resulting simultaneous optimized CRS stacked section. The CRS stacked section obtained with the initial attributes from the result of pragmatic approach in Figure 5.4 already has a high quality. The optimization procedure can further increase the accuracy of the wavefield attributes. Attributes after simultaneous are smoother can be important for model building.

Nelder Mead optimization method

The CRS stacked section obtained with the Nelder Mead method is displayed in Figure 5.6. It shows better continuity of horizons at all time levels and produced a better image of conflicting dip areas. The CRS stacked section increase the lateral resolution in the areas with significant variation of the event curvature. The reflections are more continuous and appear clearer. The continuity of reflection events in the CRS stacked section increased greatly and the signal-to-noise (S/N) ratio improved compared to the CMP stacked sections (Figure 5.2) and pragmatic approach CRS stacked section (Figure 5.4).

The coherence section for the dominant events associated with the Nelder Mead optimized CRS stack is shown in Figure 5.7. The events associated with the highest coherence at each particular zero-offset (ZO) location allow to identify the detected events and to estimate the reliability of the image as well of its associated wavefield attributes. In the coherence section most reflections can be identified while are visible in the CMP stack and CRS stack. The reflection events are clearly defined for times 0-2.5 s traveltime correspond with high coherence values and associated with the reflector. Due of the lower signal-to-noise (S/N) ratio and geometrical spreading loss the coherence decreases with increasing recording time. And the image of seismic events below 2.5 s traveltime have lower coherence values. These events are influenced by the salt plug areas.

The optimized emergence angle sections, α, for the dominant events are shown in Figure 5.8. The improvement of the emergence angle section can readily be observed, due to the simple relation between the emergence angle and the slopes of the zero-offset (ZO) events. Angle of emergence around 0° correspond to almost horizontal reflections. And higher values of emergence angle at 3 s traveltime indicate diffractions in this section.

The optimized radius of curvature of the normal wave, R_N section for the dominant events are depicted in Figure 5.9. The same condition as above applies to this section. The upper part of this section has very large values of R_N associated with reflections almost flat. Plane reflectors are associated by large values of R_N.

And the optimized radius of curvature of the NIP wave, R_{NIP} section for the dominant events are shown in Figure 5.10. For the stratified areas, the values of R_{NIP} continously increases smoothly with increasing traveltime indicating that this parameter is associated with the reflector depth. The difference in coherence between the pragmatic approach initial CRS stacked (Figure 5.5) and the Nelder Mead optimized CRS stack (Figure 5.7) is shown in Figure 5.11. The improvement of the coherence section can readily be observed at the coherence section associated with the Nelder Mead optimized section.

Powel conjugate direction optimization method

The CRS stacked section obtained with the Powell conjugate direction optimized method is displayed in Figure 5.12. It shows better continuity of horizons at all time levels and produced a better image of conflicting dip areas compared to the CRS stack of the pragmatic approach in Figure 5.4. We do not see specific differences in the sections for the Powell conjugate direction or the Nelder Mead approach. Moreover, the Powell conjugate direction method has a substantial computational advantage against the Nelder Mead method currently used in the CRS attribute search. A factor of 2 in computing time was observed for the simultaneous search of the parameters in the 2-D CRS stack using the Powell conjugate direction approach. For multi-parameter stacking approaches its possible of the CPU time is used in the CRS method can be reduced. Compared to the CMP stacked section (Figure 5.2) and pragmatic approach CRS stacked section (Figure 5.4), the CRS stacked section increase the lateral resolution in the areas with significant variation of the events curvature. The reflections are more continuous and appear clearer.

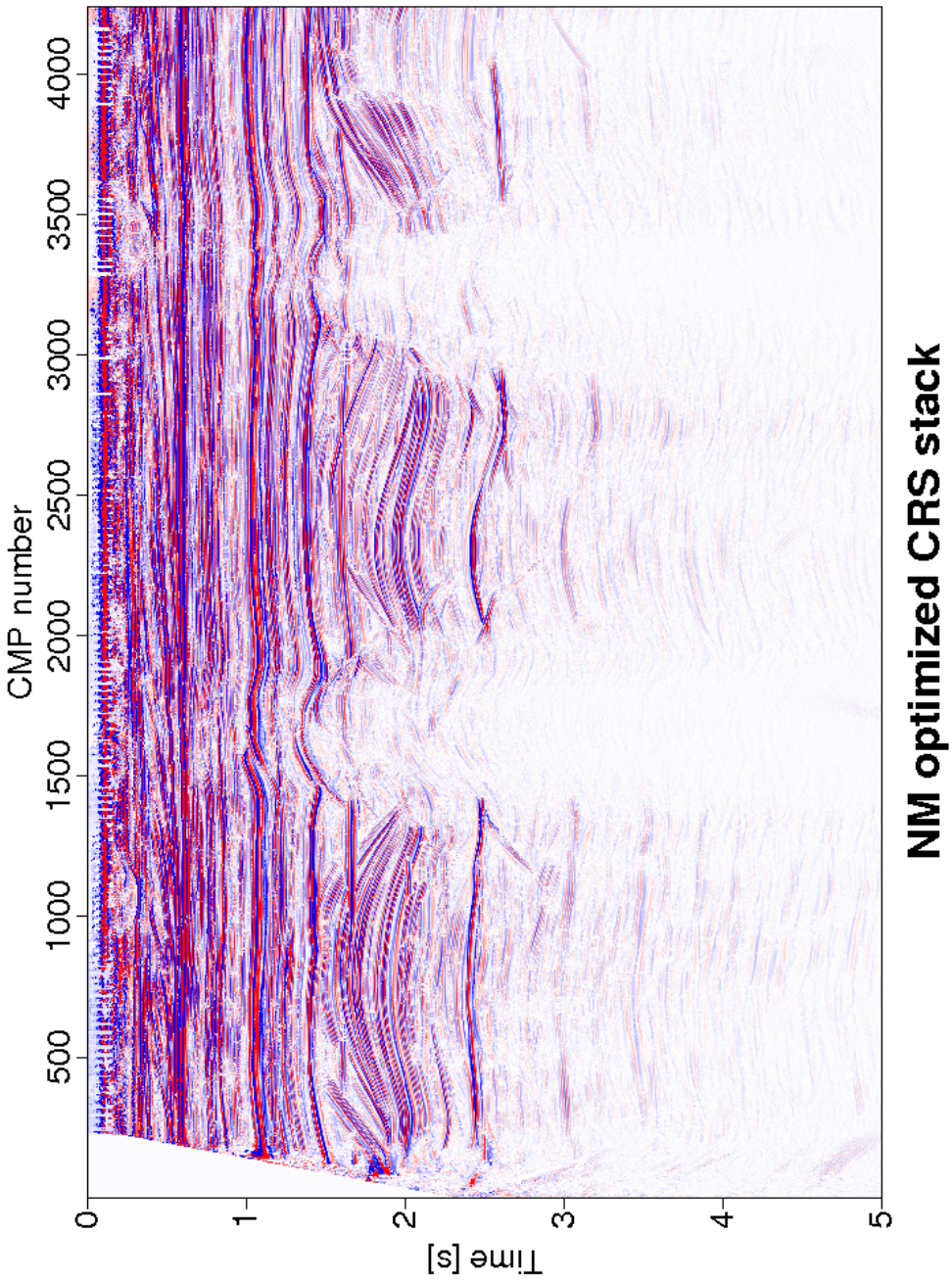

Figure 5.6: Field data: CRS stack result of the Nelder Mead optimization.

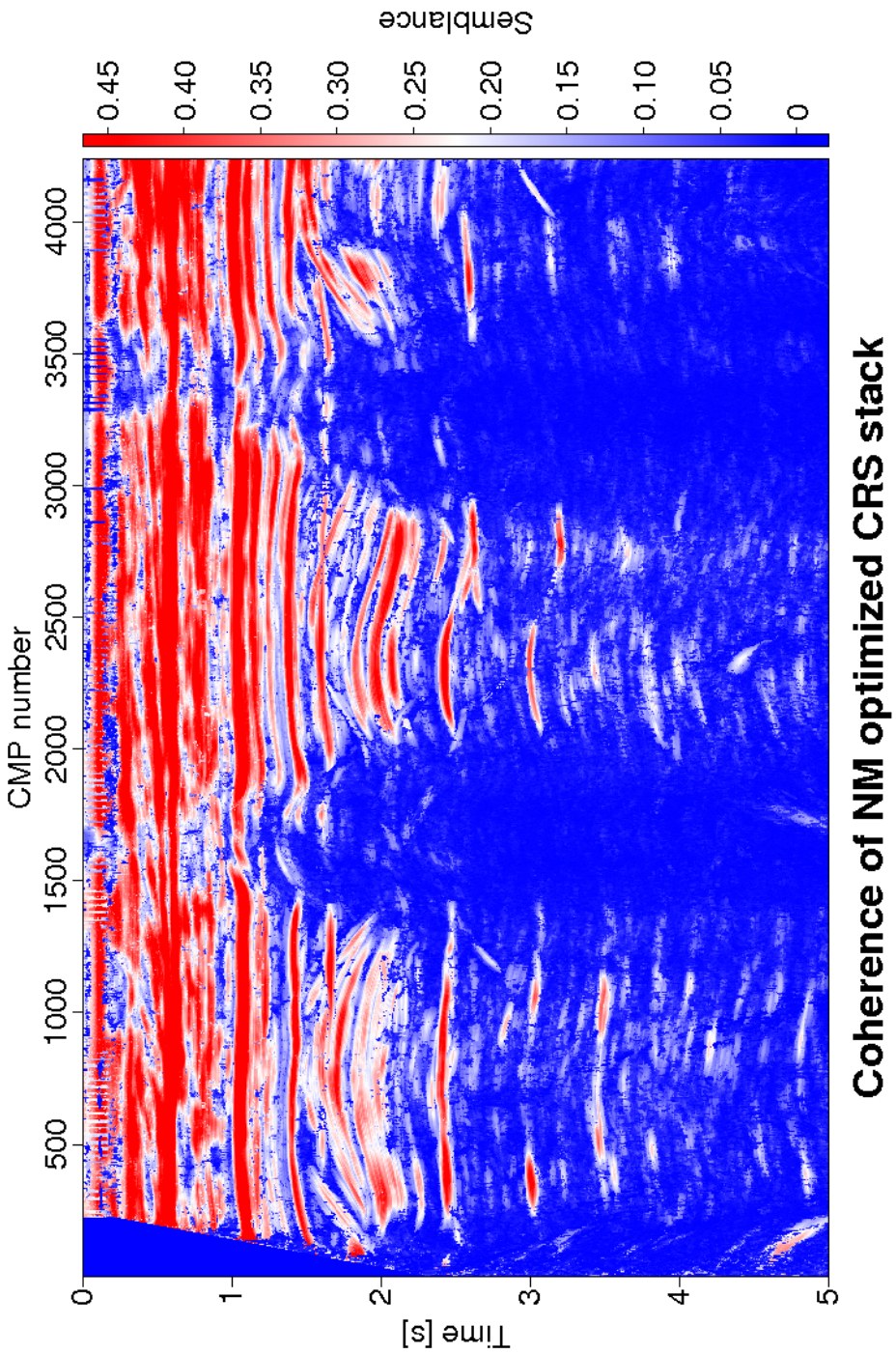

Figure 5.7: Field data: coherence section associated with the Nelder Mead optimized CRS stacked section shown in Figure 5.6 smoother than coherence section of the pragmatic approach shown in Figure 5.5.

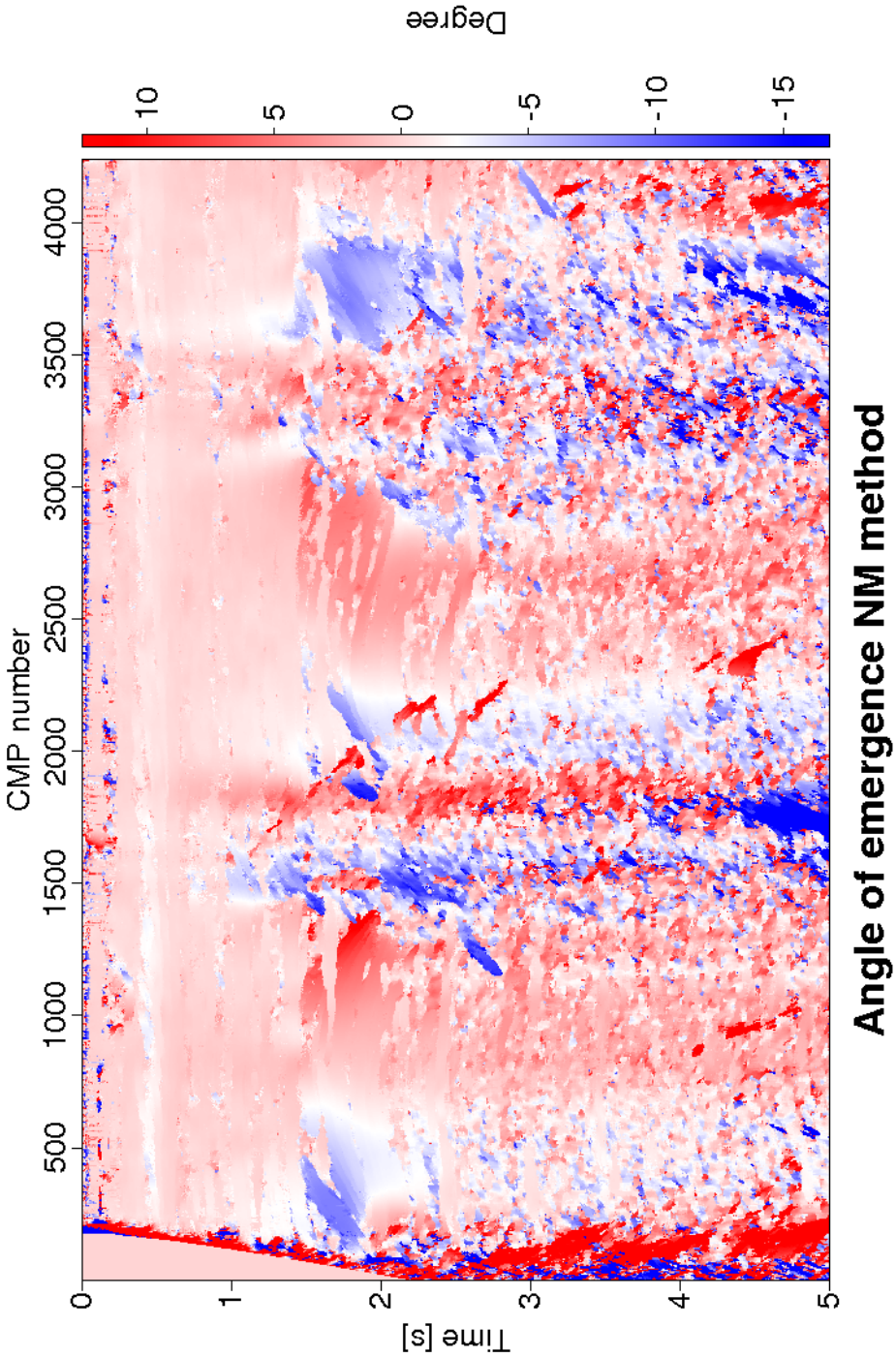

Figure 5.8: Field data: angle of emergence associated with the Nelder Mead optimized CRS stacked section shown in Figure 5.6.

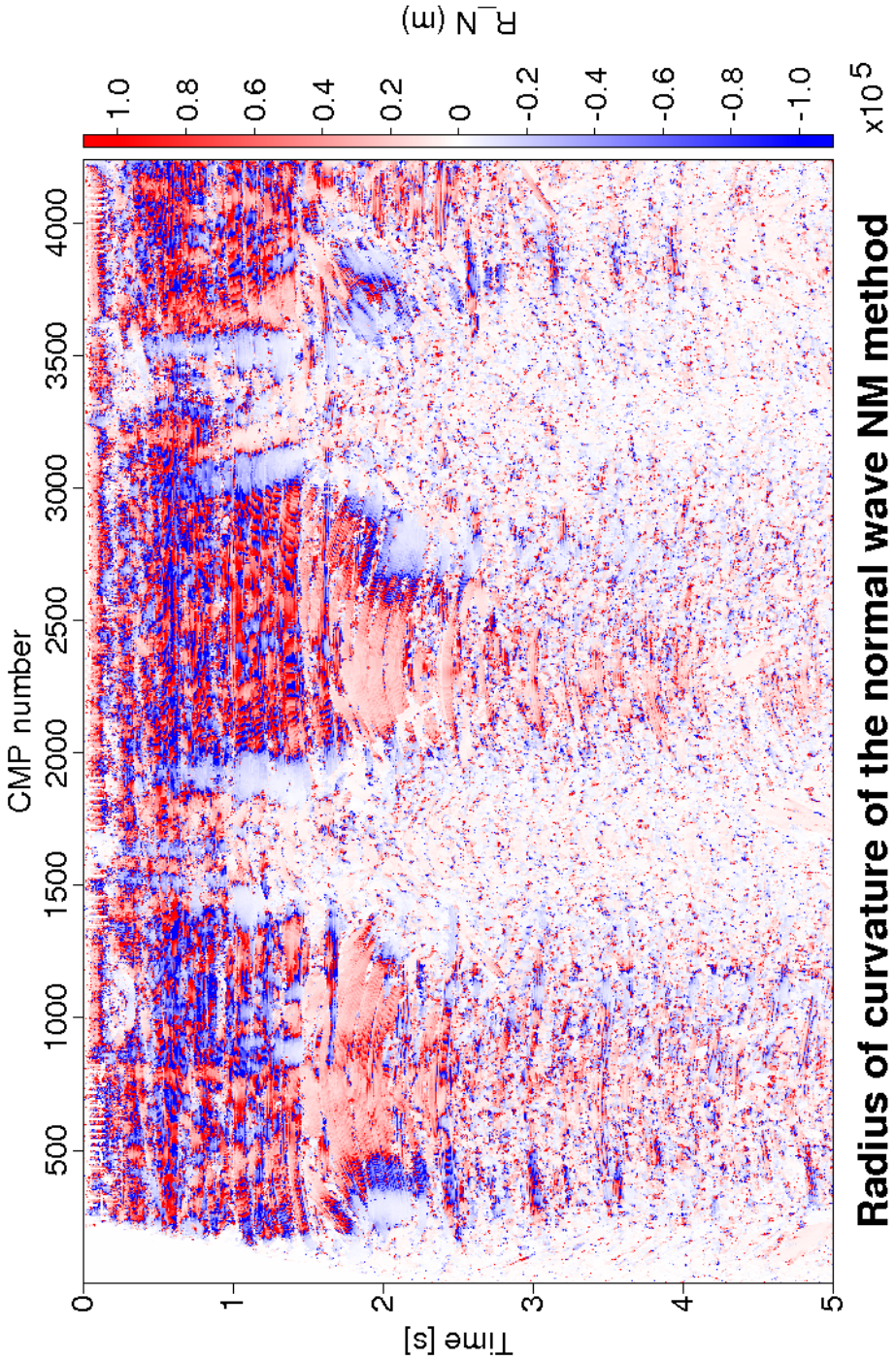

Figure 5.9: Field data: radius of curvature of the normal wave associated with the Nelder Mead optimized CRS stacked section shown in Figure 5.6.

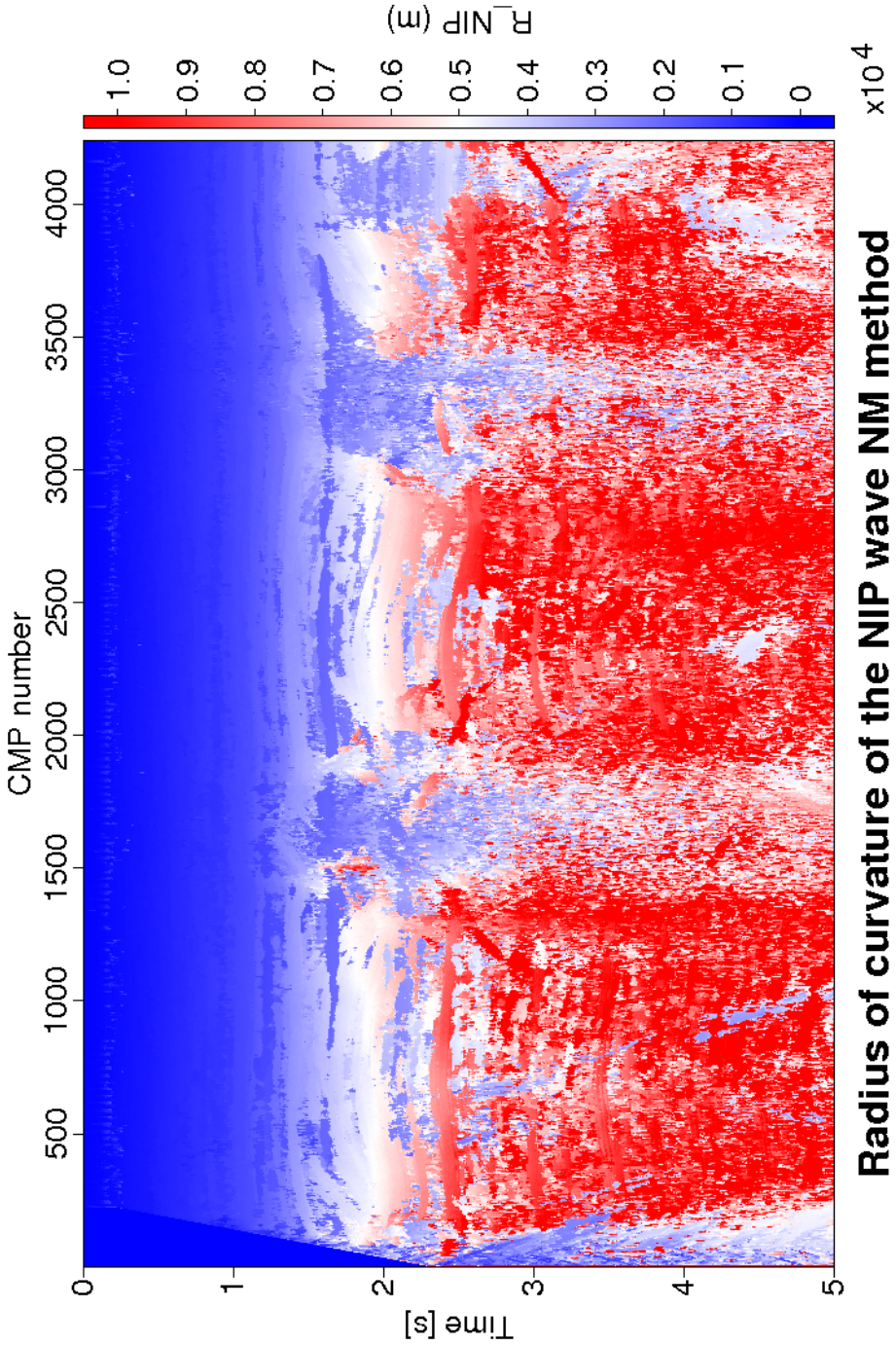

Figure 5.10: Field data: radius of curvature of the NIP wave associated with the Nelder Mead optimized CRS stacked section shown in Figure 5.6.

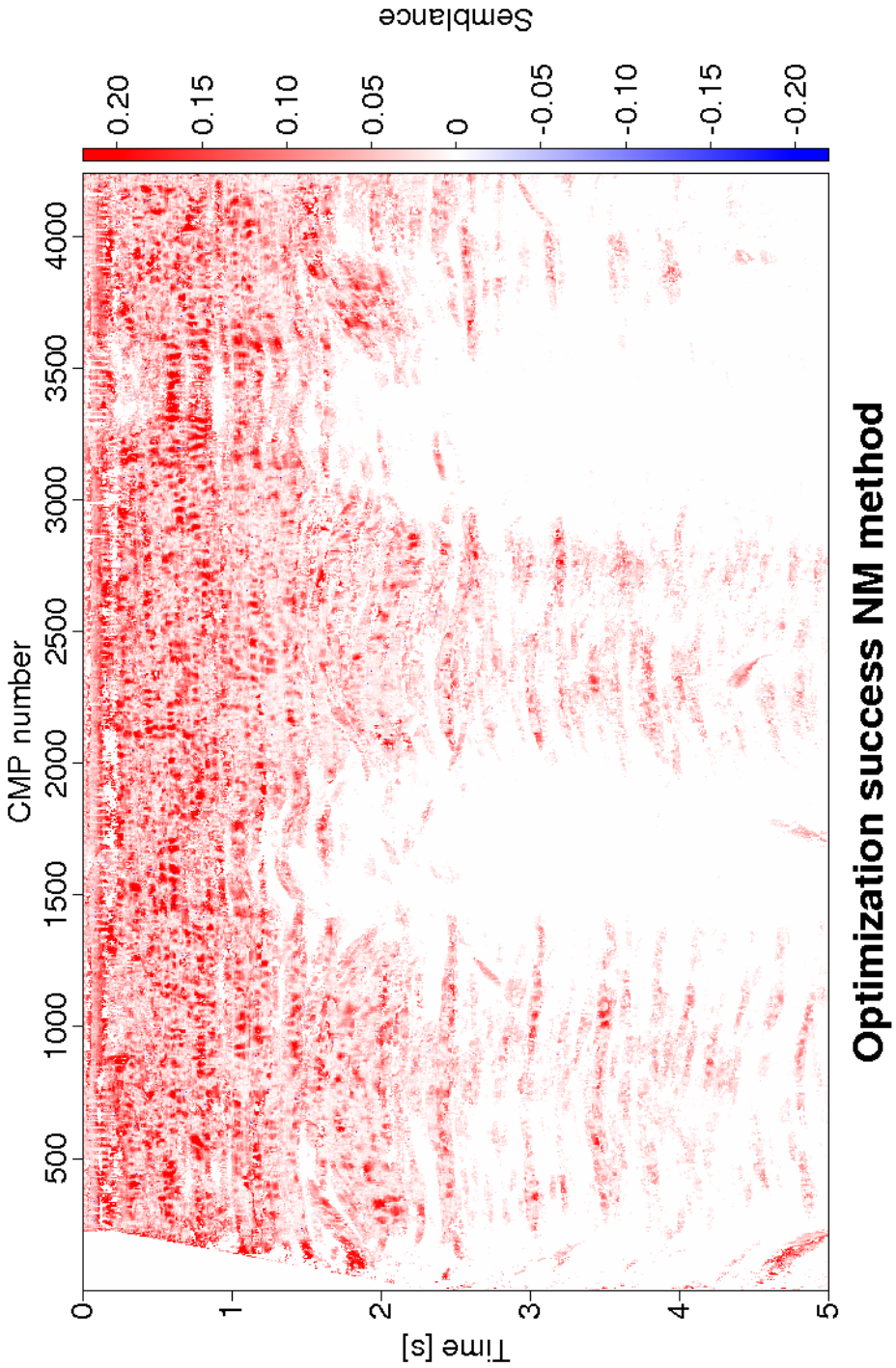

Figure 5.11: Field data: difference in coherence between the pragmatic approach CRS stacked section (Figure 5.5) and the Nelder Mead optimized CRS stacked section (Figure 5.7).

The coherence section for the dominant events associated with the Powell conjugate direction optimized CRS stack is shown in Figure 5.13. The coherence section of the Powell conjugate direction method displays a little bit more scatter than the coherence section of the Nelder Mead method (Figure 5.7), but both sections are very similar and it does not appear that the difference in coherence has a major effect on the attributes.

The optimized emergence angle sections, α, for the dominant events are shown in Figure 5.14. The consistency of the optimized emergence angle section can readily be observed, due to the simple relation between the emergence angle and the slopes of the zero-offset (ZO) events. Angle of emergence around 0° correspond with almost horizontal reflections. And higher values of emergence angle at 3 s traveltime indicates the diffractions in this section.

The optimized radius of curvature of the normal wave, R_N, and the section of radius of curvature of the NIP wave, R_{NIP} sections for the dominant events are depicted in Figure 5.15 and Figure 5.16, respectively. The differences coherence between the pragmatic approach initial CRS stacked (Figure 5.5) and the Powell conjugate direction optimized CRS stack (Figure 5.13) is shown in Figure 5.17. The improvement of the coherence section can readily be observed at the coherence section associated with the Powell conjugate direction optimized section compared to the pragmatic approach section.

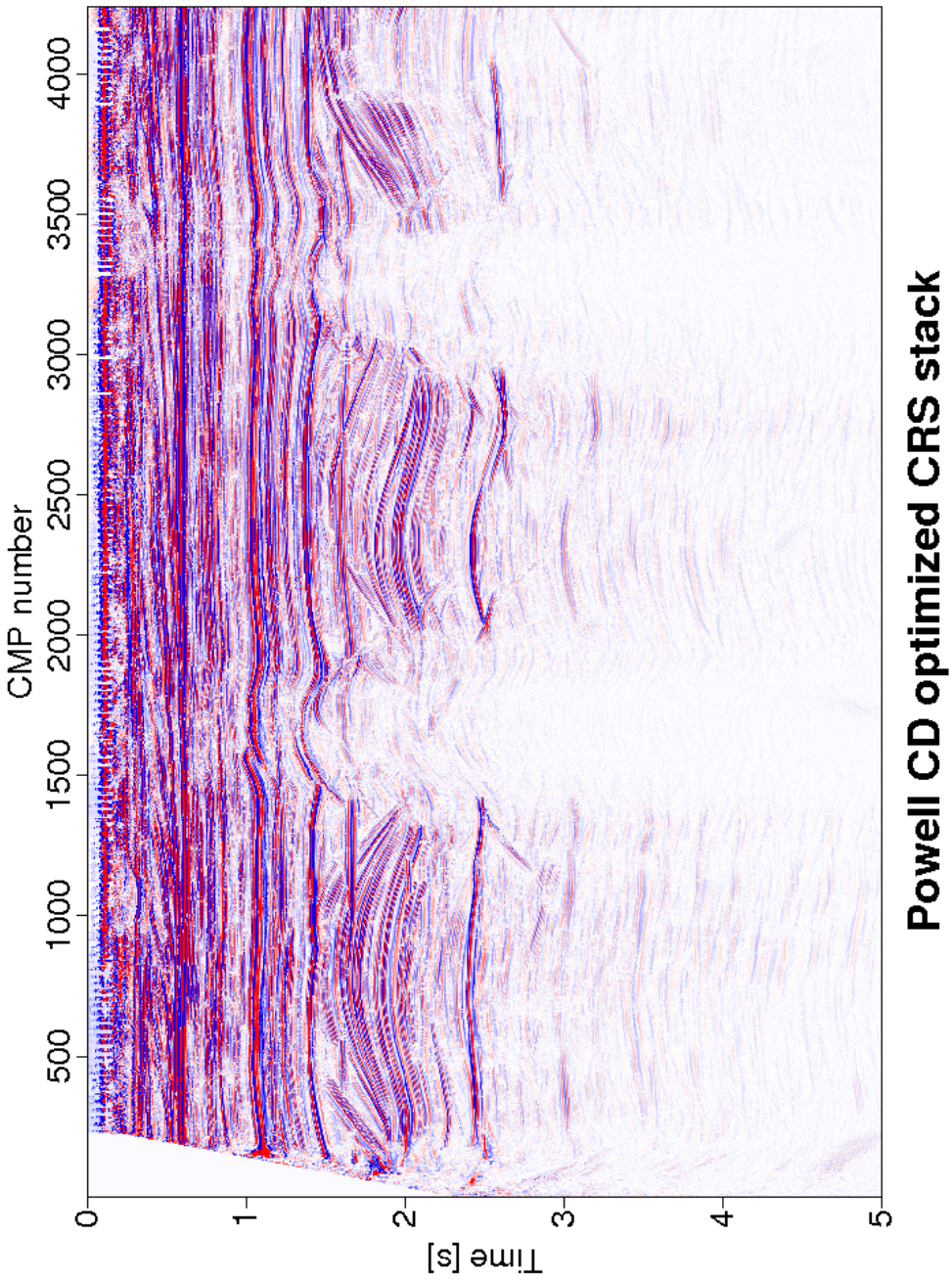

Figure 5.12: Field data: CRS stack result of the Powell CD optimization.

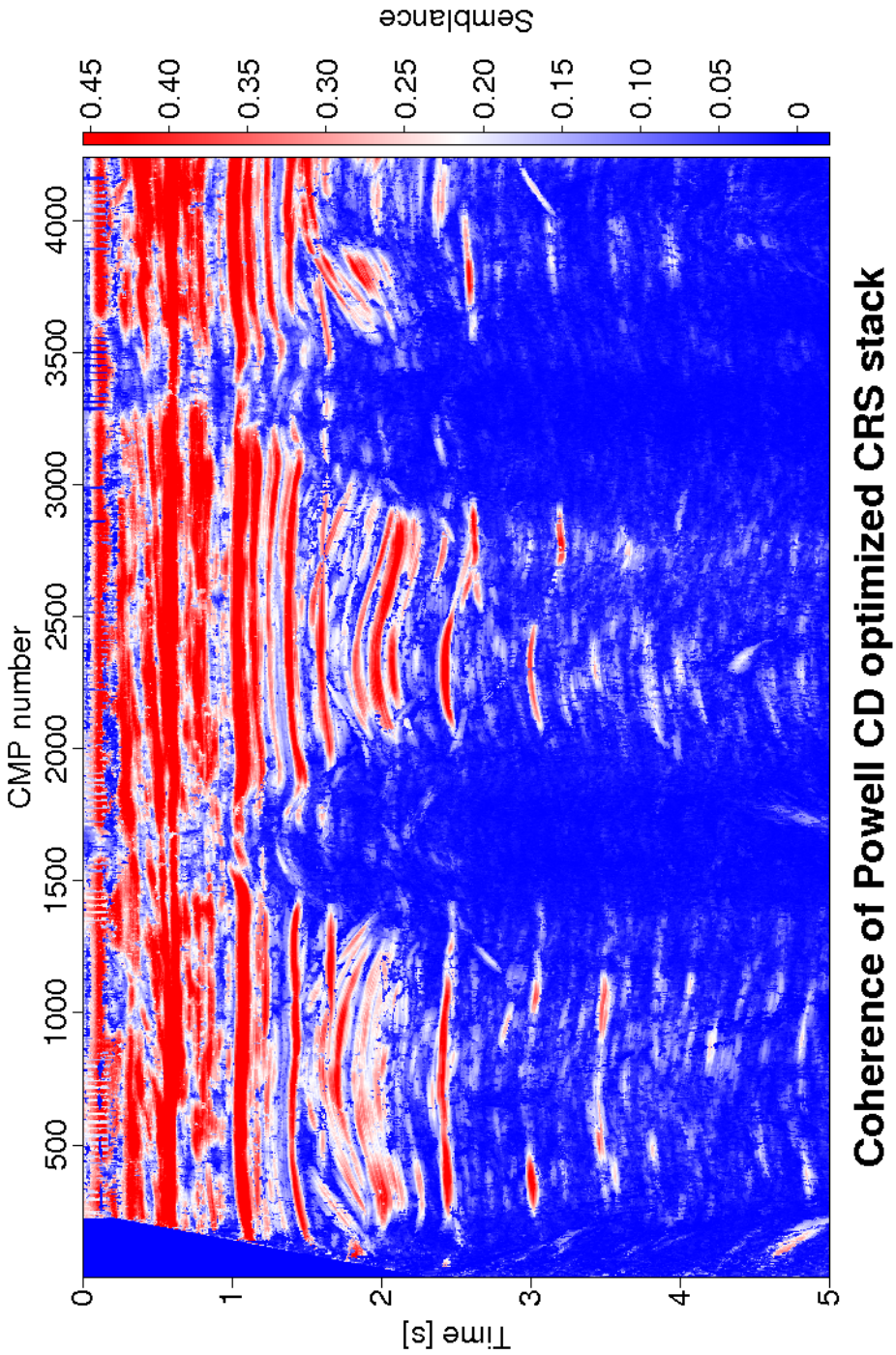

Figure 5.13: Field data: coherence section associated with the Powell CD optimized CRS stacked section shown in Figure 5.12 smoother than coherence section of the pragmatic approach shown in Figure 5.5.

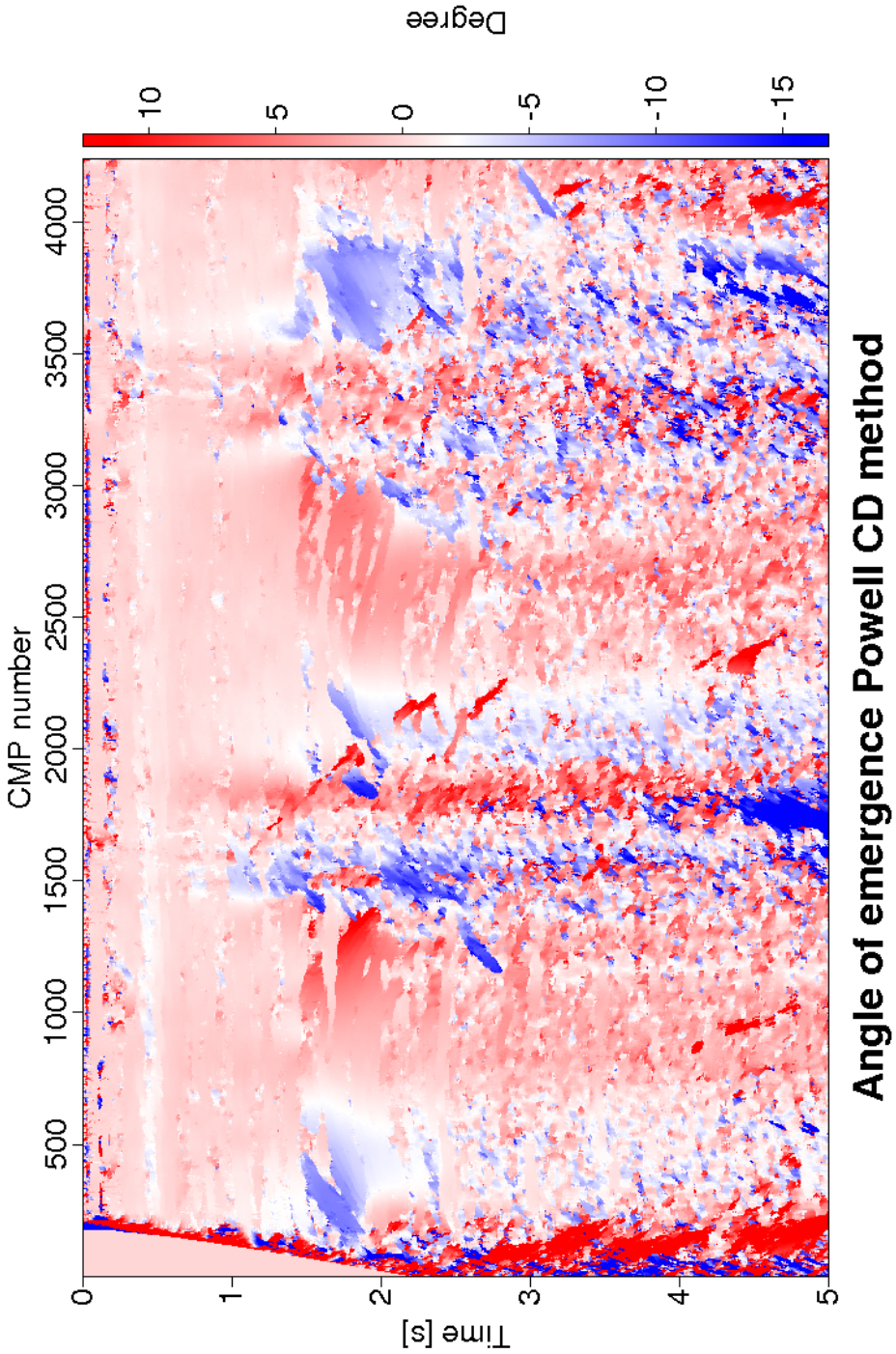

Figure 5.14: Field data: angle of emergence associated with the Powell CD optimized CRS stacked section shown in Figure 5.12.

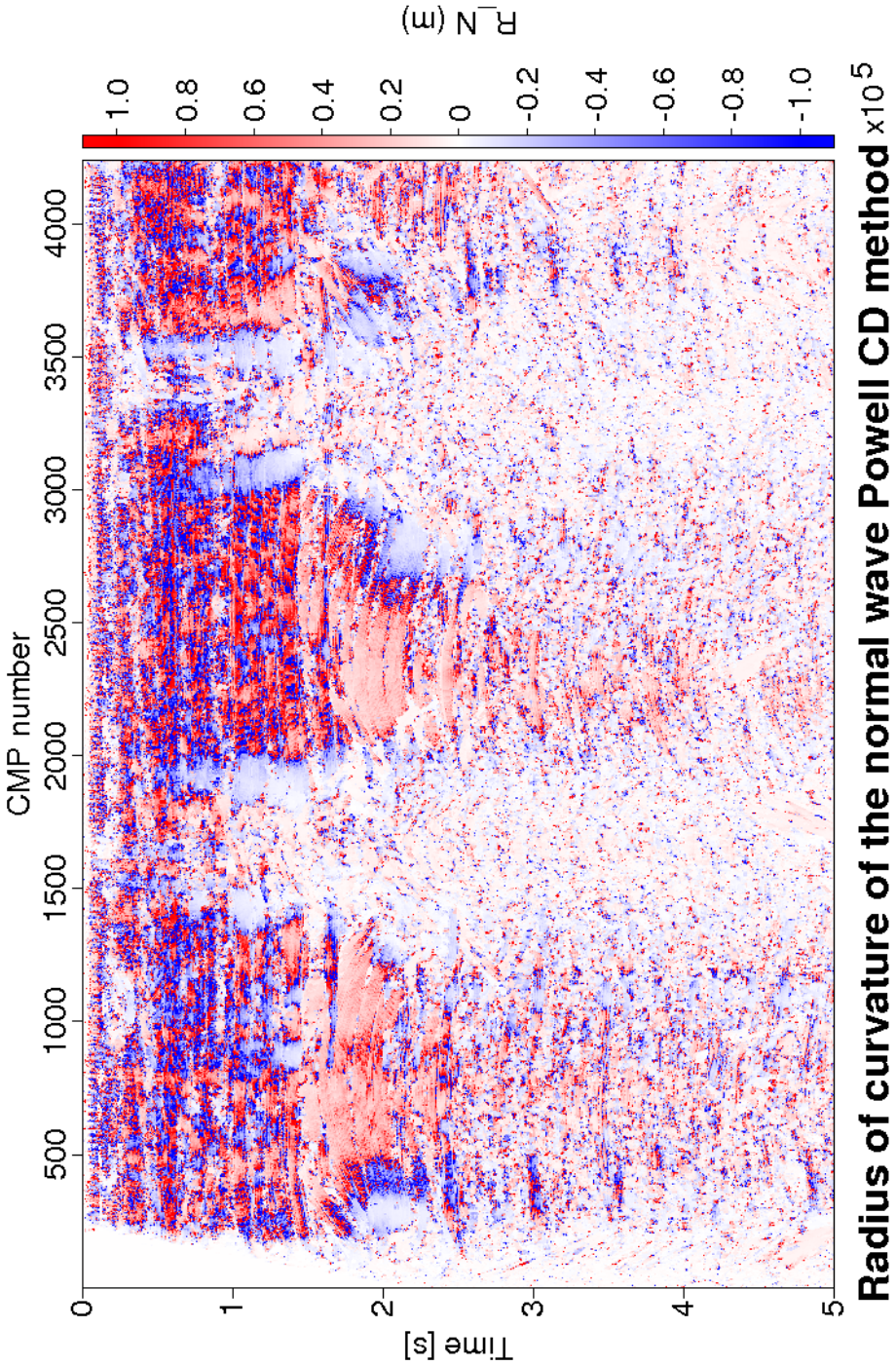

Figure 5.15: Field data: radius of curvature of the normal wave associated with the Powell CD optimized CRS stacked section shown in Figure 5.12.

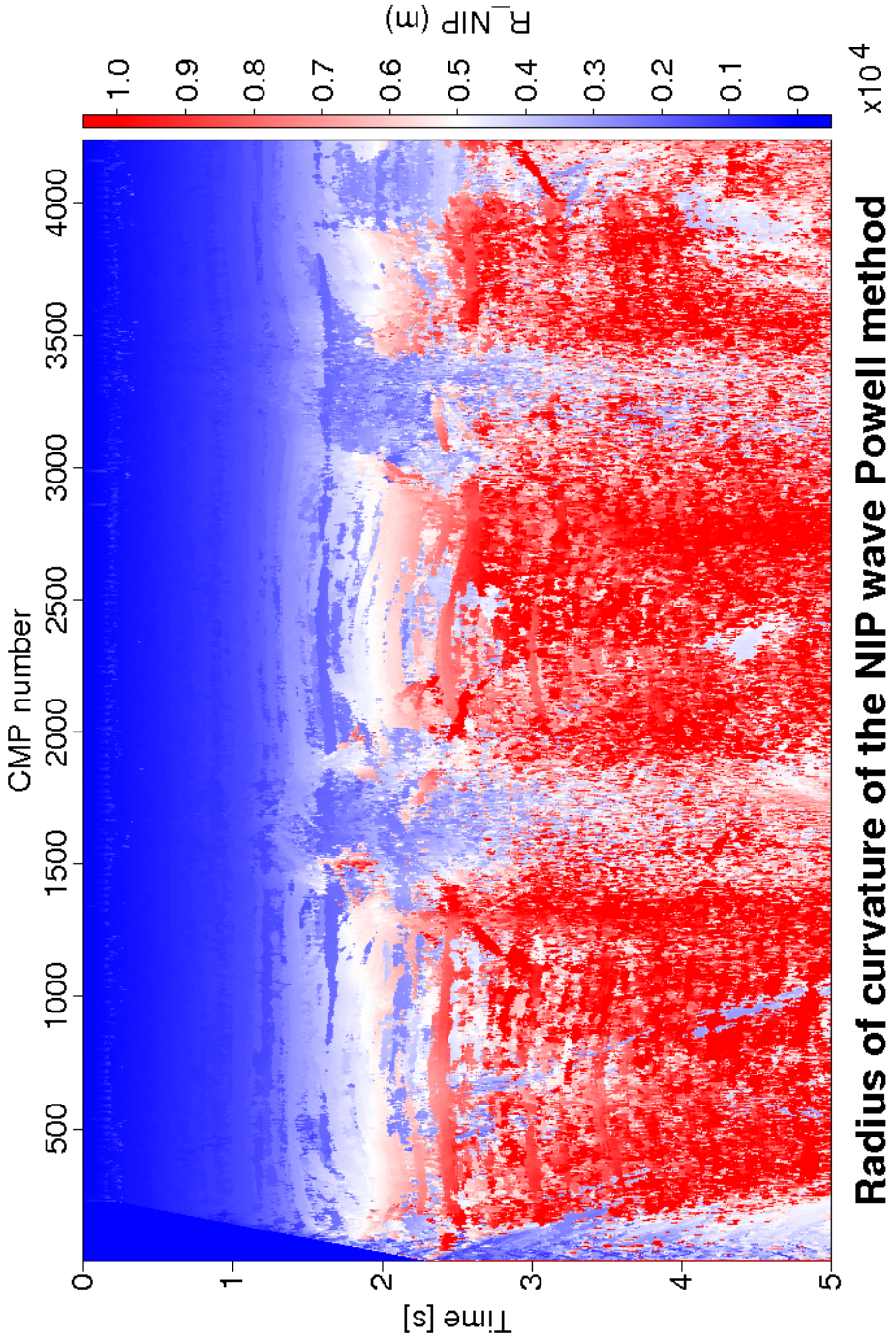

Figure 5.16: Field data: radius of curvature of the NIP wave associated with the Powell CD optimized CRS stacked section shown in Figure 5.12.

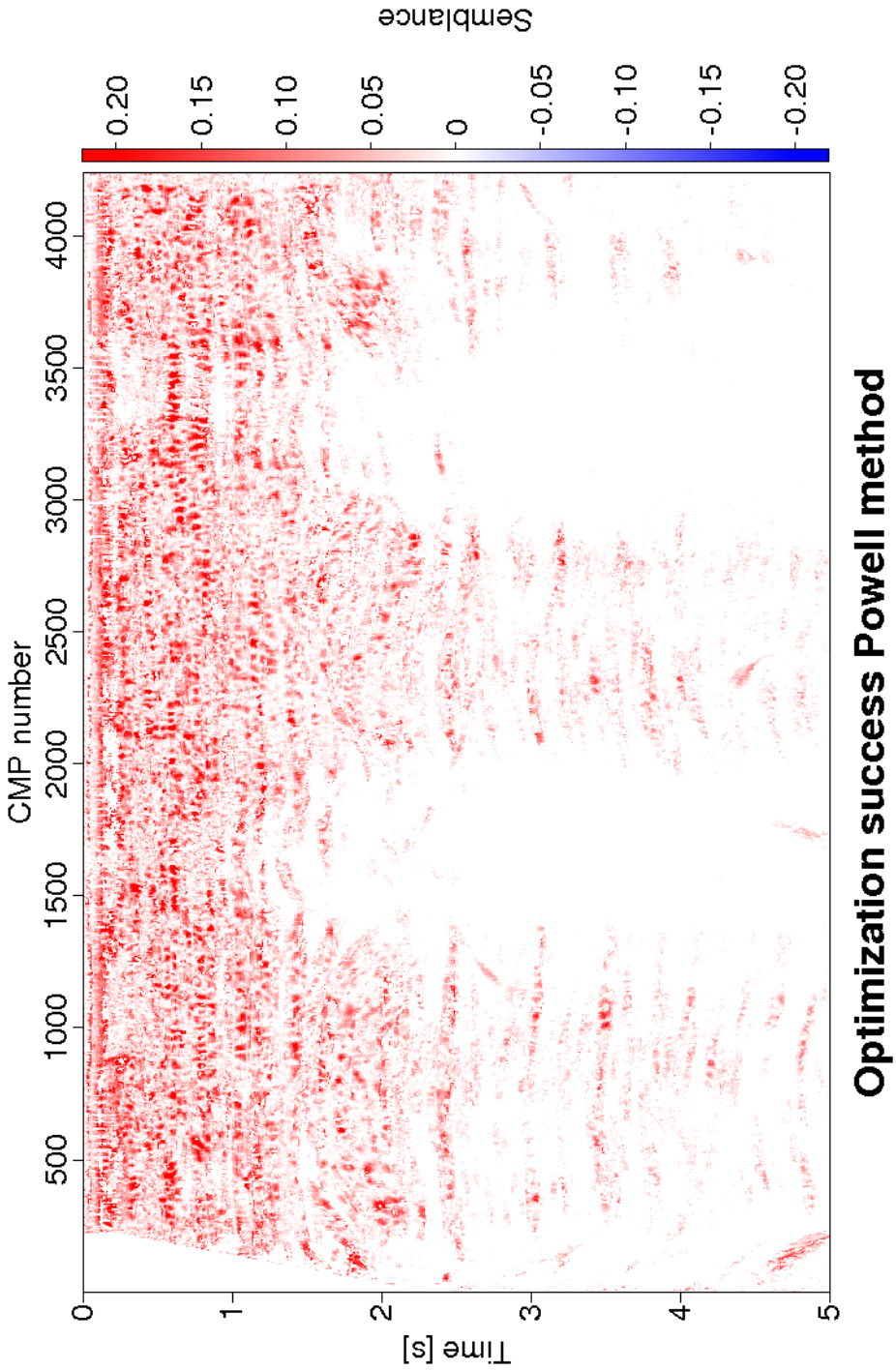

Figure 5.17: Field data: difference in coherence between the pragmatic approach CRS stacked section (Figure 5.5) and the Powell conjugate direction optimized CRS stacked section (Figure 5.13).

Figure 5.18 shows enlarged images of the simultaneous optimized CRS stacked sections for the Nelder Mead optimization method and the Powell conjugate direction method in the areas of CMP 1100-2200. Overall both images almost look similar and no differences can be observed between the Nelder Mead stacked section and the Powell conjugate direction stacked section (Figure 5.18b). Computational time on field data was 2 times faster than the Nelder Mead stacked section (Figure 5.18a).

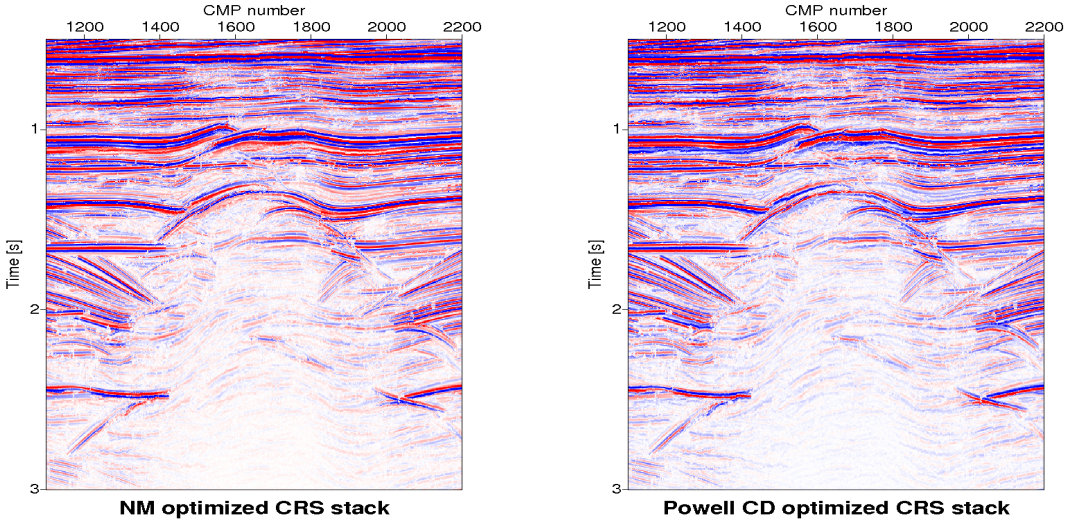

(a) (b)

Figure 5.18: ZO CRS stacked sections: comparison between the Nelder Mead optimization method and Powell conjugate direction optimization method with the same initial values in the areas of CMP 1100-2200. The Powell conjugate direction optimization method (b) is 2 times faster in computational time compared to the Nelder Mead optimization method (a).

Figure 5.19 shows enlarged images of the coherence CRS stacked sections for the Nelder Mead optimization method and the Powell conjugate direction method in the areas of CMP 1100-2200. The Powell conjugate direction stacked section Figure 5.19b has a little bit scatter compared to the Nelder Mead stacked section Figure 5.19a. But both images are look similar and it does not appear that the differences in coherence sections has a major effect on the attributes (shows in Figure 5.20, Figure 5.21, and Figure 5.22).

Figure 5.20 shows enlarge the angle of emergence sections, α, for the Nelder mead optimization method and the Powell conjugate direction method in the areas of CMP 1100-2200. Both sections are very similar and no differences can be observed.

Figure 5.21 and Figure 5.22 show enlarge radius of curvature of the N wave sections, R_N, and radius of curvature of the NIP wave sections, R_{NIP}, for the Nelder mead optimization method and the Powell conjugate direction method in the areas of CMP 1100-2200. Both sections are very similar and no differences can be observed.

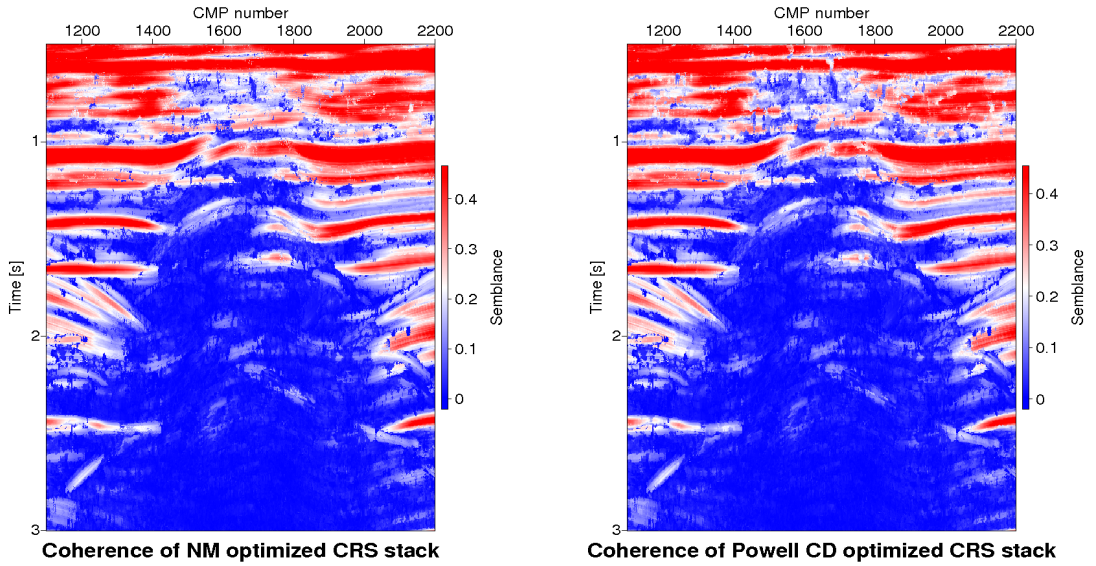

(a) (b)

Figure 5.19: Coherence section: comparison between the Nelder Mead optimization method (a) and Powell conjugate direction optimization method (b) in the areas of CMP 1100-2200. The stacks of both methods look similar and it does not appear that the differences in coherence has a major effect on the attributes.

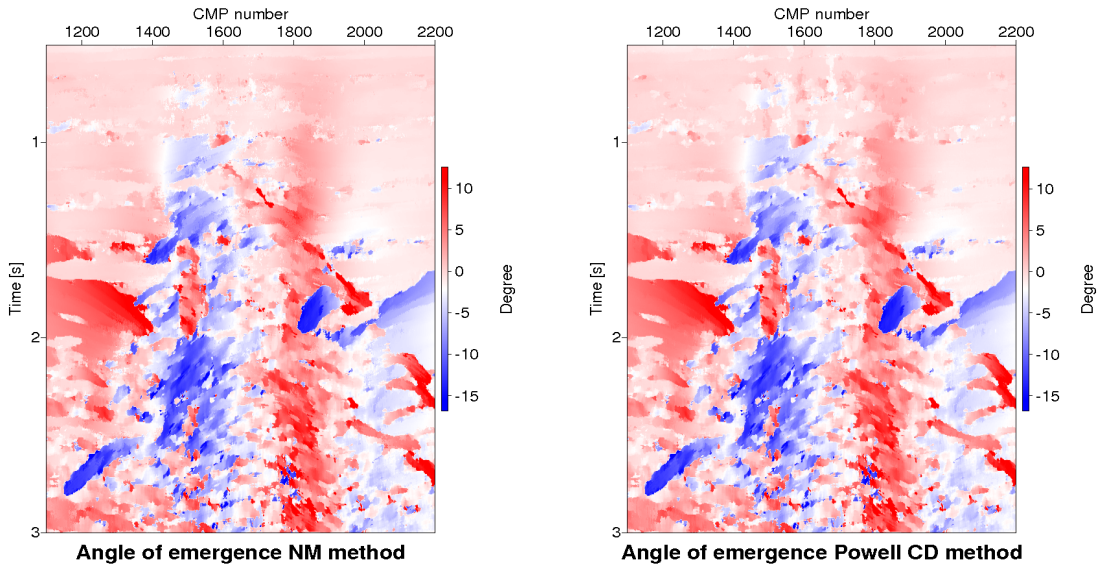

(a) (b)

Figure 5.20: Results of the automatic CRS parameter searches: α. Angle of emergence section for Nelder Mead optimization method (a) and Powell conjugate direction optimization method (b) in the areas of CMP 1100-2200. Both sections are very similar and no specific differences can be observed.

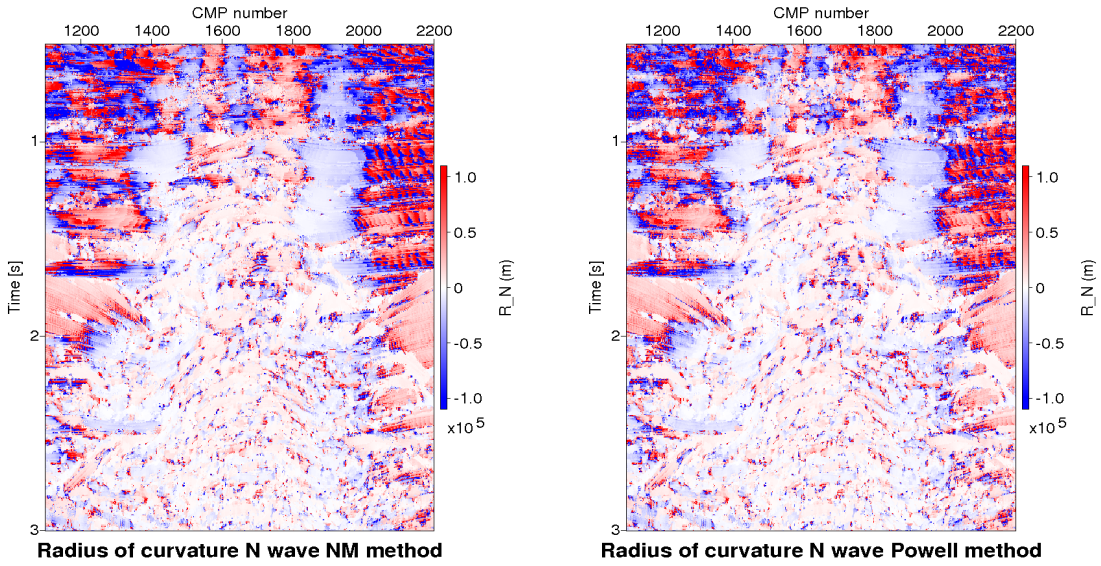

(a) (b)

Figure 5.21: Results of the automatic CRS parameter searches: R_N. Radius of curvature of the N wave section for Nelder Mead optimization method (a) and Powell conjugate direction optimization method (b) in the areas of CMP 1100-2200. Both sections are very similar and no specific differences can be observed.

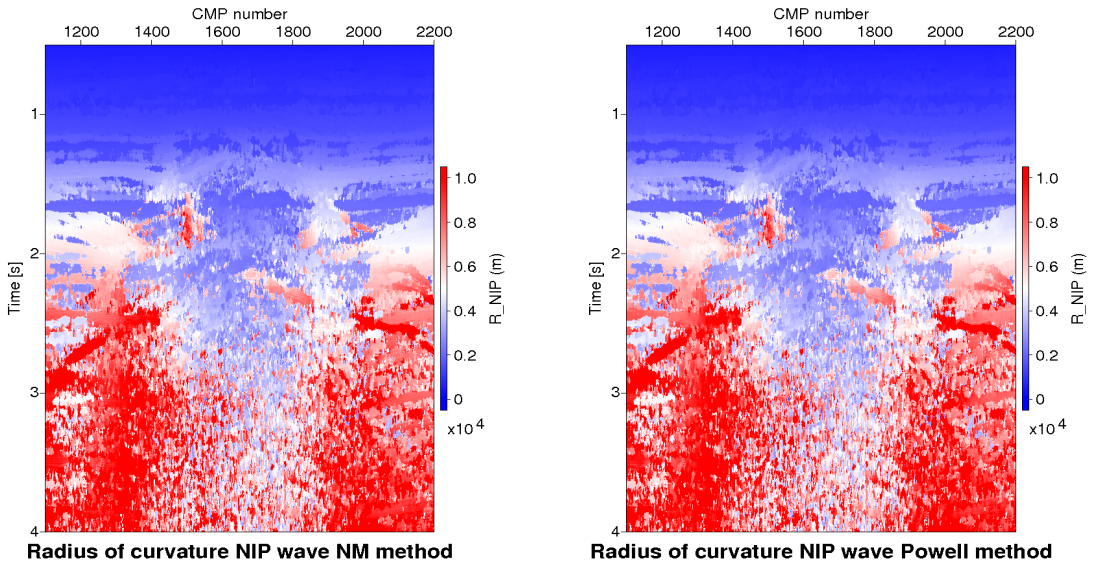

(a) (b)

Figure 5.22: Results of the automatic CRS parameter searches: R_{NIP}. Radius of curvature of the NIP wave section for Nelder Mead optimization method (a) and Powell conjugate direction optimization method (b) in the areas of CMP 1100-2200. Both sections look similar and no specific differences can be observed.

5.3 Conclusions

The application of the simultaneous optimization of the CRS stack method on the field data set shows that the new method has a substantial computational advantage against the Nelder Mead method currently used in the CRS attribute search. A factor of 2 in computing time was observed for the simultaneous search of the parameters in the 2-D CRS stack using the Powell conjugate direction approach. Results of the automatic three attributes CRS parameter searches obtained with the Powell conjugate direction method are very similar and no differences can be observed compared to the Nelder Mead method currently used in the CRS attributes search.

The Powell conjugate direction optimization method increased the continuity of reflection events most significantly, and also improved the signal-to-noise (S/N) ratio compared to the CMP stacked section. This quality improvement is observed at the top of the salt plugs and in deeper section below 2.5 s traveltime. Structurally, the study area can be subdivided into three major parts: Tertiary, Upper Cretaceous, and Zechstein. Most horizons have continuous structures and can be easily identified. The base of Tertiary at 1 s traveltime, the base of Upper Cretaceous at 1.5 s traveltime, and the base of Zechstein at 2.5 s traveltime are well identified. Such an inversion algorithm of the attributes, the CRS wavefield attributes provide the information required to build a depth model. Although the performance of the CRS stack strongly depends on the local complexity of the recorded wavefield. Nevertheless, all primary events that can be sufficiently accurately approximated by a hyperboloid given by the CRS stacking operator are well imaged in the CRS stacked section.

Chapter 6

Global optimization method

This chapter shows the application of the global optimization method using an arbitrary initial guess to demonstrate the advantages of this method in finding the solution to avoid being trapped into local solutions. The pragmatic approach based on three one-parameter search processes to define the CRS parameters as an input for the initial values for the optimization procedure can be replaced based on a priori information for the geological structure, best guess or local slopes (Santos et al., 2011). I investigated the optimization results based on the choice of the initial values to demonstrate the advantages of this method finding the solution. In this implementation we still using the pragmatic approach results for the R_{NIP} and R_N as an initial values, and the arbitrary value for the angle.

6.1 Synthetic data example

I used the same acquisition parameters of the pre-stack data and the basic processing parameters for the zero-offset simulation of the CRS stack for the Sigsbee synthetic data as compiled in Table 4.1 and Table 4.2, respectively. The optimization of the CRS processing procedure started with the three parameters which the arbitrary angle and R_{NIP} and R_N from the pragmatic approach results as an initial values. Then we compared the results of both method between the Powell conjugate direction optimization method and the Nelder Mead optimization method.

Figure 6.1 shows enlarged images of the coherence CRS stacked sections for the Nelder Mead optimization method and the Powell conjugate direction method. The coherence of the Nelder Mead method Figure 6.1a has a little bit scatter compared to the coherence Powell conjugate direction stacked section Figure 6.1b. This case shows the advantages of using the new method. This is possible because the strict procedures in the search of direction to avoid the wrong solutions into local minima.

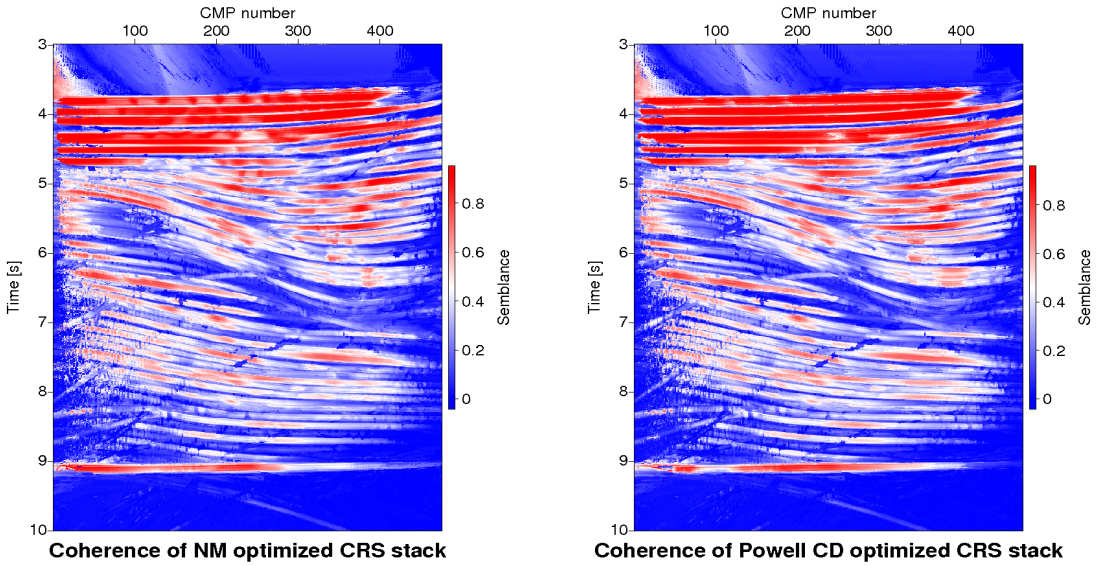

(a) (b)

Figure 6.1: Coherence section of CRS stacked: comparison between coherence of NM optimized CRS stack (a) and coherence of Powell CD optimized CRS stack (b). coherence of Powell CD optimized CRS stack (b) more smooth and better than coherence of NM optimized CRS stack (a).

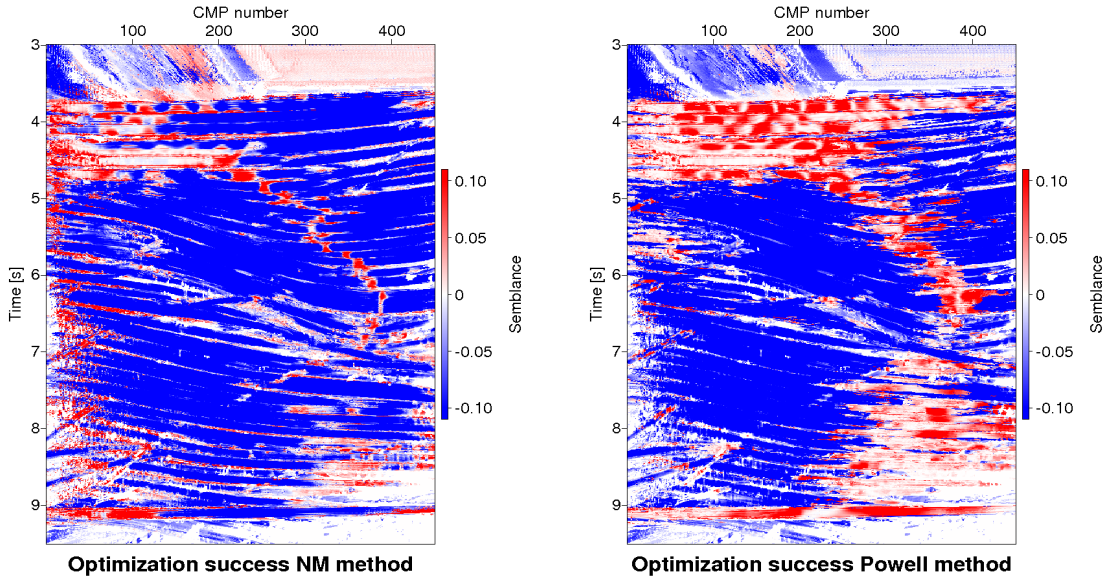

(a) (b)

Figure 6.2: Improvement of the coherence section between initial CRS stack and Powell conjugate direction optimized method (Figure 6.2b) compared to the coherence section between initial CRS stack and Nelder Mead optimized method (Figure 6.2a).

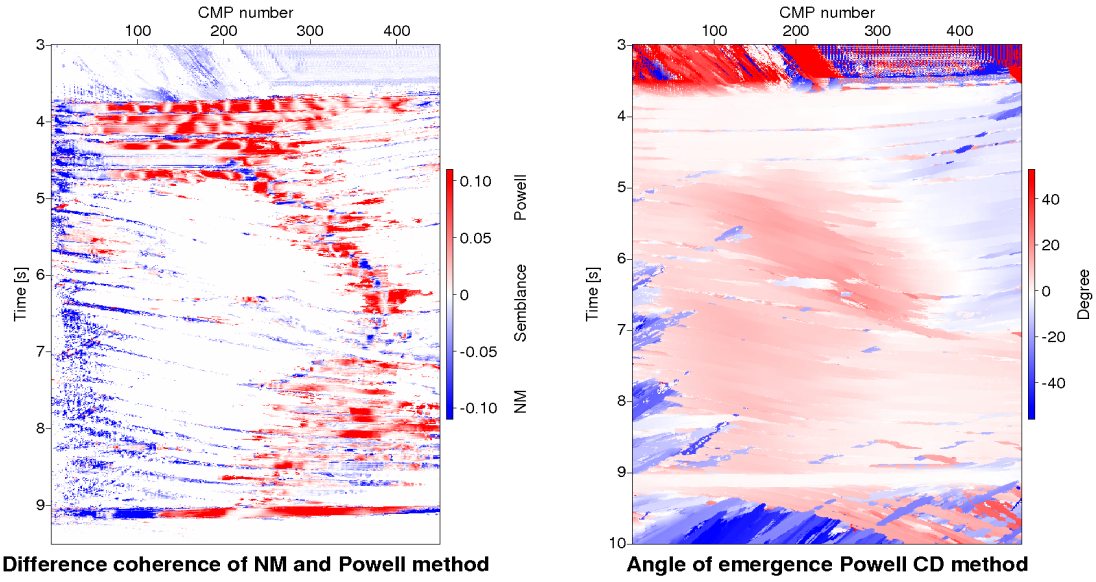

(a) (b)

Figure 6.3: Differences in coherence between the NM optimized CRS stack and Powell CD optimized CRS stack (a) and results of the automatic CRS parameter searches: α, angle of emergence section Powell CD method (b).

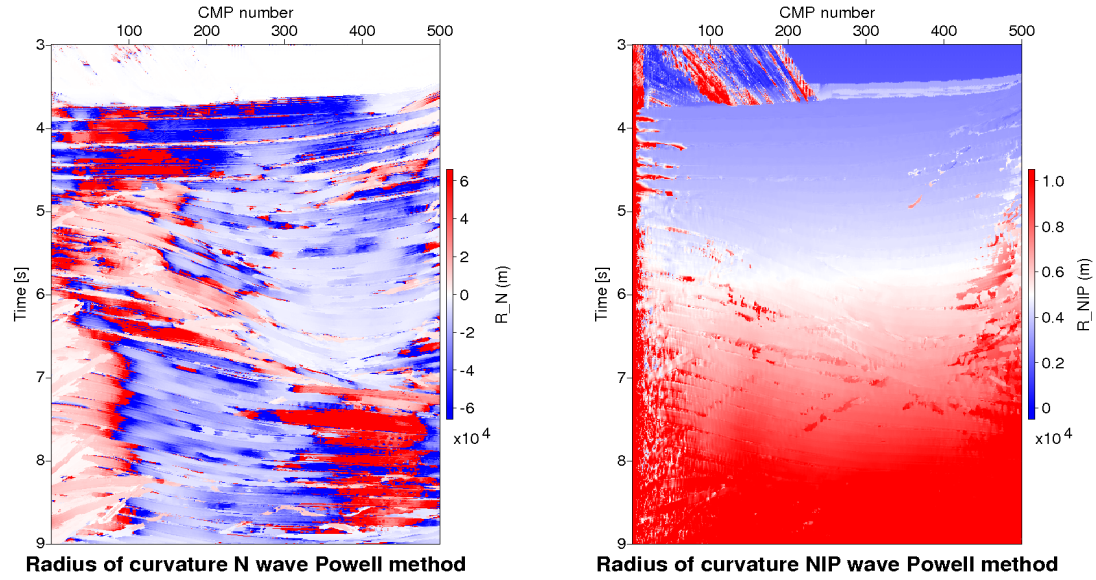

(a) (b)

Figure 6.4: Results of the automatic CRS parameter searches: R_N and R_{NIP}, radius of curvature of N wave section (a) and radius of curvature of NIP wave section (b) for the Powell conjugate direction method.

The improvement of the coherence section between the NM optimized method and the Powell conjugate direction optimized method is shown in Figure 6.2. The coherence section associated with the Powell conjugate direction optimized method (Figure 6.2b) are smoother and continuous compared to the coherence section associated with the Nelder Mead optimized method (Figure 6.2a). Specific features of the Powell conjugate direction method include the strict procedures for the search of direction which allows better results. The computing time for the global optimization required 10 times slower when comparison which using the pragmatic approach as an initial values for the optimization procedure.

Figure 6.3a shows enlarged images of the differences of the coherence CRS stacked sections between the Nelder Mead optimization method and the Powell conjugate direction method. The superior improvement of the coherence section can readily be observed at the coherence section associated with the Powell conjugate direction optimized section compared to the Nelder Mead optimized section. Figure 6.3b, 6.4a and Figure 6.4b show enlarged image results of the automatic CRS parameter searches emergence angle sections, α, radius of curvature of the N wave section, R_N, and radius of curvature of the NIP wave section, R_{NIP}, for the Powell conjugate direction method. The three attributes search show similar results and no spesific differences can be observed with the results in chapter 4 (Figure 4.19b, 4.20b and Figure 4.21b). Figure 6.5 shows enlarged images of the simultaneous optimized CRS stacked sections for the Nelder Mead optimization method and the Powell conjugate direction method. The Powell conjugate direction stacked section (Figure 6.5b) displays the reflection more continues, more clearer and the reflectors are better defined compared to the Nelder Mead stacked section (Figure 6.5a).

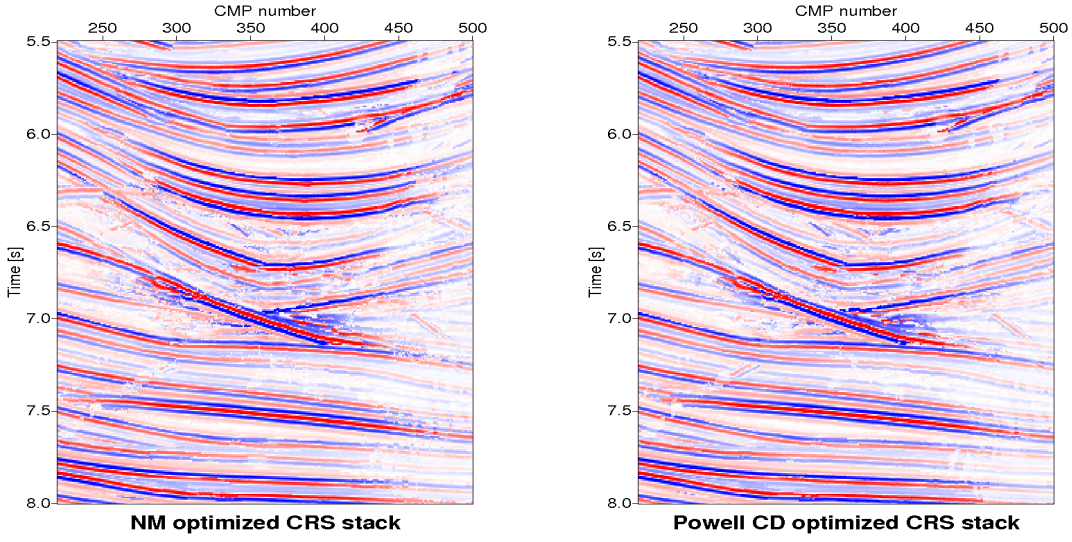

(a) (b)

Figure 6.5: ZO CRS stacked sections: comparison between the Nelder Mead method (a) and Powell conjugate direction method (b). Powell conjugate direction method stacked section has more clearer and the reflections better defined.

The CRS stacked section obtained with the Powell conjugate direction optimized method displayed in Figure 6.6 shows better continuity of horizons at all time levels and produced a better image of conflicting dip areas. We do not see specific differences in the stack sections for the Powell conjugate direction approach using initial values from the pragmatic approach result shown in Figure 4.11. These results indicate that the Powell conjugate direction method has advantages in dealing with the selection of initial value problems in finding a final solution which can not be done by the NM method currently used in the CRS attributes search. Possibility being trapped into local solutions to overcome the new method by applying strict procedures in the search direction.

The coherence section for the dominant events associated with the Powell conjugate direction optimized CRS stack is depicted in Figure 6.7. This figure looks similar to the Powell conjugate direction approach using initial values from the pragmatic approach result (Figure 4.12). The events associated with the highest coherence at each particular ZO location, allows to identify the detected events and to estimate the reliability of the image as well of its associated wavefield attributes.

Figure 6.8 to 6.10 display three CRS parameter sections. The optimized emergence angle section for the dominant events is shown in Figure 6.8. This image looks similar to the optimized emergence angle section of the Powell conjugate direction approach using initial values from the pragmatic approach result (Figure 4.13) and no specific differences can be observed. The consistency of the optimized emergence angle section can readily be observed, due to the simple relation between the emergence angle and the slopes of the ZO events.

The optimized radius of curvature of the normal wave section for the dominant events are depicted in Figure 6.9. This section looks similar to the Powell conjugate direction approach using initial values from the pragmatic approach result (Figure 4.14). The same applies to the section that is related to the curvature of the ZO events.

The optimized radius of curvature of the NIP wave for the dominant events are shown in Figure 6.10. This image looks similar to the Powell conjugate direction approach using initial values from the pragmatic approach result (Figure 4.15). For the stratified areas above and left to the salt, the values of R_{NIP} continously increases with increasing traveltime. Below the salt, the section is dominated by the tails of bow-tie structures and diffraction patterns stemming from the top and possibly also the botttom of the salt body.

Figure 6.11 display difference in coherence between the Nelder Mead optimization method and the Powell conjugate direction optimization method. The superior improvement of the coherence section can readily be observed by using the new method.

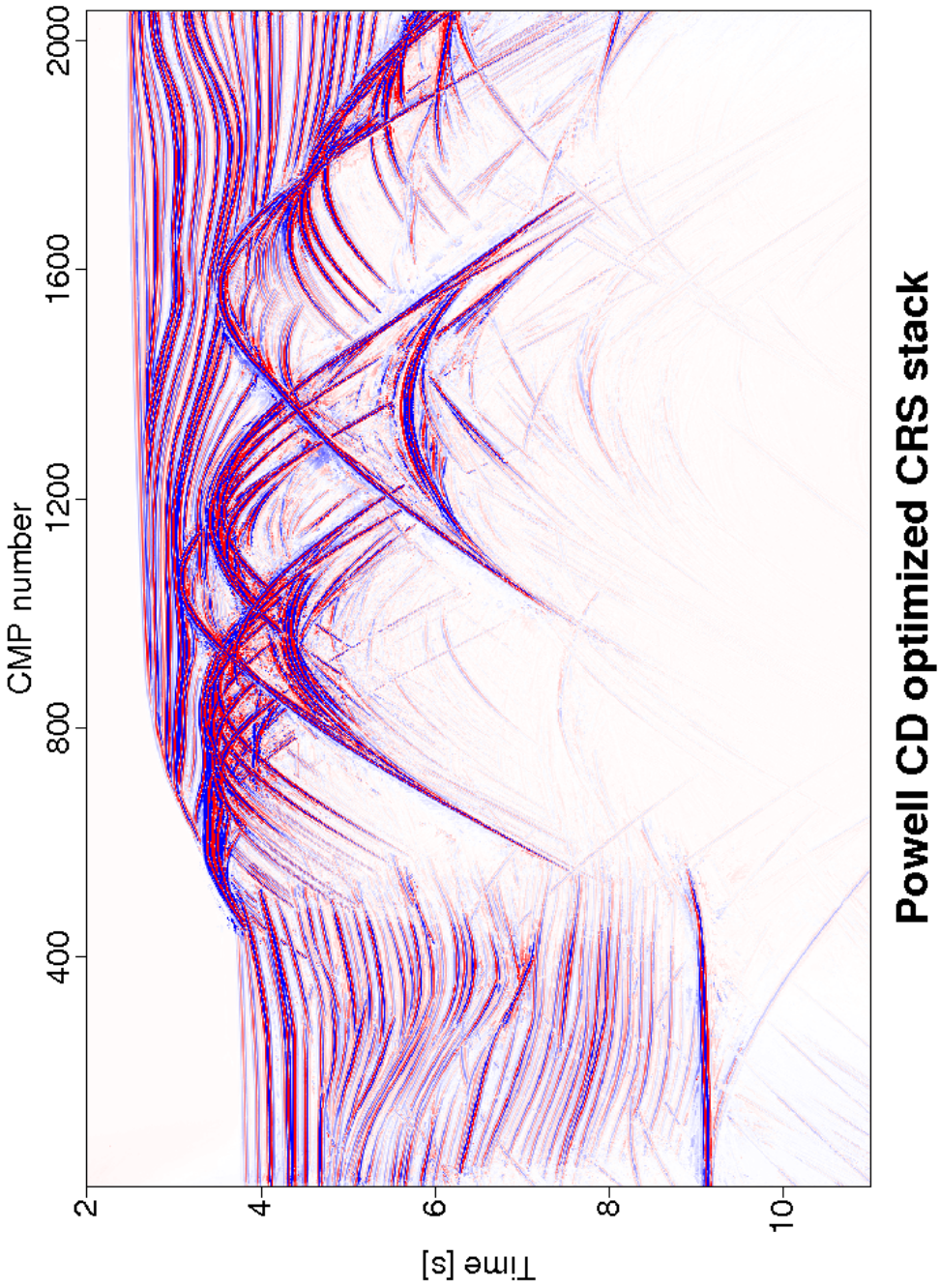

Figure 6.6: Global optimization Sigsbee data: CRS stack result of the Powell CD optimization.

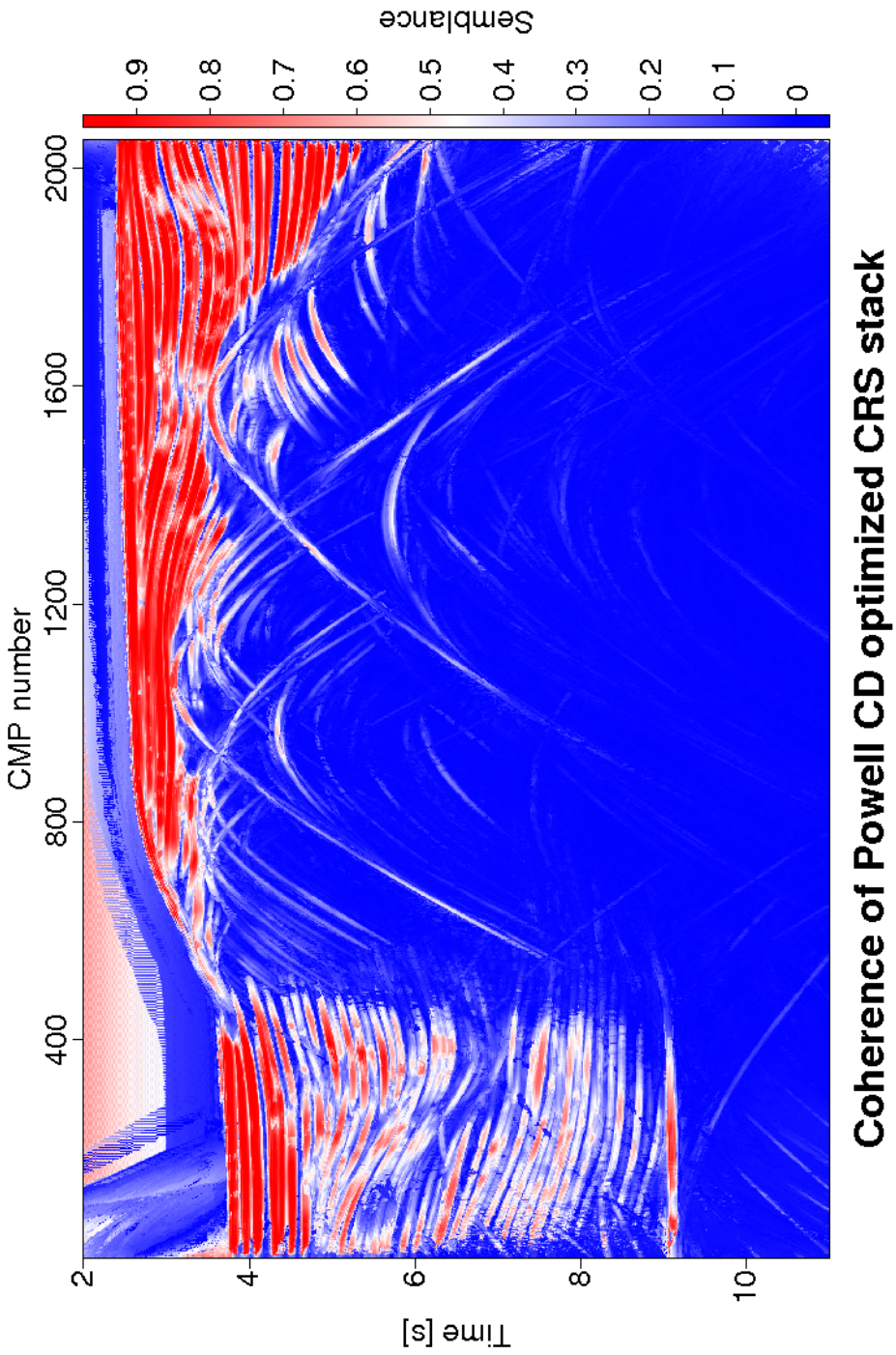

Figure 6.7: Global optimization Sigsbee data: coherence section associated with the Powell CD optimized CRS stacked section shown in Figure 6.6.

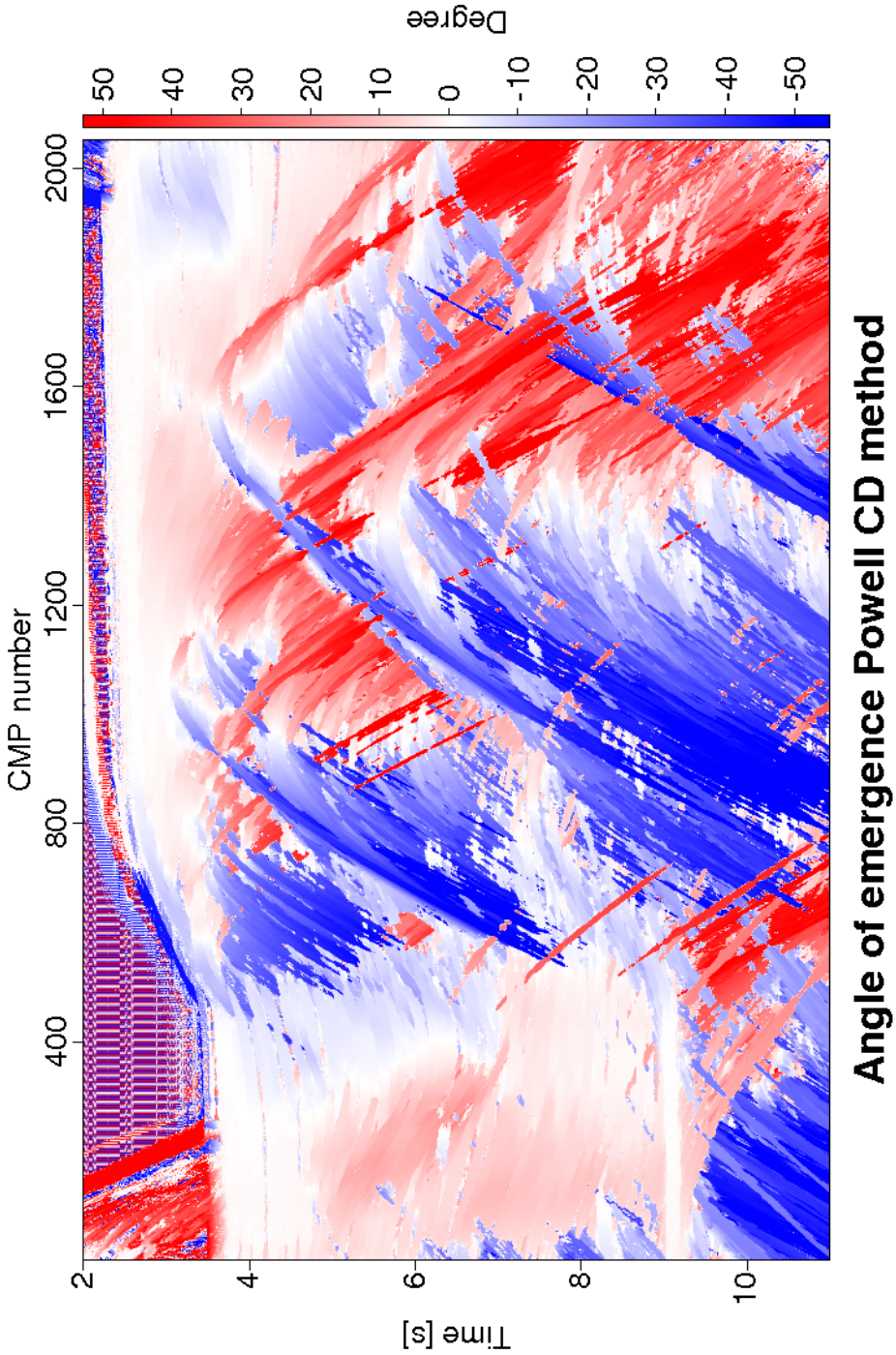

Figure 6.8: Global optimization Sigsbee data: angle of emergence associated with the Powell CD optimized CRS stacked section shown in Figure 6.6. These attributes are directly related to the slopes of the events.

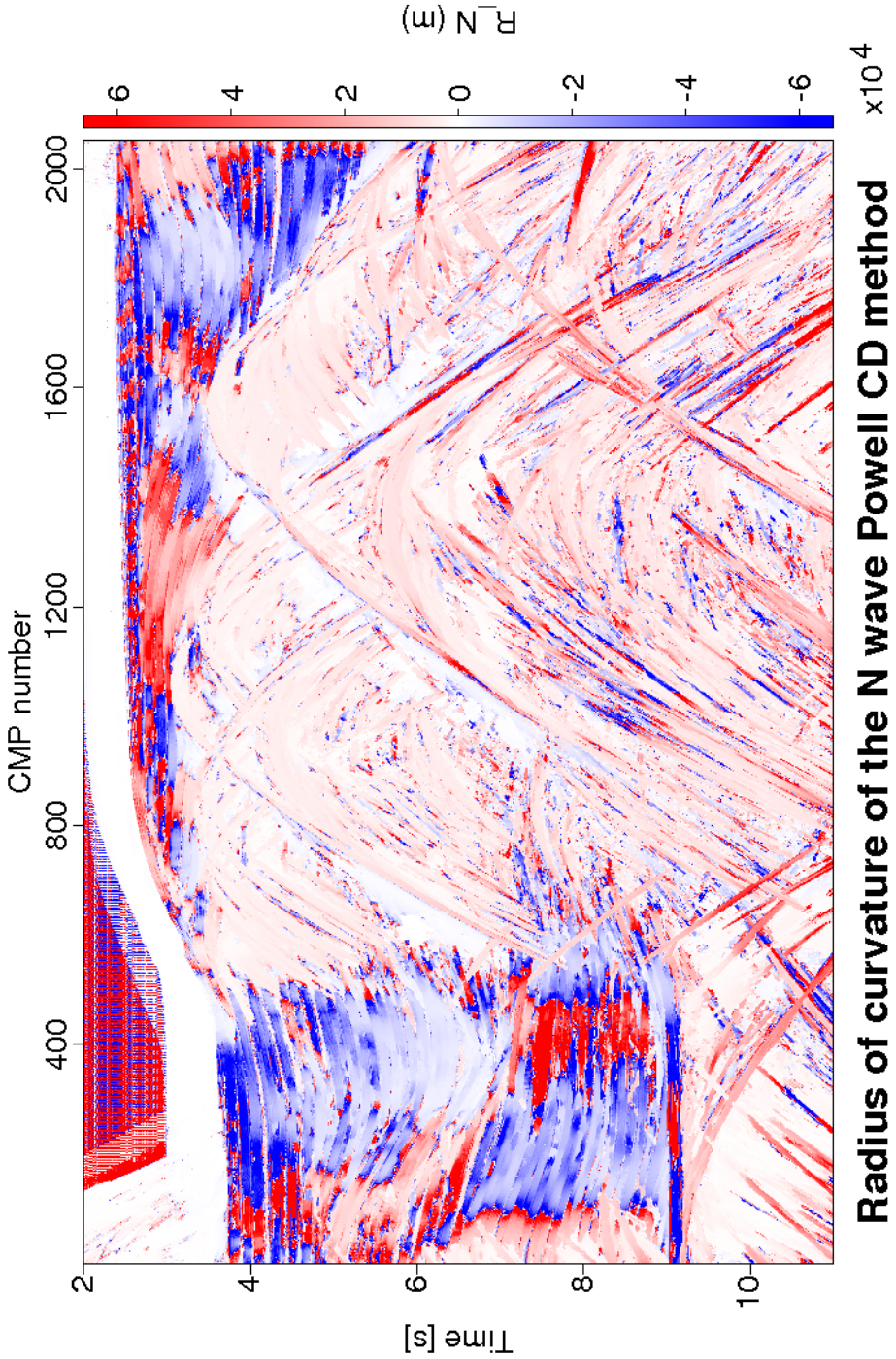

Figure 6.9: Global optimization Sigsbee data: radius of curvature of the normal wave associated with the Powell CD optimized CRS stacked section shown in Figure 6.6. These attributes are directly related to the curvatures of the events in the ZO section.

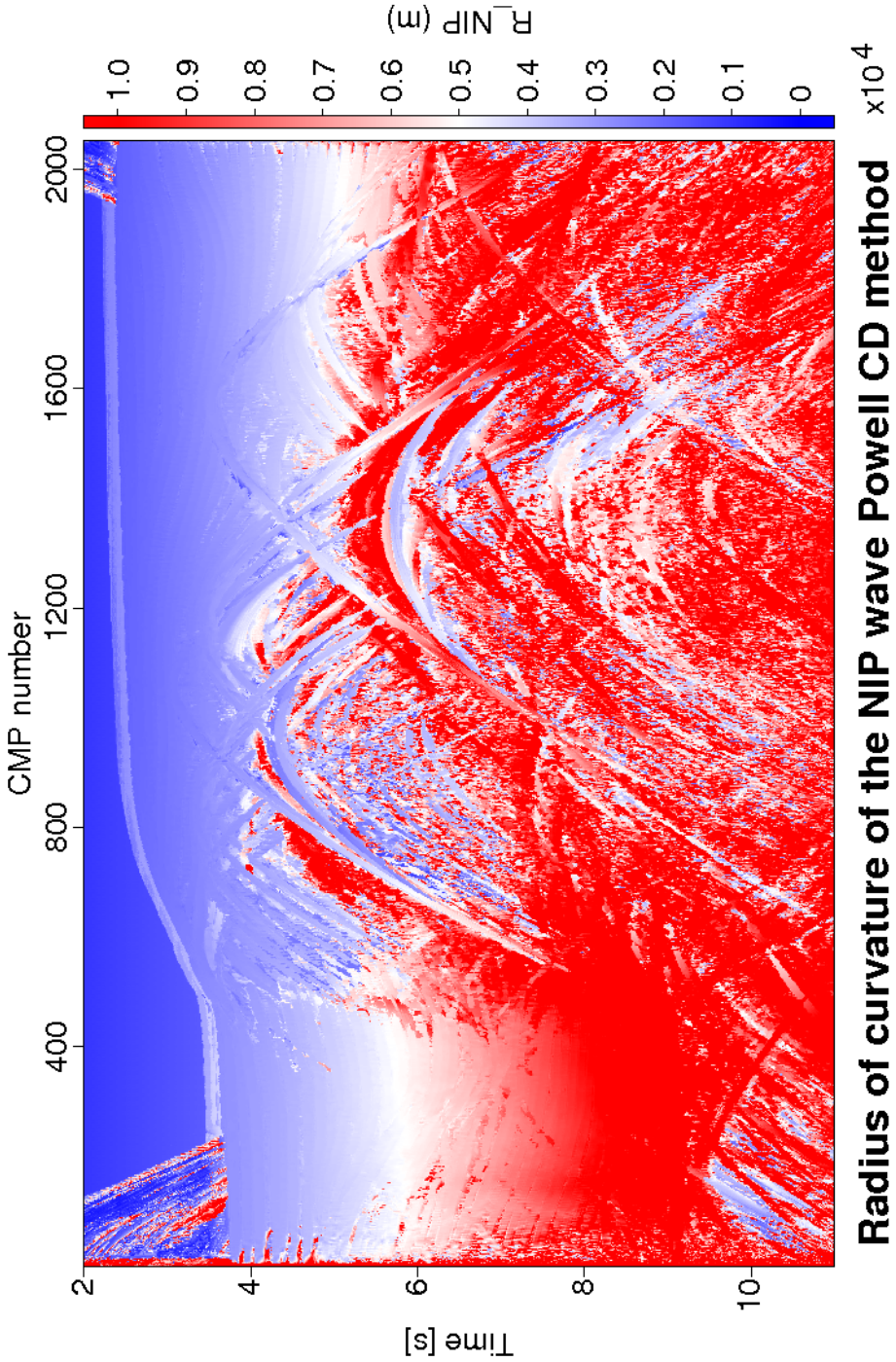

Figure 6.10: Global optimization Sigsbee data: radius of curvature of the NIP wave associated with the Powell CD optimized CRS stacked section shown in Figure 6.5. These section is calculated from the emergence angle section of the dominant events in Figure 6.8 and the stacking velocity section obtained from automatic CMP stack.

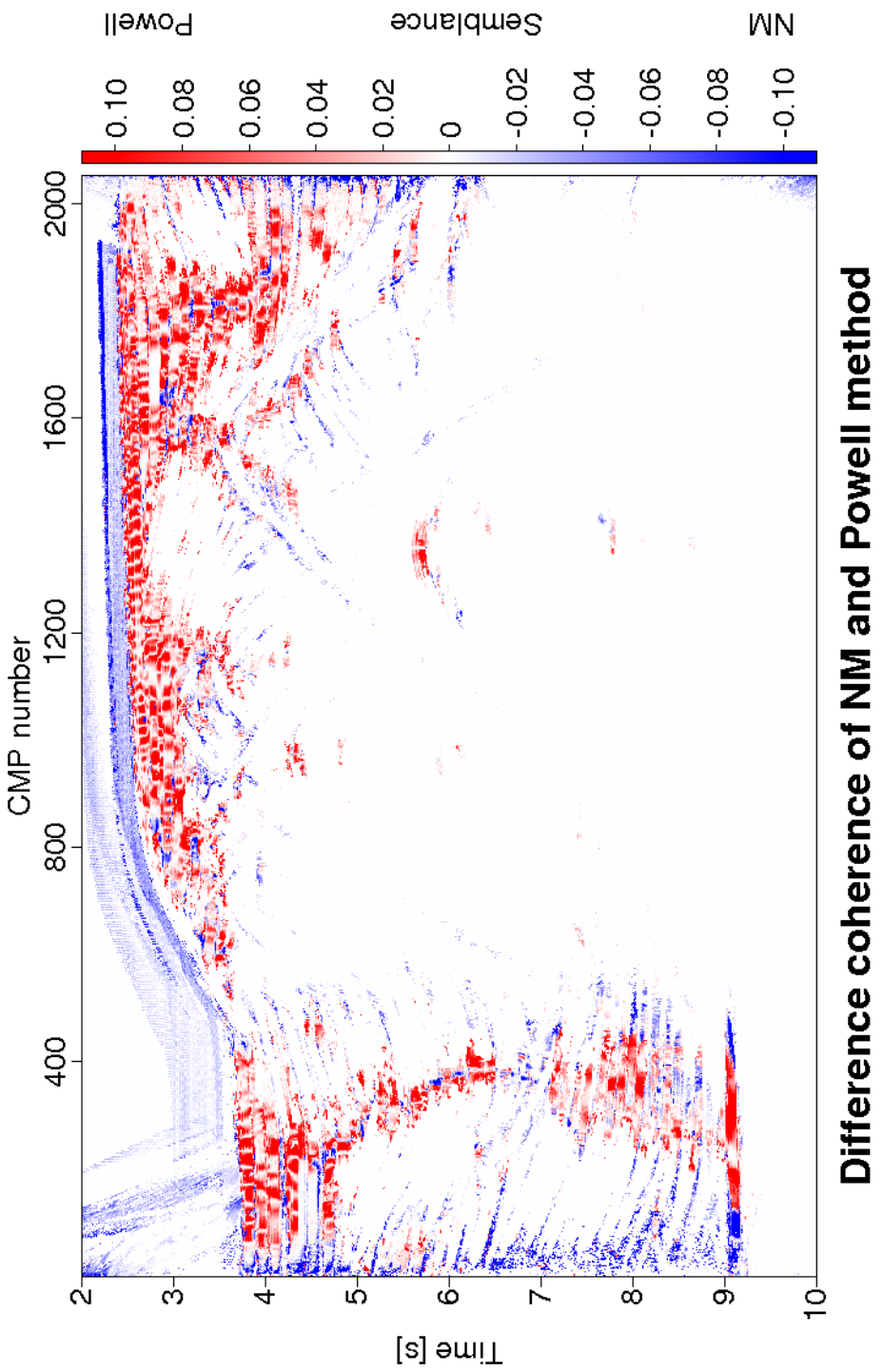

Figure 6.11: Global optimization Sigsbee data: difference in coherence between the Nelder Mead optimized method and the Powell conjugate direction optimized method.

6.2 Field data example

I used the same acquisition parameters and the basic processing parameters for the zero-offset simulation of CRS stack for the field data as compiled in Table 5.1 and Table 5.2, respectively.

Figure 6.12 shows enlarged images of the coherence CRS stacked sections for the Nelder Mead optimization method and the Powell conjugate direction optimization method. The coherence section of the Powell conjugate direction method Figure 6.12b appear more smooth and improved compared to the coherence section of the Nelder Mead method Figure 6.12a.

The improvement coherence section between initial CRS stack and the Nelder Mead optimized method compared to the coherence section between initial CRS stack and the Powell conjugate direction optimized method is shown in Figure 6.13. Coherence section associated with the Powell conjugate direction optimized method (Figure 6.13b) more smooth and continue compared to the coherence section associated with the Nelder Mead optimized method (Figure 6.13a). Specific features of the Powell conjugate direction method in the strict procedures the search of direction which allow better result. The computing time for the global optimization required 20 times slower when comparison which using the pragmatic approach as an initial values for the optimization procedure.

The superior improvement of the coherence section can readily be observed at the coherence section associated with the Powell conjugate direction optimized section. Figure 6.14a shows enlarged images the differences of the coherence CRS stacked sections between the Nelder Mead optimization method and the Powell conjugate direction method.

Figure 6.14b, 6.15a and Figure 6.15b show enlarged images of the automatic CRS parameter searches for the emergence angle sections, α, radius of curvature for the N wave section, R_N, and radius of curvature for the NIP wave section, R_{NIP}, for the Powell conjugate direction method. The three attributes search shows the similar results and no spesific differences can be observed with the results in chapter 5 (Figure 5.20b, 5.21b and Figure 5.22b).

Figure 6.16 shows enlarged images of the simultaneous optimized CRS stacked sections for the Nelder Mead optimization method and the Powell conjugate direction method. The Powell conjugate direction stacked section (Figure 6.16b) displays the reflection more continues, more clearer and the reflectors are better defined compared to the Nelder Mead stacked section (Figure 6.16a).

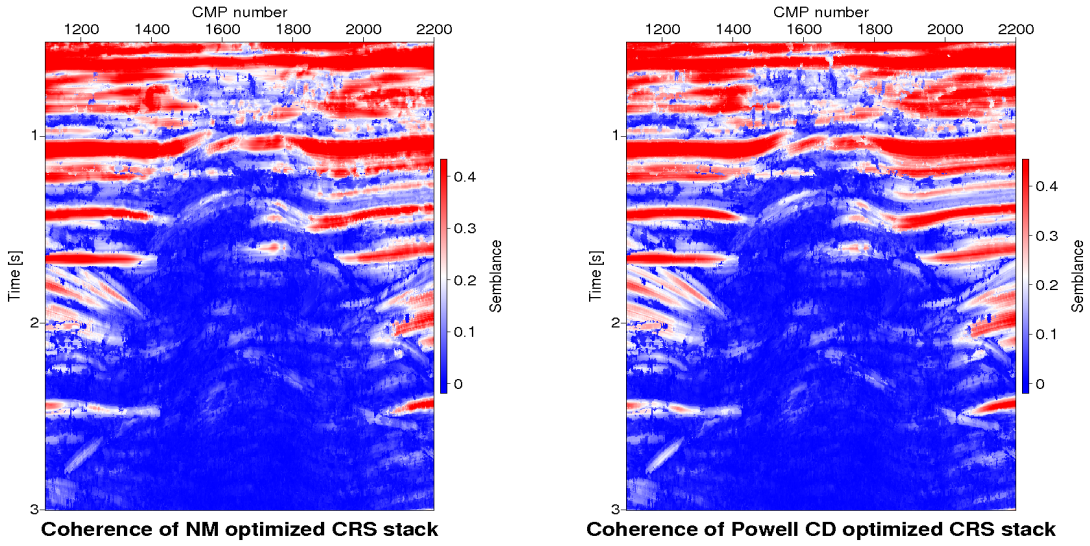

(a) (b)

Figure 6.12: Coherence section of CRS stacked: comparison between coherence of NM optimized CRS stack (a) and coherence of Powell CD optimized CRS stack (b). coherence of Powell CD optimized CRS stack (b) more smooth and better than coherence of NM optimized CRS stack (a).

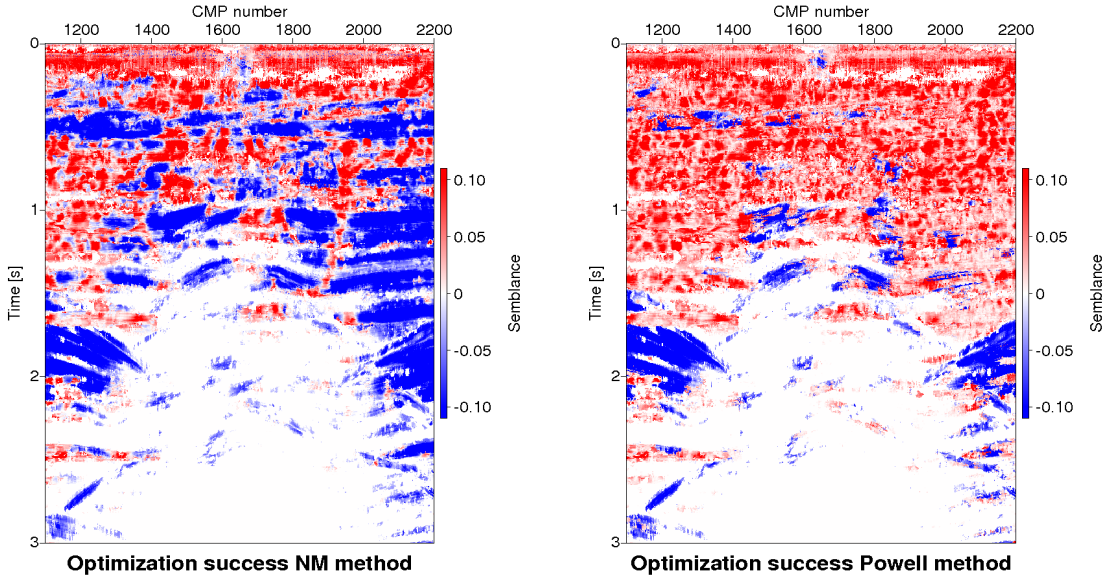

(a) (b)

Figure 6.13: Improvement of the coherence section between initial CRS stack and the Powell conjugate direction optimized method (Figure 6.15b) compared to the coherence section between initial CRS stack and the Nelder Mead optimized method (Figure 6.15a).

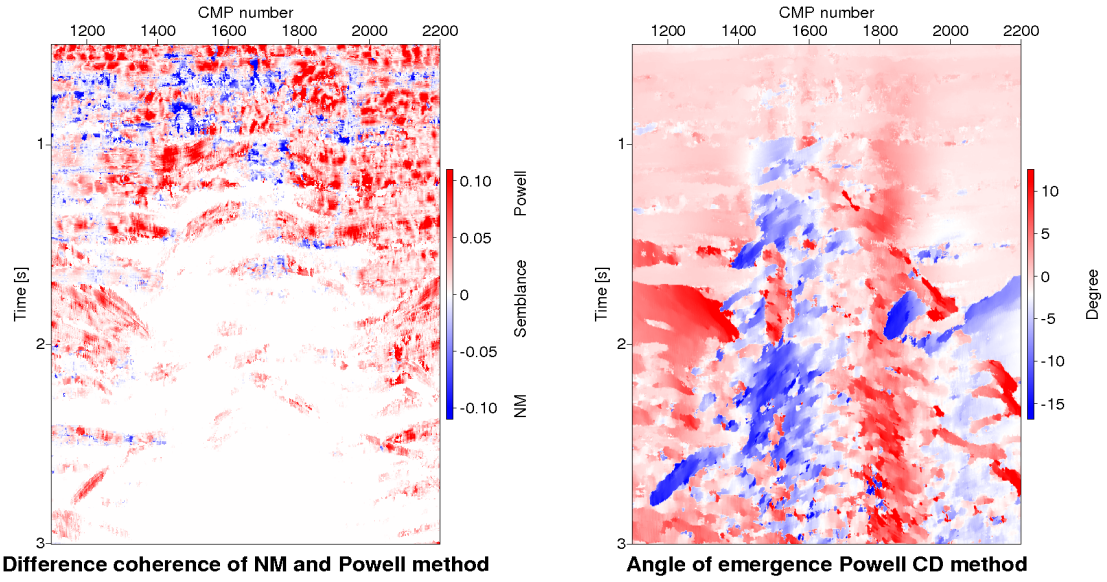

(a) (b)

Figure 6.14: Differences in coherence between the NM optimized CRS stack and Powell CD optimized CRS stack (a) and results of the automatic CRS parameter searches: α, angle of emergence section Powell CD method (b).

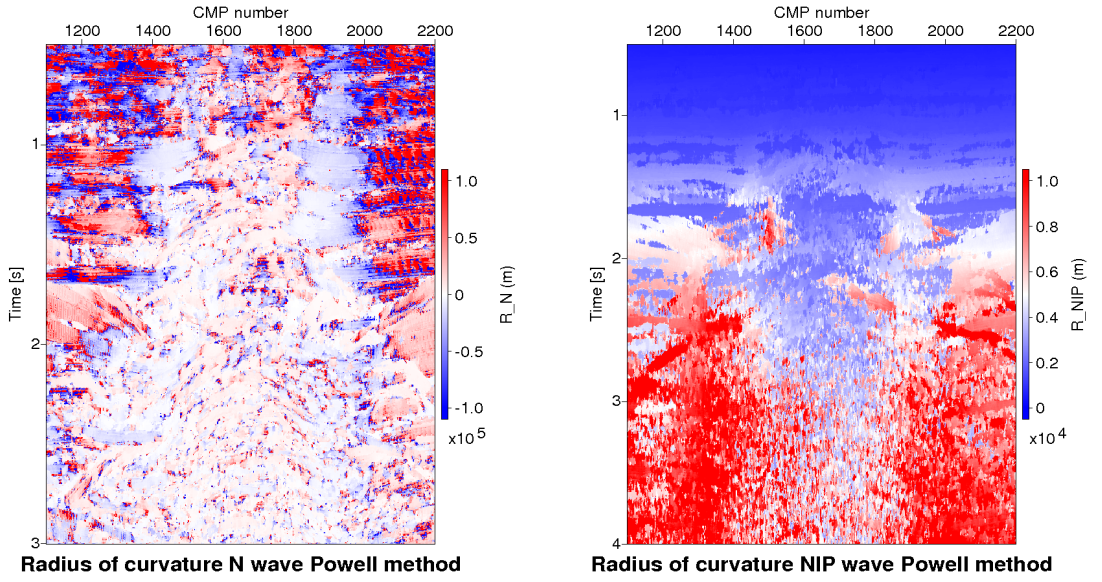

(a) (b)

Figure 6.15: Results of the automatic CRS parameter searches: R_N and R_{NIP}, radius of curvature of N wave section (a) and radius of curvature of NIP wave section (b) for the Powell conjugate direction method.

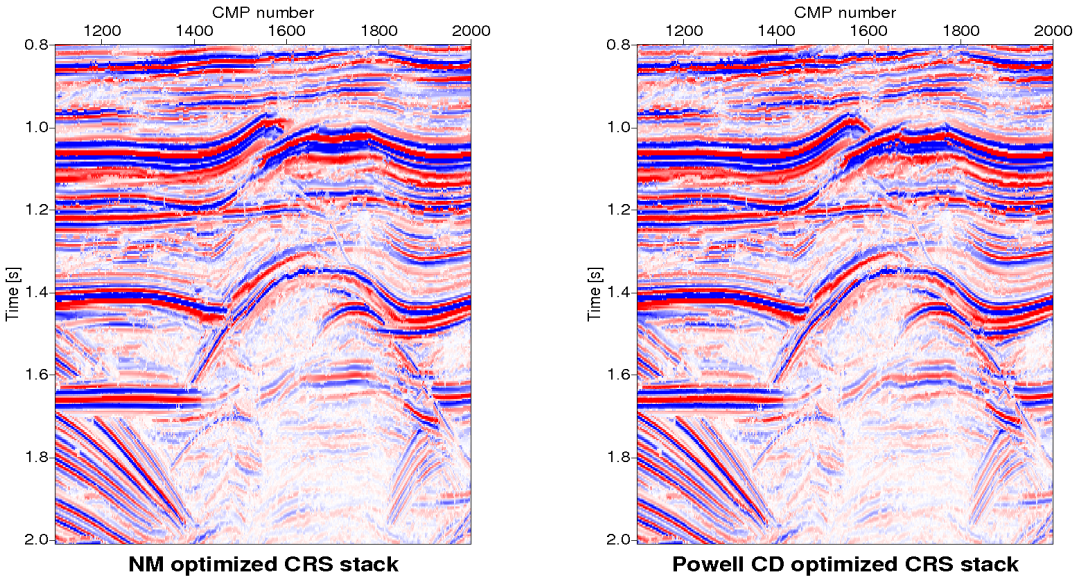

(a) (b)

Figure 6.16: ZO CRS stacked sections: comparison between the Nelder Mead optimization method (a) and Powell conjugate direction optimization method (b) in the areas of CMP 1100-2000. Powell conjugate direction method stacked section has more clearer and the reflections better defined.

The CRS stacked section obtained with the Powell conjugate direction optimized method is displayed in Figure 6.17. We do not see specific differences in the stack sections for the Powell conjugate direction approach using initial values from the pragmatic approach result shown in Figure 5.12. The possibility being trapped into local solutions to overcome the Powell conjugate direction method by applying strict procedures in the search direction. These results indicate that the new method has advantages in dealing with the selection of initial value problems in finding a final solution.

The coherence section for the dominant events associated with the Powell conjugate direction optimized CRS stack is shown in Figure 6.18. This figure looks similar to the Powell conjugate direction approach using initial values from the pragmatic approach result (Figure 5.13). In the coherence section most reflections can be identified which are visible in the CMP stack and CRS stack.

The reflection events are clearly defined for times 0-2.5 s traveltime correspond with high coherence values and associated with the reflector. The base of Tertiary at 1 s traveltime and the base of Upper Cretaceous at 1.5 s traveltime has cleary and can be easily identified. And the image of seismic events below 2.5 s traveltime have a lower coherence values which correspond to the salt plug areas. The events associated with the highest coherence at each particular zero-offset (ZO) location, allows to identify the detected events and to estimate the reliability of the image as well of its associated

wavefield attributes.

Figure 6.19 to 6.21 displays the sections of the CRS attributes obtained by automatic search with the Powell CD method. The optimized emergence angle sections for the dominant events are shown in Figure 6.19. This image looks similar to the optimized emergence angle section of the Powell conjugate direction approach using initial values from the pragmatic approach result (Figure 5.14) and no specific differences can be observed. Angle of emergence around 0° correspond to almost horizontal reflections. And higher values of emergence angle at 3 s traveltime indicates the diffractions in this section. The consistency of the optimized emergence angle section can readily be observed, due to the simple relation between the emergence angle and the slopes of the ZO events.

The optimized radius of curvature for the normal wave section for the dominant events are depicted in Figure 6.20. This section looks similar to the Powell conjugate direction approach using initial values from the pragmatic approach result (Figure 5.15). The upper part of this section has very large values of R_N associated to almost flat reflections. Plane reflector is characterized by the large values of R_N. The same applies to the section which is related to the curvature of the ZO events.

The optimized radius of curvature for the NIP wave for the dominant events are displayed in Figure 6.21. This image looks similar to the Powell conjugate direction approach using initial values from the pragmatic approach result (Figure 5.16). For the stratified areas, the values of R_{NIP} continously increases with increasing traveltime since this attributes associated to the reflector depth in a constant velocity medium. Overall, no differences can be observed from the result of the automatic three CRS parameter searches using global optimization when compared to the Powell conjugate direction approach using initial values from the pragmatic approach. The superior improvement of the coherence section can readily be observed by using the new method. The differences of coherence comparison between Nelder Mead optimization method and Powell conjugate direction optimization method is shown in Figure 6.22.

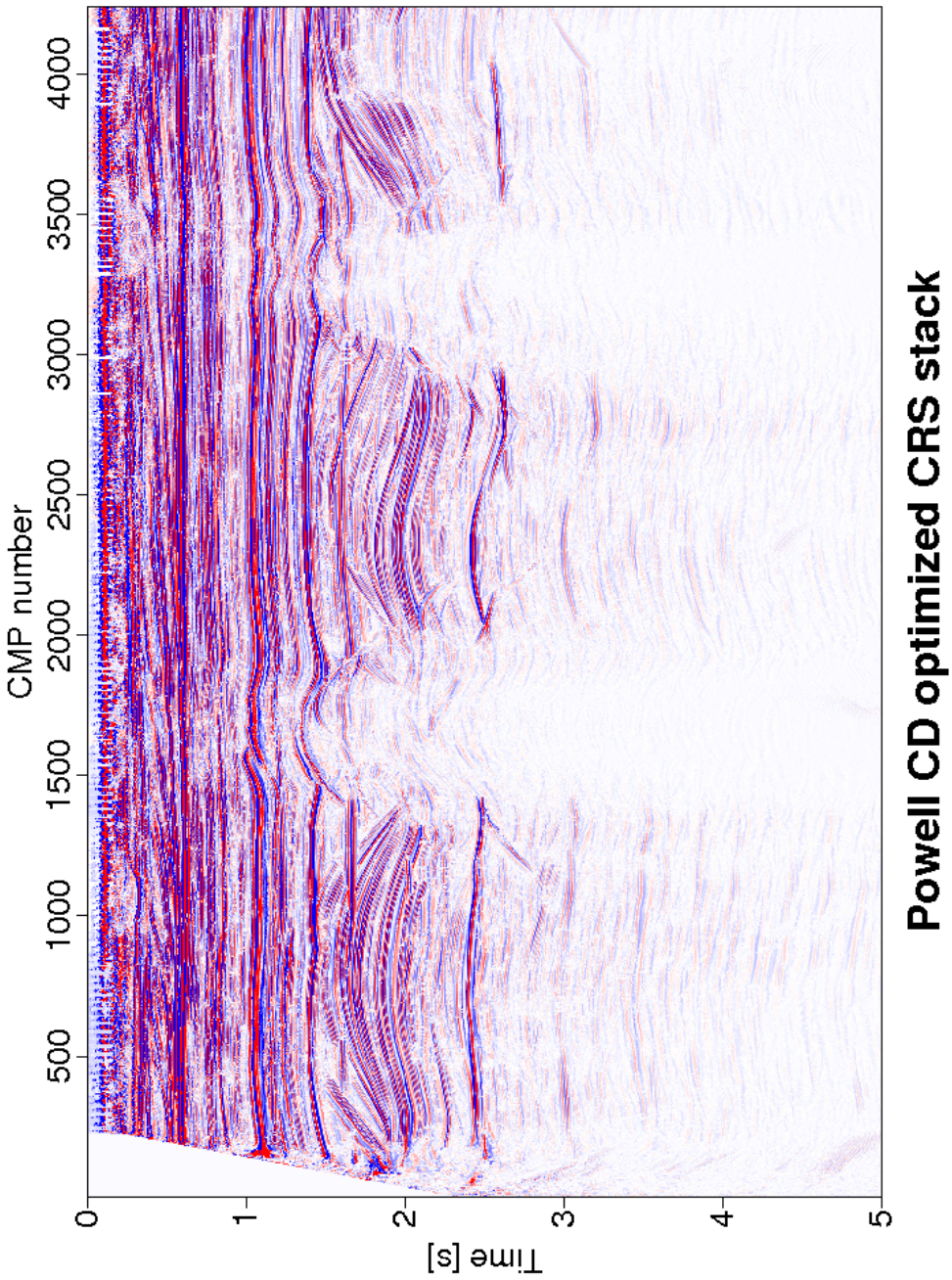

Figure 6.17: Global optimization field data: CRS stack result of the Powell CD optimization.

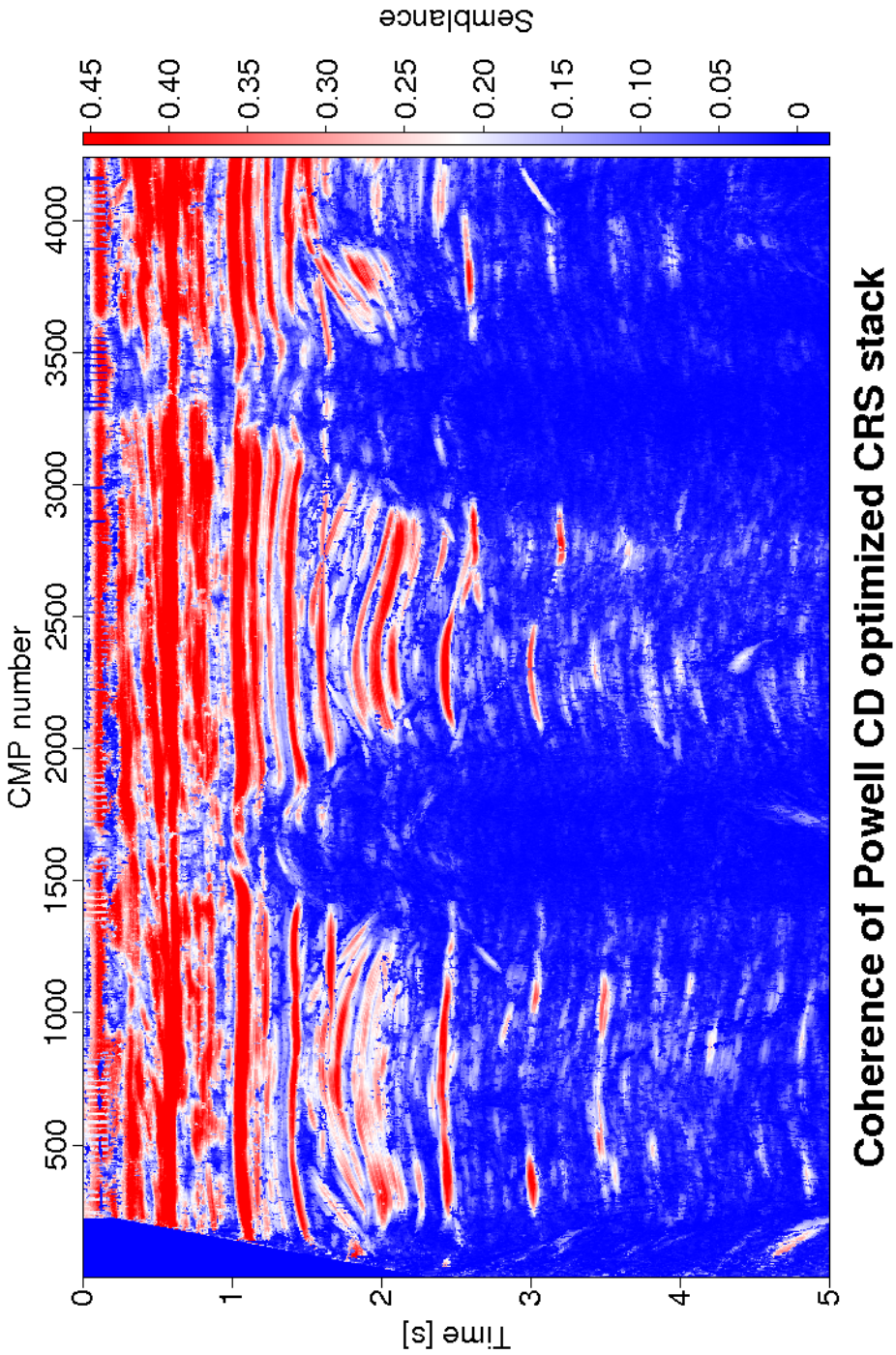

Figure 6.18: Global optimization field data: coherence section associated with the Powell CD optimized CRS stacked section shown in Figure 6.16.

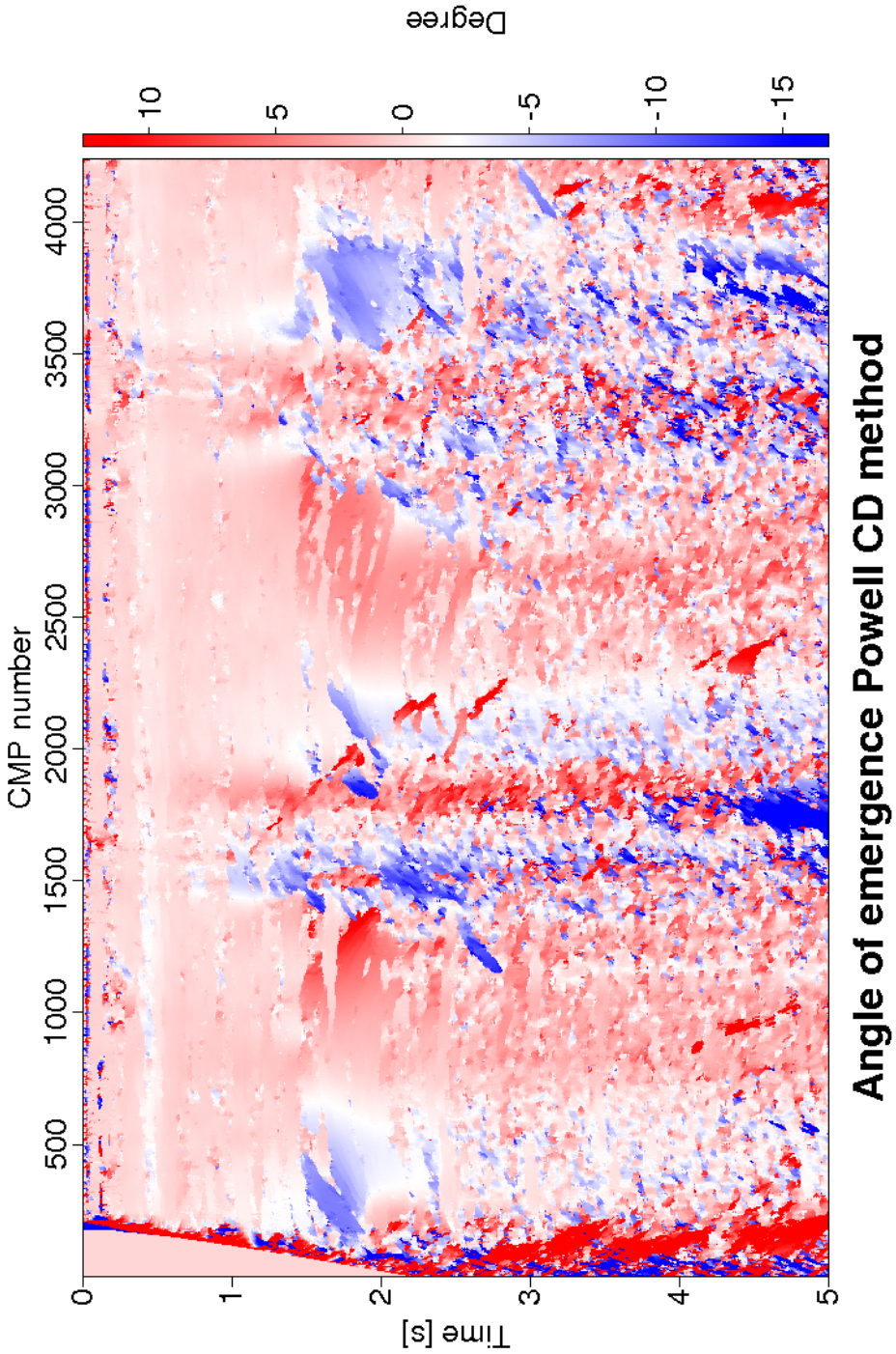

Figure 6.19: Global optimization field data: angle of emergence associated with the Powell CD optimized CRS stacked section shown in Figure 6.16. These attributes are directly related to the slopes of the events.

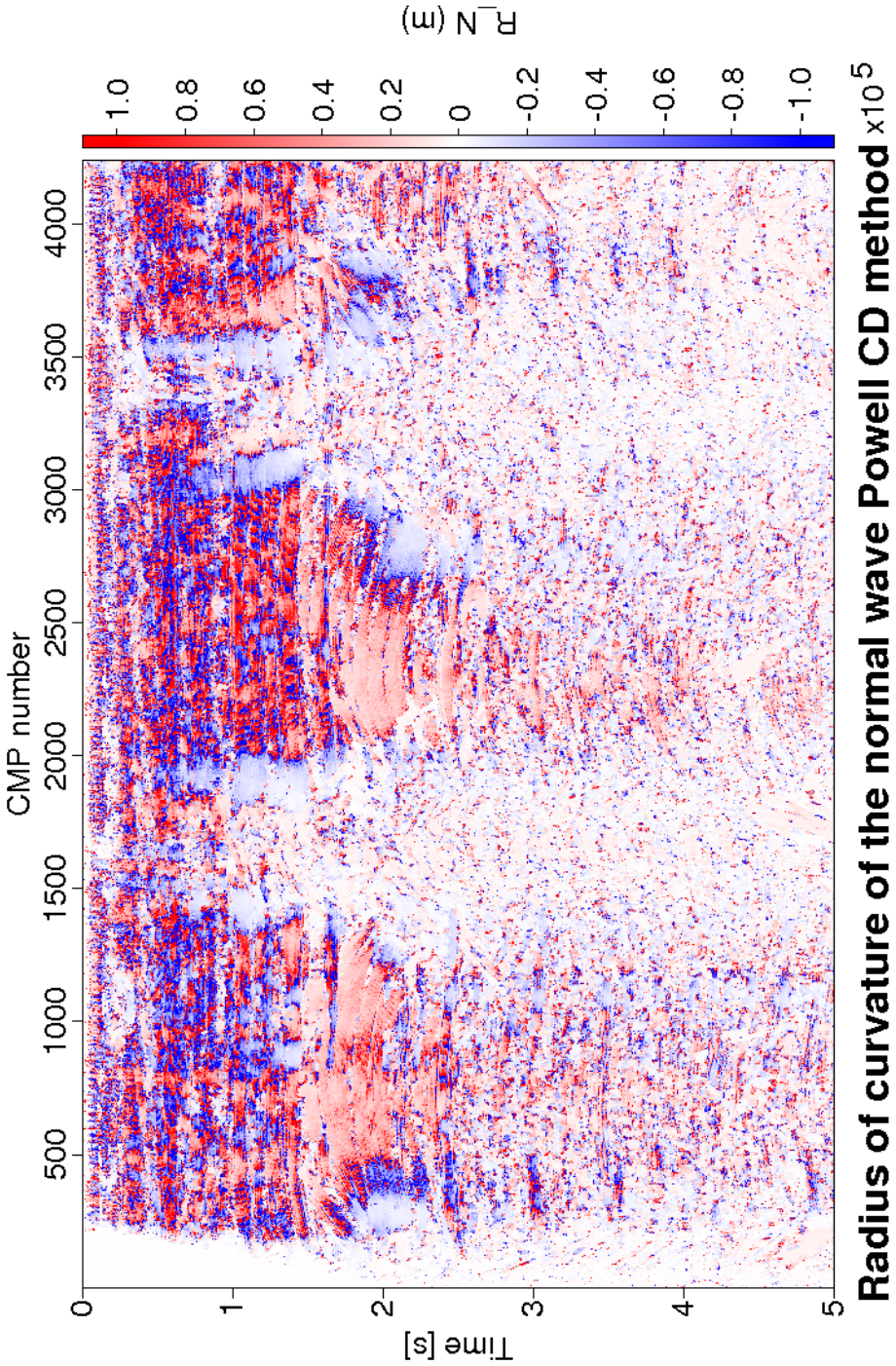

Figure 6.20: Global optimization field data: radius of curvature for the normal wave associated with the Powell CD optimized CRS stacked section shown in Figure 6.16. These attributes are directly related to the curvatures of the events in the ZO section.

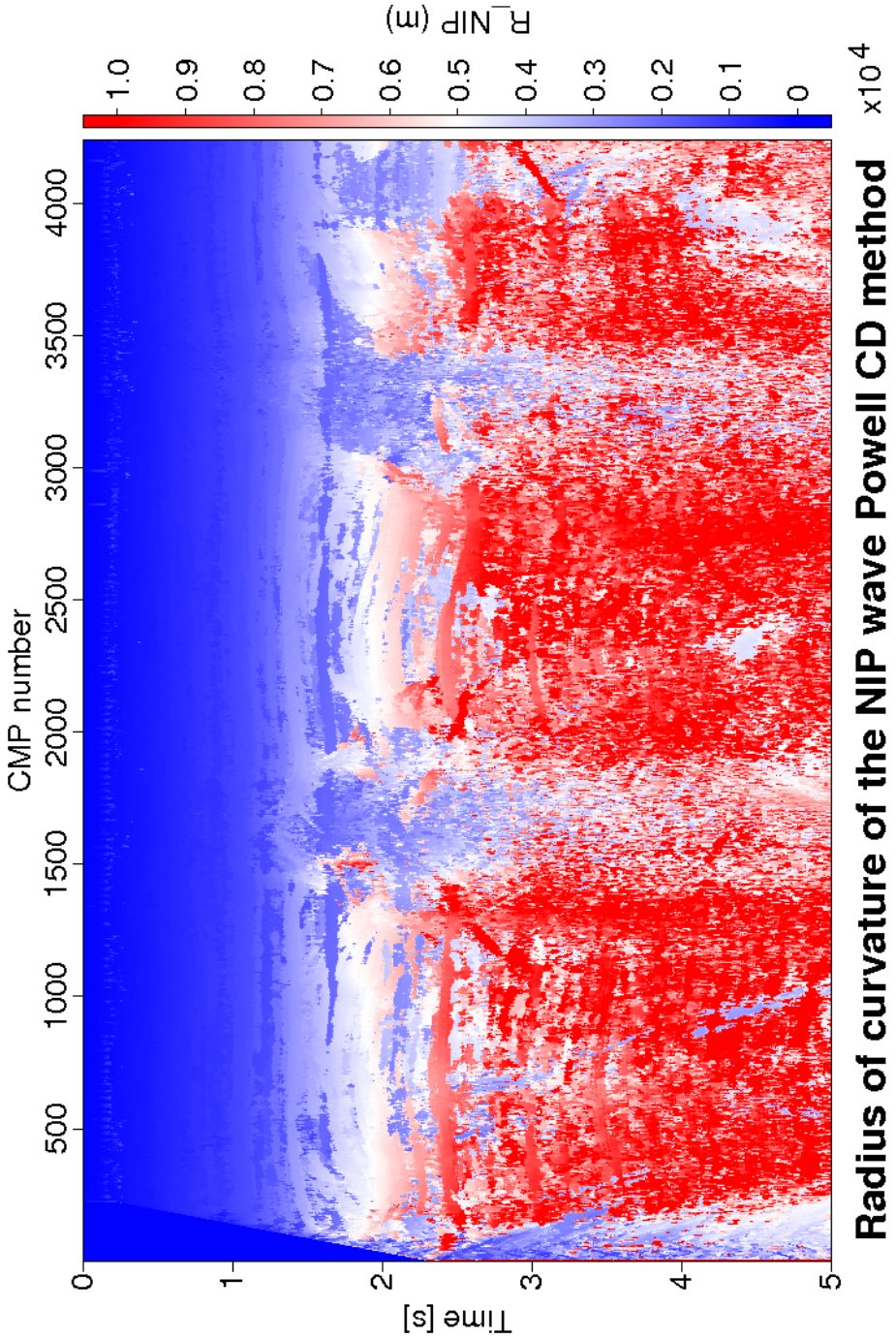

Figure 6.21: Global optimization field data: radius of curvature for the NIP wave associated with the Powell CD optimized CRS stacked section shown in Figure 6.14. These section is calculated from the emergence angle section of the dominant events in Figure 6.17 and the stacking velocity section obtained from automatic CMP stack.

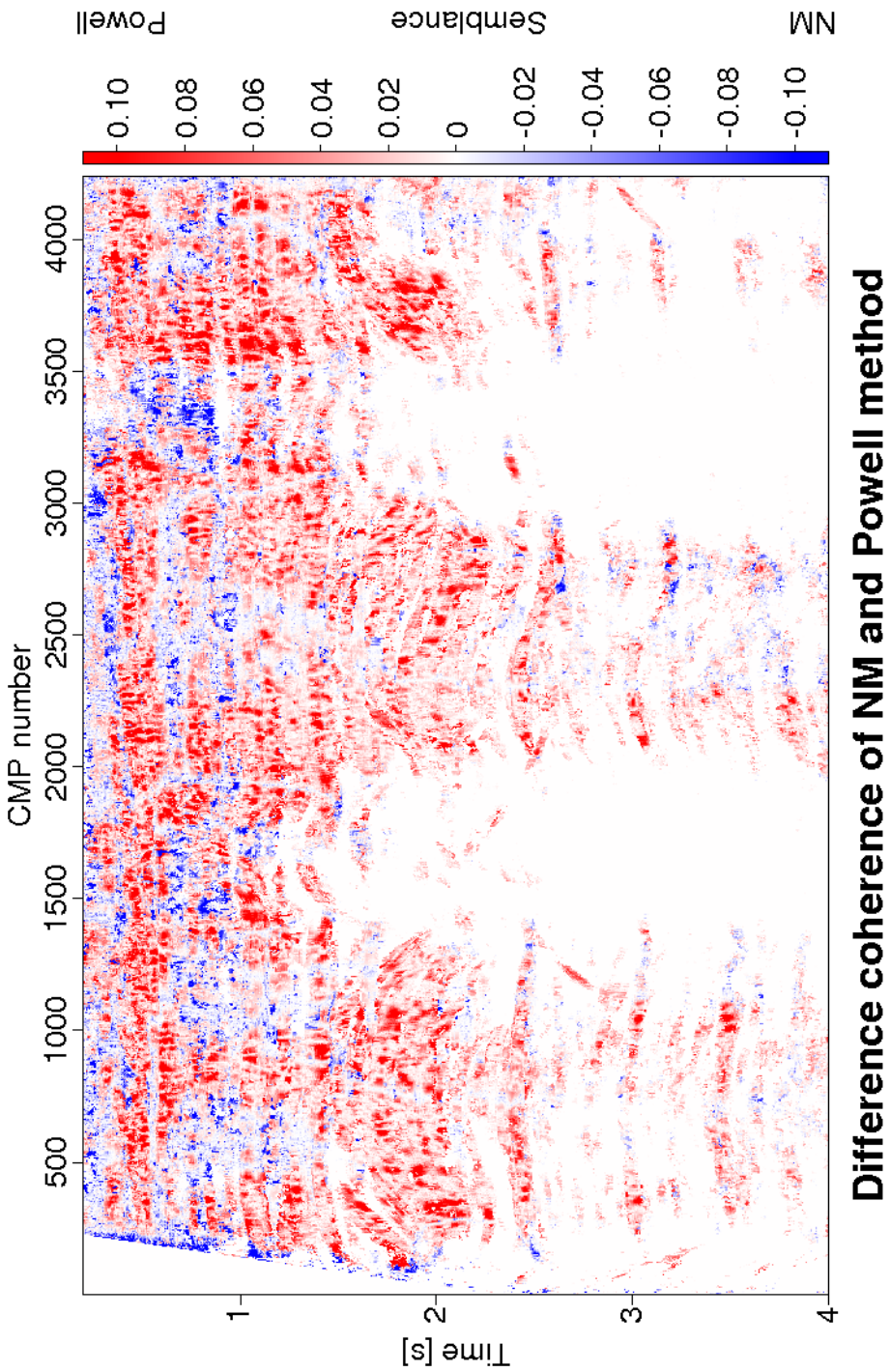

Figure 6.22: Global optimization field data: difference in coherence between the Nelder Mead optimized method and the Powell conjugate direction optimized method.

6.3 Conclusions

The optimization CRS stack result depends the choice of the initial wavefield attributes. The results of the global optimization of the CRS stacked section obtained with the Nelder Mead optimization method show more blur and scatter occurs when compared to the CRS stacked section obtained with the Powell conjugate direction optimization method. This scatter may be a results of getting trapped in a local minima. The best solution may also not be achieved in case the maximum number of iterations is exceeded. However, a specific feature of the Powell conjugate direction approach is its ability to avoid being trapped in local minima. Strict procedures in the search direction allows this method to find the right solution.

Overall one can conclude, that the application of the new method leads to comparable especially when we use arbitrary initial values. Result of the global optimization of the CRS stacked section obtained with the Powell conjugate direction optimization method provides very good quality. The application of the simultaneous optimization of the CRS stack method on the Sigsbee 2A synthetic data set and field data set shows that the new method provides very good solutions and can avoids being trapped into wrong solutions that can not be done by the Nelder Mead optimization method. The results shows appear smoother and improved when compared to the Nelder Mead results. Result of the automatic three CRS parameter searches sections displays similarity to the Powell conjugate direction approach using initial values from the pragmatic approach.

Chapter 7

Conclusion and Outlook

We have proposed a new strategy for the optimization of the simultaneous estimation of the CRS stack attributes, which allows to improve the image of pre-stack seismic reflection data. The method comprises the conjugate direction approach based on the Powell search method. The strategy is based on the conjugate direction method with its well known convergence properties and iterative Powell search method. The algorithm is robust and easy to implement. The use of the conjugate direction method leads to a highly efficient iterative search method to speed up the convergence rate while no derivatives need to be calculated. The iterative Powell search method for the control of the search direction prevents the premature convergence into local minima.

The 2-D CRS stack application using Powell conjugate direction optimization method have shown significant improvements in simulating zero-offset (ZO) sections compared to the conventional CMP stacked section and the pragmatic approach CRS stacked section. This optimization algorithm can be further increasing the accuracy of the Common Reflection Surface (CRS) wavefield attributes. Reflections are more continuous and the reflectors are better defined in the CRS stacked section. I have presented the application to the Sigsbee 2A synthetic data example and a field data example from Northern Germany. The quality improvement is observed on the Sigsbee 2A synthetic data example at the top of salt the bow-tie structures and diffraction patterns stemming are well simulated. As well as, for field data example the quality improvement is observed at the top of the salt plugs and in deeper section below 2.5 s traveltime. Most horizons have continuous structures and can be easily identified.

The improvement of coherence section between the pragmatic approach initial CRS stack and the Powell conjugate direction optimization method display more blur when compared to the CRS stacked section obtained with Nelder Mead optimization method. But it does not appear that the differences in coherence sections has a major effect on the three attributes. No specific differences can be observed from the CRS stacked sections and three kinematic wavefield attributes of both method.

The application to the complex Sigsbee 2A synthetic data example and a field

data example show that the new method provides solutions with higher stability and faster convergence. Moreover, this method has a substantial computational advantage against the Nelder Mead method currently used in the CRS attribute search. Examples show that the new method reduces the requirements in computational time by 55% (2 times faster) was observed for the simultaneous search of the parameters in the 2-D CRS stack using this method on the field data example.

The other advantage of this method turned out to be its globality. The application of the global optimization of the simultaneous estimation of the CRS stack method on the Sigsbee 2A synthetic data set and field data set shows that the new method provides very good solutions and can avoids being trapped into wrong solutions which can not be achieved by the Nelder Mead optimization method. The superior improvement result of the coherence section can readily be observed and significantly better described by the new method. Overall one can conclude, that the application of the new method leads to comparable results, even for the case of arbitrary starting values in a global application.

In this thesis, optimization of the simultaneous estimation of the CRS stack method was implemented for the 2-D case only. The application of the CRS stack for 2-D is also applicable for 3-D models. The concepts of the CRS stack approach have been shown by (Höcht, 2002) and transferred to the 3-D case provides a consistent subset of the 3-D zero-offset volume. The 3-D implementation of the pragmatic search strategy have already been implemented by (Müler, 2003). One possible topic of future research could be to extend the method for 3-D implementation of the CRS stack strategy and also for new other operators applicable to all coherence based optimization, i.e., i-CRS.

Another major issue for the future research could be the extension of the method to implementation of inexact line search. The line search is a basic part of the optimization method. Commonly, the exact line search is expensive especially when an iterate is far from the solution of the problem. Implementation inexact line search remains as future task to reduce the computing efforts. Moreover, the implementation of the initial values for the optimization based on a priori information from geological structure, best guess or local slope would be remains as challenge task for the future research topics.

Used software

In the course of this thesis several computers running the free GNU/Linux operation system were used.

The optimized CRS stack method developed during this work was written in C++. The program is based on the 2-D ZO CRS stack code as implemented by Mann (2002).

For simple processing and visualisation of the data, the free Seismic Un*x (SU) package was used. Additional figures were generated using gnuplot, inkscape, gimp and dia diagram editor.

The thesis it self was written on a PC with the free operating system Debian GNU/Linux with the type setting system LaTeX.

Acknowledgments

I am grateful to **Prof. Dr. Dirk Gajewski** for the supervision of this work and for help in any kind of occuring questions and problems. He gave me the opportunity to study in the Institute of Geophysics at the University of Hamburg.
I would like to thank following colleagues and students of the Institute of Geohysics, University of Hamburg, who contributed to this study:

- **Dr. Claudia Vanelle** and **Dr. Ekkehart Tessmer** for support in organize administration and computer administration.
- **Dr. Jürgen Mann** for the 2-D ZO CRS code code.
- **Dr. Daniela Theis** for the discussions and some advice about the method.
- **Benjamin Schwarz** for the continous discussions and many helps about the code, **Oksana Zhebel** assist for my presentations.
- **Sergius Dell** provided an introduction a lot of codes and scripts used in this thesis.
- **Christel Mynarik** and **Paola Dal Corso** for the assistance in administration and help me when the first time came to Hamburg.

The synthetic dataset for numerical tests was kindly provided by the **SMAART JV** consortium. The marine dataset was kindly provided by BP with assistance of **RWE Dea AG** (Hamburg).
I gratefully acknowledge the **Institute of Geohysics, University of Hamburg**, the Wave Inversion technology (**WIT**) consortium, and also Applied Geophysics Group

for discussion. **Directorate General of Higher Education (DIKTI)**, National Education Department of Republic Indonesia for the financial support during the study.
The finally, my wife **Yeti Mareta Undaryati** and our son **Sultan Syauqi Adliananda Minarto** and also our new baby **Lubnaa Aulia Taniananda Minarto** for their patience and support.

Erklärung

Hiermit versichere ich, die vorliegende Arbeit selbstständig angefertigt und nur die angegebenen Hilfsmittel verwendet zu haben.
Diese Arbeit hat in gleicher oder änlicher Form noch keiner Prüfungsbehörde vorgelegen.

Hamburg, den 22 January 2014

Eko Minarto

Bibliography

Brent, R. P. (1973). Algorithms for minimization without derivatives.

Fomel, S. (2007). Velocity-independent time-domain seismic imaging using local event slopes. *Society of Exploration Geophysicists.*, 72(3):139–147. DOI: 10.1190/1.2714047.

Ghosh, S., Gajewski, D., Dell, S. and Nath, S. K. (2010). Stacking attributes from local slopes. *American Geophysical Union, Fall Meeting* 2010.

Hertweck, T., Schleicher, J., and Mann, J. (2007). Data stacking beyond CMP. *The Leading Edge*, 26, no. 7, 818-827.

Höcht, G. (1998). *The common reflection surface stack.* Master's thesis, University of Karlsruhe.

Höcht, G. (2002). *Traveltime approximations for 2D and 3D media and kinematic wavefield attributes*. PhD thesis, University of Karlsruhe.

Hubral, P. (1983). Computing true amplitude reflections in alaterally in homogeneous earth. 48:1051–1062. DOI: 10.1190/1.1441528.

Hubral, P. and Krey, T. (1980). Interval velocities from seismic reflection traveltime measurements.

Jäger, R., Mann, J., Höcht, G., and Hubral, P. (2001). Common-reflection-surface stack: Image and attributes. *Geophysics*, 66:97–109.

Lagarias, Jeffrey, C., James, A. R., Margaret, H. W., and Paul, E. W. (1998). Convergence properties of the nelder mead simplex method in low dimensions. *SIAM Journal on Optimization*, 9(1):112–147.

Mann, J. (2002). *Extensions and Applications of the Common-Reflection-Surface Stack Method.* PhD thesis, University of Karlsruhe.

Mayne, W. H. (1962). Common reflection point horizontal data stacking techniques. *Geophysics*, 27. DOI:10.1190/1.1439118.

Müller, A. (2003). *The 3D Common-Reflecion-Surface Stack Theory and Application*. Master's thesis, University of Karlsruhe.

Müller, T. (1998). Common reflection surface stack versus nmo/stack and nmo/dmo/stack. *Extended Abstract*.

Müller, T. (1999). *The common reflection surface stack method seismic imaging without explicit knowledge of the velocity model*. PhD thesis, University of Karlsruhe.

Nelder, J. A. and Mead, R. (1965). A simplex method for function minimization. *Computer Journal*, 7:308–313.

Nocedal, J. and Wright, S. J. (1999). *Numerical Optimization. Springer : Series in Operations Research. ISBN 0-387-98793-2.*, volume 0-387-98793-2.

Santos, L., Schleicher, J., Costa, J. C., and Novais, A. (2011). Fast estimation of common-reflection-surface parameters using local slopes. *Society of Exploration Geophysicists*, 76(2):23–34. DOI: 10.1190/1.3553001.

Schleicher, J., Tygel, M., and Hubral, P. (1993). Parabolic and hyperbolic paraxial two-point traveltimes in 3d media. *Geophys. Prosp.*, 41(4):495–514.

Sheriff, R. E. and Geldart, L. P. (1995). *Exploration Seismology, 2nd edition*. Cambridge University Press.

Shohei, M., Tsuji, T., Matsuoka, T., Nishizaka, N., and Ikeda, M. (2012). Global optimization by simulated annealing for common reflection surface stacking and its application to low-fold marine data in southwest Japan. *Exploration Geophysics*, 10.1071/EG12008.

Stewart, G. W. (1973). Conjugate direction methods for solving system of linear equations. *Numeric Math.*, 21:285–297.

Sun, W. and Yuan, Y. X. (2006). Optimization theory and methods : nonlinear programming. *Springer*.

Taner, M. T. and Koehler, F. (1969). Velocity spectra-digital computer derivation and application of velocity function. *Geophysics*, 34(6):859–881.

Tygel, M., Müller, T., Hubral, P., and Schleicher, J. (1997). Eigenwave based multiparameter traveltime expansions. *SEG, Expanded Abstract*, pages 1770–1773. 67th Annua International Meeting.

Weise, T. (2009). *Global Optimization Algorithms - Theory and Application* -. http://www.it-weise.de/.

Yilmas, O. (2001). *Seismic data analysis - Processing, inversion, and interpretation of seismic data*. Society of Exploration Geophysics.

Ziegler, P. (1990). *Geological Atlas of Western and Central Europe, 2nd edition*. Shell, The Hague.